

AD-A151 967

OPTIMAL OPEN LOOP AND NONLINEAR FEEDBACK CONTROL FOR
REMOTE ORBITAL CAPTURE(U) AIR FORCE INST OF TECH
WRIGHT-PATTERSON AFB OH J W WIDHALM 1985

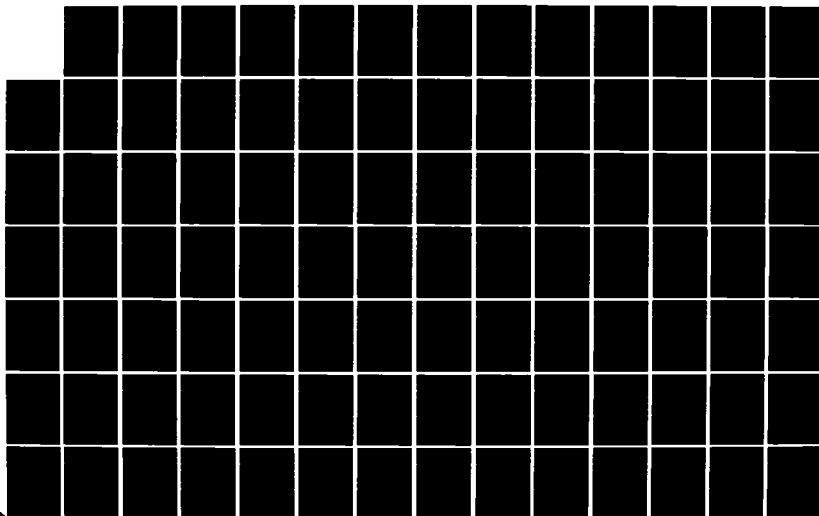
1/2

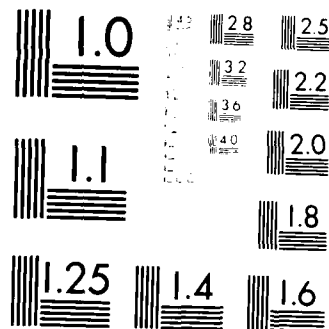
UNCLASSIFIED

AFIT/CI/NR-85-32D

F/G 22/1

NL





MICROCOPY RESOLUTION TEST CHART
NATIONAL BUREAU OF STANDARDS-1963-A

UNCLASS

SECURITY CLASSIFICATION OF THIS PAGE (When Data Entered)

REPORT DOCUMENTATION PAGE		READ INSTRUCTIONS BEFORE COMPLETING FORM
1. REPORT NUMBER AFIT/CI/NR 85- 32D	2. GOVT ACCESSION NO.	3. RECIPIENT'S CATALOG NUMBER
4. TITLE (and Subtitle) Optimal Open Loop And Nonlinear Feedback Control For Remote Orbital Capture	5. TYPE OF REPORT & PERIOD COVERED THESIS/DISSERTATION	
	6. PERFORMING ORG. REPORT NUMBER	
7. AUTHOR(s) Joseph William Widhalm, Jr.	8. CONTRACT OR GRANT NUMBER(s)	
9. PERFORMING ORGANIZATION NAME AND ADDRESS AFIT STUDENT AT: University of Illinois	10. PROGRAM ELEMENT, PROJECT, TASK AREA & WORK UNIT NUMBERS	
11. CONTROLLING OFFICE NAME AND ADDRESS AFIT/NR WPAFB OH 45433	12. REPORT DATE 1985	
	13. NUMBER OF PAGES 102	
14. MONITORING AGENCY NAME & ADDRESS (if different from Controlling Office)	15. SECURITY CLASS. (of this report) UNCLASS	
	15a. DECLASSIFICATION/DOWNGRADING SCHEDULE	
16. DISTRIBUTION STATEMENT (of this Report) APPROVED FOR PUBLIC RELEASE; DISTRIBUTION UNLIMITED		
17. DISTRIBUTION STATEMENT (of the abstract entered in Block 20, if different from Report)		
18. SUPPLEMENTARY NOTES APPROVED FOR PUBLIC RELEASE: IAW AFR 190-1 LYNN E. WOLAVER, 18 Feb 85 Dean for Research and Professional Development AFIT, Wright-Patterson AFB OH		
19. KEY WORDS (Continue on reverse side if necessary and identify by block number)		
20. ABSTRACT (Continue on reverse side if necessary and identify by block number) ATTACHED		

DD FORM 1 JAN 73 1473

EDITION OF 1 NOV 65 IS OBSOLETE

UNCLASS

85

03

11

047

SECURITY CLASSIFICATION OF THIS PAGE (When Data Entered)

AD-A151 967

MICROFILM COPY

OPTIMAL OPEN LOOP AND NONLINEAR FEEDBACK
CONTROL FOR REMOTE ORBITAL CAPTURE

BY

JOSEPH WILLIAM WIDHALM JR.

B.S., University of Illinois, 1967
M.S., Air Force Institute of Technology, 1974

THESIS

Submitted in partial fulfillment of the requirements
for the degree of Doctor of Philosophy in
Aeronautical and Astronautical Engineering
in the Graduate College of the
University of Illinois at Urbana-Champaign, 1985

Urbana, Illinois

Accession For	
NTIS GRA&I	<input checked="checked" type="checkbox"/>
DTIC TAB	<input type="checkbox"/>
Unannounced	<input type="checkbox"/>
Justification	
By	
Distribution/	
Availability Codes	
and/or	
Price	
A-1	



OPTIMAL OPEN LOOP AND NONLINEAR FEEDBACK
CONTROL FOR REMOTE ORBITAL CAPTURE

Joseph William Widhalm Jr., Ph.D.
Department of Aeronautical and Astronautical Engineering
University of Illinois at Urbana-Champaign, 1985

Optimal open loop and nonlinear feedback control histories are presented for the problem of detumbling (passivating) a target satellite by a remotely operated robot spacecraft. Detumbling is required so that the robot spacecraft, sometimes called a teleoperator or orbital maneuvering vehicle (OMV), can return the target satellite to low-Earth orbit for servicing and repair. The dynamics of the coupled two-body system are described with equations of motion derived from an Eulerian formulation (the Hooker-Margulies equations). Two degrees of rotational freedom are allowed at the joint which connects the OMV and target spacecraft, and the joint is allowed to translate on the surface of the OMV. The initial condition of the axially symmetric target satellite is free spin and precession. Representative masses and inertias are assumed for each body. The detumbling controls, which are the external (thruster) and internal (joint) torques applied by the OMV, are found from optimal control theory and Liapunov stability theory. Applying optimal control theory yields a nonsingular two-point-boundary-value-problem which is solved numerically for the open loop controls over a specified time interval. Control

constraints on the thrusters and one of the joint torques are also considered. Liapunov stability theory is used to derive a nonlinear feedback control law which results in the asymptotic stability of a set of equilibria for the two-body system. This control law is analyzed numerically and compared to the results of optimum open loop control. Also presented is an example in which open loop controls nearly detumble the target satellite and feedback controls complete detumbling. In all cases the constraint force and torque at the joint are determined. Detumbling is shown to be a very benign process requiring only very small control torques and producing only small constraint loads.

TABLE OF CONTENTS

Chapter		Page
	LIST OF TABLES	vii
	LIST OF FIGURES	viii
	LIST OF SYMBOLS	x
1	INTRODUCTION	
	1.1 Problem Statement and Relevance	1
	1.2 Previous Approaches	2
	1.3 The Present Approach	6
2	EQUATIONS OF MOTION	
	2.1 Introduction	11
	2.2 Review and Modification of the Hooker and Margulies Equation	12
	2.3 Elimination of the Unknown Constraint Torques	16
	2.4 Two-Body Equations for the Capture Problem	19
	2.5 Joint Constraint Force Equation	23
	2.6 Equation Verification	25
	2.7 Conclusion	27
3	CAPTURE BY CONTINUOUS OPEN LOOP OPTIMAL CONTROL	
	3.1 Introduction	28
	3.2 The Optimal Control Problem	28
	3.3 The Two-Point-Boundary-Value-Problem (TPBVP)	30
	3.4 The Reduced Order TPBVP	35
	3.5 Solving the Reduced Order TPBVP	37
	3.6 Capture With Control Constraints	39
	3.7 Results	41
	3.8 Conclusions	64
4	CAPTURE BY CONTINUOUS NONLINEAR FEEDBACK CONTROL	
	4.1 Introduction	65
	4.2 Linear Feedback Control About an Equilibrium Point	66
	4.3 Global Asymptotic Stability by Nonlinear Feedback Control	69
	4.4 Results	72
	4.5 Summary and Conclusions	77

5 CONTROL SCHEME COMPARISONS AND CONCLUSIONS

5.1	Introduction	82
5.2	Control Scheme Comparisons	82
5.3	Capture by an Open Loop Control to Feedback Control Sequence	85
5.4	Summary and Conclusions	95
5.5	Suggestions for Further Research	99
	LIST OF REFERENCES	101
	VITA	103

LIST OF TABLES

Table	Title	Page
1	State Boundary Conditions	37
2	System Mass Properties	42
3	Initial Conditions	42
4	Sequence of Initial Conditions	43
5	Control and Constraint Load Ranges for Unconstrained Optimal Open Loop Control and Feedback Control	84
6	System State Summary for the Open Loop- Feedback Case	87

LIST OF FIGURES

Figure	Title	Page
1	OMV-Target System	5
2	Body 0 Angular Rate Histories (Case 1)	45
3	Body 1 $\dot{\gamma}_1$ and $\dot{\gamma}_2$ Histories (Case 1)	47
4	Body 1 $\dot{\gamma}_1$ History (Case 1)	48
5	External Torque Histories (Case 1)	49
6	Internal Torque Histories (Case 1)	50
7	Constraint Load Histories (Case 1)	51
8	Body 0 Angular Rate Histories (Case 2)	53
9	Body 1 $\dot{\gamma}_1$ and $\dot{\gamma}_2$ Histories (Case 2)	54
10	Body 1 $\dot{\gamma}_1$ History (Case 2)	55
11	Internal Torque Histories (Case 2)	56
12	Constraint Load Histories (Case 2)	57
13	Body 0 Angular Rate Histories (Case 3)	58
14	Body 1 $\dot{\gamma}_1$ and $\dot{\gamma}_2$ Histories (Case 3)	59
15	Body 1 $\dot{\gamma}_1$ History (Case 3)	60
16	External Torque Histories (Case 3)	61
17	Internal Torque Histories (Case 3)	62
18	Constraint Load Histories (Case 3)	63
19	Joint Motion Histories (Feedback)	74
20	Body 1 $\dot{\gamma}_1$ and $\dot{\gamma}_2$ Histories (Feedback)	75
21	Body 1 $\dot{\gamma}_1$ History (Feedback)	76
22	External Torque Histories (Feedback)	78
23	Internal Torque Histories (Feedback)	79

Figure	Title	Page
24	Constraint Load Histories (Feedback)	80
25	Body 0 Angular Rate Histories (Composite) . .	89
26	Body 1 γ_1 and $\dot{\gamma}_2$ Histories (Composite)	90
27	Body 1 $\dot{\gamma}_1$ History (Composite)	91
28	External Torque Histories (Composite)	92
29	Internal Torque Histories (Composite)	93
30	Constraint Load Histories (Composite)	94

LIST OF SYMBOLS

m_λ	=	mass of body λ
m	=	total mass
\mathbf{I}_λ	=	inertia dyadic of body λ about center of mass
$\bar{\omega}_\lambda$	=	angular velocity of body λ
$\bar{\mathbf{F}}_\lambda$	=	total external force on body λ
$\bar{\mathbf{F}}'_\lambda$	=	non-gravitational external force on body λ
$\bar{\mathbf{T}}_\lambda$	=	total external torque on body λ
$\bar{\mathbf{T}}'_\lambda$	=	non-gravitational external torque on body λ
$\bar{\mathbf{p}}_\lambda$	=	planetocentric position vector of c.m. of body λ
$\bar{\mathbf{F}}^H_{\lambda j}$	=	interaction force on body λ transmitted through joint j
$\bar{\mathbf{T}}^H_{\lambda j}$	=	torque on body λ transmitted through joint j
J_λ	=	the set of joints on body λ
$\bar{\mathbf{T}}^C_{\lambda j}$	=	gimbal constraint torque on body λ at joint j
S	=	the set of bodies in the topological tree
\mathbf{l}	=	unit dyadic
γ	=	planet's gravitational constant
$\bar{\mathbf{c}}$	=	planetocentric position vector of satellite composite c.m.
$\hat{\mathbf{c}}$	=	unit vector in direction of $\bar{\mathbf{p}}$
$\bar{\mathbf{T}}^{\text{SD}}_{\lambda j}$	=	spring-damper torque on body λ at joint j
$\hat{\mathbf{g}}_i$	=	unit vector along rotation axis of joint
γ_i	=	angle of rotation about axis $\hat{\mathbf{g}}_i$
r	=	number of rotational degrees of freedom
$\bar{\omega}_0$	=	angular velocity of the reference body
$\bar{\mathbf{z}}_{ij}$	=	the i 'th through j 'th elements of the vector $\bar{\mathbf{z}}$

CHAPTER 1

INTRODUCTION

1.1 Problem Statement and Relevance

The in-orbit servicing and repair of satellites is a new area of space operations now possible because of the capabilities of the Space Shuttle. In April 1984 a Space Shuttle crew successfully captured and repaired a satellite, the Solar Maximum spacecraft, for the first time. A significant part of that effort was the detumbling or passivating of the satellite which had to be accomplished before the repair could begin. The detumbling proved to be quite difficult even though the angular rates of the satellite were very small.

Many of the satellites which could benefit from in-orbit servicing or repair are in orbits beyond the reach of the Space Shuttle. To retrieve these satellites to the Space Shuttle's orbit, a remotely operated spacecraft, sometimes called a teleoperator or orbital maneuvering vehicle (OMV), is required. The OMV would have to rendezvous and dock with the target satellite. Then the OMV would have to detumble or passivate the target, as the Shuttle did with the Solar Maximum spacecraft, to complete capture. Detumbling would be accomplished by applying forces and torques to the target to remove any motion relative to

the OMV and would be necessary if the target were spin-stabilized or had experienced a failure of its attitude control system. Finally, attitude maneuvers would be performed to orient the coupled two-body system for return to low-Earth orbit.

The detumbling of a target satellite by an OMV is the specific problem of concern in this work. The OMV is considered to have rendezvoused and docked with the target satellite, and detumbling is to be effected by applying torques on the target through the OMV. The absolute motion of the OMV is also to be partially controlled during detumbling by applying torques on the OMV. In the remainder of this chapter, previous approaches to the problem of remote orbital capture by an OMV are reviewed, and the approaches taken in this work are described.

1.2 Previous Approaches

Work began on the problem of remote orbital capture in the early 1970's. Efforts to define the concept and requirements of teleoperator spacecraft were made by Omega and Clingman [1] and by Smith and DeRocher [2]. At the same time the dynamics and control of remote orbital capture began to be considered. Faile, et al. [3] analyzed the response of a target spacecraft to torques applied by an OMV which had completed a rendezvous and docking with the target spacecraft. However, they assumed that the OMV was

$$\sum_{\mu \in S} \bar{F}_{\lambda\mu} \cdot \dot{\bar{J}}_{\mu} = \bar{E}_{\lambda} + \sum_{j \in J_{\lambda}} \bar{T}_{\lambda j}^C$$

$$- \sum_{\mu \neq \lambda} m_{\mu} \bar{\mathcal{L}}_{\lambda\mu} \times [\ddot{\bar{D}}_{\lambda\mu}^R + 2\bar{\omega}_{\lambda} \times \dot{\bar{D}}_{\lambda\mu}^R] \quad (2.15)$$

By the same argument, motion of the joints on some other body, μ , relative to the mass center of body μ can be allowed. Referring back to equation (2.3), such motion is treated by using the more complete form of the second derivative of $\bar{D}_{\mu\lambda}$, as in equation (2.13), rather than the form given by equation (2.12). Substituting as before leads to the conclusion that the expression for \bar{E}_{λ} in equation (2.15), as given by equation (2.11), must be changed by substituting

$$m[\ddot{\bar{D}}_{\mu\lambda}^R + 2\bar{\omega}_{\mu} \times \dot{\bar{D}}_{\mu\lambda}^R + \bar{\omega}_{\mu} \times (\bar{\omega}_{\mu} \times \bar{D}_{\mu\lambda})]$$

for the term $m\bar{\omega}_{\mu} \times (\bar{\omega}_{\mu} \times \bar{D}_{\mu\lambda})$. With this change, equation (2.15) becomes the attitude equation of motion for body λ properly accounting for joint motions relative to any of the bodies the joints connect.

2.3 Elimination of the Unknown Constraint Torques

Examining equation (2.15) reveals the explicit appearance of the constraint torques, $\bar{T}_{\lambda j}^C$, while the constraint forces, $\bar{F}_{\lambda j}^H$, have been eliminated. Hooker [7] shows how to eliminate the constraint torques from equation (2.15) by considering the attitude motion of the complete system

The restriction that the joints on body λ must be fixed relative to the center of mass of body λ is contained in equations (2.6) and (2.7) where Hooker and Margulies [6] assumed the vector $\bar{D}_{\lambda\mu}$ to be fixed in body λ so that

$$\ddot{\bar{D}}_{\lambda\mu} = \dot{\bar{\omega}}_{\lambda} \times \bar{D}_{\lambda\mu} + \bar{\omega}_{\lambda} \times [\bar{\omega}_{\lambda} \times \bar{D}_{\lambda\mu}] . \quad (2.12)$$

If, on the other hand, motion of a joint on body λ with respect to body λ (e.g. along the surface of body λ) is allowed, $\bar{D}_{\lambda\mu}$ is then no longer fixed in body λ , so equation (2.12) becomes

$$\ddot{\bar{D}}_{\lambda\mu} = \ddot{\bar{D}}_{\lambda\mu}^R + 2\bar{\omega}_{\lambda} \times \dot{\bar{D}}_{\lambda\mu}^R + \dot{\bar{\omega}}_{\lambda} \times \bar{D}_{\lambda\mu} + \bar{\omega}_{\lambda} \times [\bar{\omega}_{\lambda} \times \bar{D}_{\lambda\mu}] , \quad (2.13)$$

where superscript R indicates differentiation with respect to time relative to the reference frame fixed in body λ .

Substituting equation (2.13) into equation (2.6) yields

$$\begin{aligned} - \sum_{\mu \neq \lambda} m_{\mu} \bar{\mathcal{L}}_{\lambda\mu} \times \ddot{\bar{D}}_{\lambda\mu} &= - X_{\lambda} \cdot \dot{\bar{\omega}}_{\lambda} - \bar{\omega}_{\lambda} \times X_{\lambda} \cdot \bar{\omega}_{\lambda} \\ &- \sum_{\mu \neq \lambda} m_{\mu} \bar{\mathcal{L}}_{\lambda\mu} \times [\ddot{\bar{D}}_{\lambda\mu}^R + 2\bar{\omega}_{\lambda} \times \dot{\bar{D}}_{\lambda\mu}^R] . \end{aligned} \quad (2.14)$$

Further substitution of equation (2.14) into equation (2.3) and then equation (2.3) into Euler's equation now leads directly to the attitude equation of motion for body λ in which the joints on body λ are free to translate relative to the center of mass of body λ . The final result is given here as

$$\begin{aligned}
X_\lambda &= [m_\lambda \bar{D}_\lambda^2 + \sum_{\mu \neq \lambda} m_\mu \bar{D}_{\lambda\mu}^2] \mathbf{1} \\
&- [m_\lambda \bar{D}_\lambda \bar{D}_\lambda + \sum_{\mu \neq \lambda} m_\lambda \bar{D}_{\lambda\mu} \bar{D}_{\lambda\mu}].
\end{aligned} \quad (2.7)$$

Substituting equation (2.6) into equation (2.3) and then equation (2.3) into Euler's equation leads directly to the attitude equation of motion of body λ under the influence of gravity gradient torque. That equation given by Hooker and Margulies [6] is written in an equivalent form by Hooker [7] as

$$\sum_{\mu \in S} \phi_{\lambda\mu} \cdot \dot{\bar{\omega}}_\mu = \bar{E}_\lambda + \sum_{j \in J_\lambda} \bar{T}_{\lambda j}^C, \quad (2.8)$$

where $\phi_{\lambda\mu}$ is the dyadic,

$$\begin{aligned}
\phi_{\lambda\lambda} &= \phi_\lambda + m_\lambda [\bar{D}_\lambda^2 \mathbf{1} - \bar{D}_\lambda \bar{D}_\lambda] \\
&+ \sum_{\mu \neq \lambda} m_\mu [\bar{D}_{\lambda\mu}^2 \mathbf{1} - \bar{D}_{\lambda\mu} \bar{D}_{\lambda\mu}],
\end{aligned} \quad (2.9)$$

$$\phi_{\lambda\mu} (\mu \neq \lambda) = -m [\bar{D}_{\mu\lambda} \cdot \bar{D}_{\mu\lambda} \mathbf{1} - \bar{D}_{\mu\lambda} \bar{D}_{\mu\lambda}], \quad (2.10)$$

and \bar{E}_λ is the vector

$$\begin{aligned}
\bar{E}_\lambda &= 3\gamma\bar{\rho}^{-3} \hat{\rho} \times \phi_{\lambda\lambda} \cdot \hat{\rho} - \bar{\omega}_\lambda \times \phi_{\lambda\lambda} \cdot \bar{\omega}_\lambda \\
&+ \bar{T}_\lambda' + \sum_{j \in J_\lambda} \bar{T}_{\lambda j}^{SD} + \bar{D}_\lambda \times \bar{F}_\lambda' \\
&+ \sum_{\mu \neq \lambda} \bar{D}_{\lambda\mu} \times \{ \bar{F}_\mu' + m\bar{\omega}_\mu \times [\bar{\omega}_\mu \times \bar{D}_{\mu\lambda}] + m\gamma\bar{\rho}^{-3} [1 - 3\hat{\rho}\hat{\rho}] \cdot \bar{D}_{\mu\lambda} \}.
\end{aligned} \quad (2.11)$$

$$\bar{F}_\lambda + \sum_{j \in J_\lambda} \bar{F}_{\lambda j}^H = m_\lambda \ddot{\bar{\rho}}_\lambda \quad (2.1)$$

and

$$\begin{aligned} \phi_\lambda \cdot \dot{\bar{\omega}}_\lambda + \bar{\omega}_\lambda \times \phi_\lambda \cdot \bar{\omega}_\lambda = \bar{T}_\lambda + \sum_{j \in J_\lambda} \bar{T}_{\lambda j}^H \\ + \sum_{j \in J_\lambda} \bar{\mathcal{L}}_{\lambda j} \times \bar{F}_{\lambda j}^H, \end{aligned} \quad (2.2)$$

where $\bar{\mathcal{L}}_{\lambda j}$ is the vector from the center of mass of body λ to the joint, j , on body λ . The hinge forces, $\bar{F}_{\lambda j}^H$, are then eliminated from Euler's equation by summing Newton's equation over the bodies, μ , connected to the body, λ , at each joint, j . An expression for $\bar{F}_{\lambda j}^H$ results, which can be substituted into the last term of Euler's equation to yield

$$\begin{aligned} \sum_{j \in J_\lambda} \bar{\mathcal{L}}_{\lambda j} \times \bar{F}_{\lambda j}^H = \bar{D}_\lambda \times \bar{F}_\lambda + \sum_{\mu \neq \lambda} \bar{D}_{\lambda \mu} \times \bar{F}_\mu \\ - \sum_{\mu \neq \lambda} m_\mu \bar{\mathcal{L}}_{\lambda \mu} \times \ddot{\bar{D}}_{\lambda \mu} + m \sum_{\mu \neq \lambda} \bar{D}_{\lambda \mu} \times \ddot{\bar{D}}_{\mu \lambda}, \end{aligned} \quad (2.3)$$

$$\text{where } \bar{D}_\lambda = - \sum_{\mu \neq \lambda} m_\mu m^{-1} \bar{\mathcal{L}}_{\lambda \mu} \quad (2.4)$$

$$\text{and } \bar{D}_{\lambda \mu} = \bar{D}_\lambda + \bar{\mathcal{L}}_{\lambda \mu}. \quad (2.5)$$

Here $\bar{\mathcal{L}}_{\lambda \mu}$ means the vector from the center of mass of body λ to the joint, j , leading to body μ . From equation (2.3) it can be shown that

$$- \sum_{\mu \neq \lambda} m_\mu \bar{\mathcal{L}}_{\lambda \mu} \times \ddot{\bar{D}}_{\lambda \mu} = - X_\lambda \cdot \dot{\bar{\omega}}_\lambda - \bar{\omega}_\lambda \times X_\lambda \cdot \bar{\omega}_\lambda, \quad (2.6)$$

where X_λ is the dyadic defined by Hooker and Margulies [6] as

the revised n-body equations the two-body equations for the capture problem are derived. The equation for the constraint torque on the joint given by Hooker [7] also becomes modified to account for joint motion in the process of rederiving the system equations. The constraint force on the joint is found by directly applying Newton's equation for the translational motion of either the OMV or the target. The resulting equation for the constraint force confirms that the joint motion must be prescribed and is not directly determined by the constraint force on the joint. Finally, the methods used to verify the system attitude equations, the constraint torque equation, and the constraint force equation are discussed. Various test cases are used along with the principle of conservation of angular momentum to compare computer generated results with known results. The expression for the system angular momentum is derived because of its importance to the verifying process.

2.2 Review and Modification of the Hooker and Margulies Equation

To see how the Hooker and Margulies [6] derivation must be changed to account for joint translation, that derivation must be traced carefully. Following their development, Newton's and Euler's equations for body λ in an n-body system are:

CHAPTER 2

EQUATIONS OF MOTION

2.1 Introduction

An Eulerian derivation of the equations of attitude motion of multi-body satellites has been presented by Hooker and Margulies [6] and Hooker [7]. These equations are appropriate for a system of n rigid bodies connected by joints which allow relative motion between the bodies through rotations at the joints. Two restrictions are imposed on the system in this formulation. First, chains of connected bodies may not form closed loops. Second, joint positions must be fixed with respect to the bodies they connect. Otherwise, the axes of rotation at each joint, arbitrary external forces and torques, and arbitrary internal torques at the joints may be specified. Constraint forces and torques at the joints do not appear in the final equations of motion, but methods are given to determine these quantities after the absolute angular and translational accelerations of each body are known.

Modifying these equations to allow specified joint translational motion is the subject of this chapter. First, the Hooker and Margulies derivation [6,7] is reviewed to show how the form of the equations is affected by assuming fixed joints, and then the required changes are made. From

Liapunov stability theory is employed to derive a non-linear feedback control law to effect capture. Results are presented for this control law for comparison with the open loop results of Chapter 3.

Merging the results of Chapters 3 and 4 into conclusions and suggestions for further work is the subject of Chapter 5. After comparing open loop and feedback results, an example is presented in which open loop control brings the two-body system very close to the final spin-stabilized equilibrium; then Liapunov feedback control completes the capture. From the various approaches to the capture problem, significant points are highlighted to show how the general capture problem has been brought into better perspective. Finally, several suggestions are offered for continuing this work to refine the OMV concept and requirements for rendezvous and docking and to consider target spacecraft with more general mass properties and configurations.

Also of importance as a part of the solution of the capture problem are the constraint force and torque on the joint during capture. These quantities determine the structural requirements of the joint and the force required to move the joint during capture. Equations to compute these quantities are a part of the work of Hooker and Margulies [6] and Hooker [7] but again must be modified to account for joint translational motion. The necessary changes to these equations are also developed in Chapter 2 and the aforementioned work by Conway and Widhalm [9].

With the necessary dynamic equations of the two-body system, a control strategy or control law to effect detumbling must be found. Control of multi-body systems interconnected as proposed here has not been addressed previously, but optimal control theory and Liapunov stability theory provide methods for deriving open loop and nonlinear feedback controls for such nonlinear systems. In Chapter 3 the capture problem is solved using optimal control theory. The nonsingular two-point-boundary-value-problem (TPBVP) resulting from this approach is solved numerically for the system state and open loop control histories over the specified time interval for capture. Cases in which the controls are constrained and unconstrained are presented to illustrate the effects of simplifying the control system. These results are also discussed by Conway and Widhalm [10]. In Chapter 4

capture problem proposed by Conway, et al. [5] but with the additional degree of freedom that the joint is moveable and controllable on the surface of the OMV.

To limit the complexity of the capture problem, the following assumptions are made:

1. Joint motion does not change the mass properties of the OMV.
2. All controls are continuous.
3. The target satellite is passive during capture.
4. Absolute motion of the OMV is controlled by thrusters on the OMV which do not change the mass properties of the OMV by their operation.
5. Space environmental effects (gravity gradient, solar torque, etc.) are ignored.

Solving this capture problem first requires the equations of attitude motion of the two-body system to be developed including the effects of joint motion. An Eulerian derivation is again desired because the control forces and torques appear explicitly. However, the general n-body equations given by Hooker and Margulies [6] and Hooker [7] cannot be applied directly because their derivation does not permit connecting joints to translate relative to the bodies they connect. Consequently, their derivation must be modified to account for joint translation, which is the subject of Chapter 2 and a work by Conway and Widhalm [9].

of the OMV. The initial value of $\dot{\psi}$ is determined by the initial values of γ_1 and $\dot{\gamma}_2$ for steady spin and precession from Greenwood [8].

With the initial state of the system defined, the final state must be considered. Since the two-body system is to be returned to low-Earth orbit after capture, the capture process should terminate with no relative motion between the target and the OMV. The OMV \hat{e}_3 axis should also maintain a constant orientation in space with no further active control. This is possible with the configuration proposed by Conway, et al. [5]; but, since the joint position is fixed on the OMV, there is only one scheme available, that which completely annihilates the system angular momentum. The final γ_1 , however, is limited only by the physical constraints of the system. Unfortunately, the initial cone angle, γ_1 , may not be accurately known prior to rendezvous so that the joint may not be prepositioned. Also the joint position at the start of capture may not permit a suitable target orientation relative to the OMV for the return to low orbit. If, on the other hand, the joint could move on the surface of the OMV, these problems would be eliminated. Furthermore, if the joint were moved during capture to a position on the \hat{e}_3 axis, the final two-body configuration could be spin-stabilized. Therefore, the objective of this work is to solve the

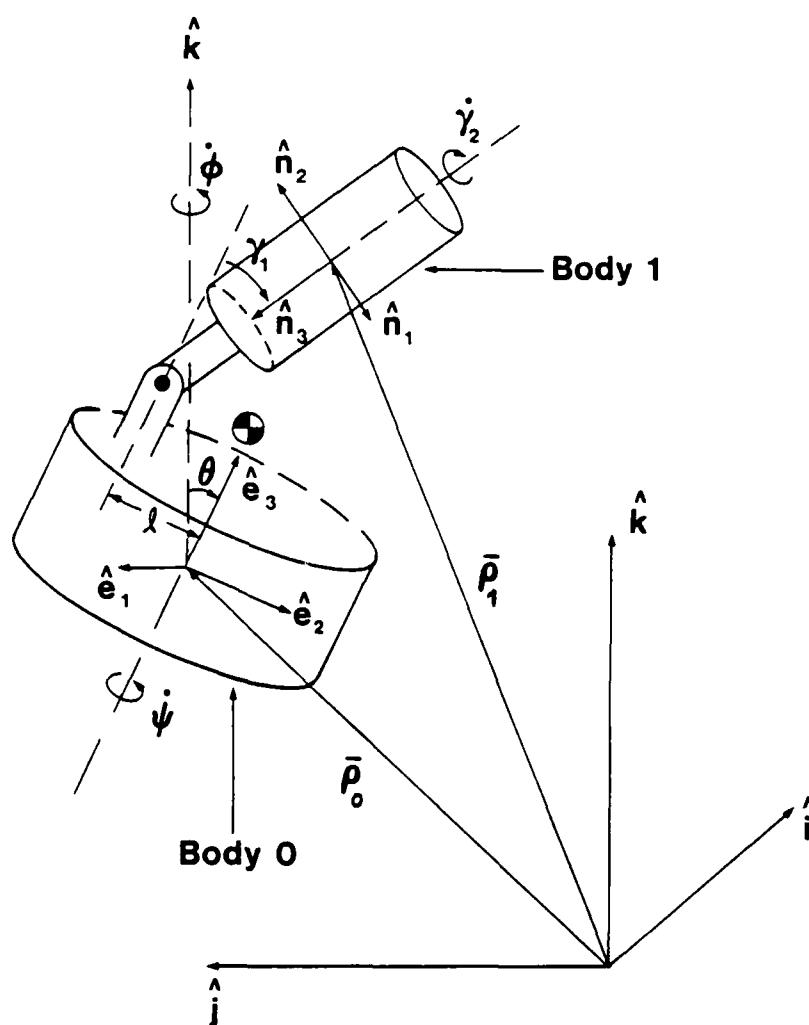
problem. Consequently, the objective here is to extend the work of Conway, et al. [5] by solving their capture problem for detumbling control histories.

1.3 The Present Approach

In extending the work of Conway, et al. [5], the capture problem they proposed is left unchanged. That is, the target satellite is to be captured from a state of steady spin and precession. The problem is particularly well posed because the docking of the OMV with the target at the joint on the OMV can be accomplished with no coupling effects between the two bodies. Consequently, the spin and precession rates of the target, as well as the spin rate of the OMV, are unchanged through the docking sequence.

To clarify the dynamic state of the two-body system after docking, reference is made to Figure 1 where the \hat{e} basis and the \hat{n} basis are fixed at the centers of mass of body 0 (OMV) and body 1 (target) respectively. The initial spin rate, $\dot{\psi}$, of the OMV is equal to the initial precession rate of the target. The initial angular momentum vectors of the OMV and the target lie on the \hat{e}_3 axis and have the same sign. The center of mass of the target is initially on the \hat{e}_3 axis. The joint position on the surface of the OMV is determined by the initial cone angle, γ_1 , and the distance in the \hat{n}_3 direction from the center of mass of the target to the surface

Figure 1. OMV-Target System



precession can be considered. As shown in Figure 1, the OMV (body 0) they propose is joined to the target (body 1) through a two degree of freedom ball and socket joint with a grappling device. An Eulerian derivation of the equations of motion of the two-body system is developed from the general n-body equations given by Hooker and Margulies [6] and Hooker [7]. System response to internal torques at the joint and external thruster torques on the OMV is analyzed by integrating the equations of motion with a set of Euler angle kinematical equations for the OMV. The output is used to drive a graphics computer display of the two-body system to show the resulting motion. Since the OMV is not considered absolutely stable, as in the previous work, the simple torque schemes applied do not yield a satisfactory capture method as evidenced by the propagation of the system orientation and angular rates. This was expected, and Conway, et al. [5] conclude that active control of internal and external torques is required for a satisfactory capture.

The problem of remote orbital capture is thus seen to have received only limited treatment. As suggested by Conway, et al. [5], a more realistic approach to the dynamics and control of the OMV-target system is essential. They clearly illustrated this point through a very specific capture problem, but they did not solve that

absolutely stable and ignored the problem of controlling the response of the OMV in applying torques to the target. Kaplan and Nadkarni [4] went farther by proposing an OMV with an articulating arm capable of four degrees of rotational freedom relative to the OMV. A grappling device on the arm was envisioned that could be driven to null its motion relative to the target for docking. The dynamic response of this system to internal torques was analyzed under two critical assumptions. First, articulating counter-masses were available to balance dynamically the mass of the articulating arm. Second, the mass of the OMV was large relative to that of the target. While simplifying the dynamic analysis, these assumptions result in an extremely massive OMV with a very complex control system for the articulating arm and counter-masses. With the hope of simplifying the OMV concept, Conway, et al. [5] continued this research with a new approach.

Conway, et al. [5] formulate a capture problem in which a 1000 Kg target spacecraft is to be retrieved from geosynchronous orbit to low-earth orbit. The OMV for this mission is assumed to use conventional propulsion and to be cylindrical in shape for transport in the cargo bay of the Space Shuttle. The target spacecraft is assumed to be symmetric about one axis so that the problem of capturing it from a torque-free steady state of spin and

of n rigid bodies. First, a reference body is selected and designated as body 0. The angular velocity of body 0 is $\bar{\omega}_0$ and has three components in a body 0 fixed frame. With the n -body system having r degrees of rotational freedom, the angular motions of the remaining $n-1$ bodies are described in terms of $\bar{\omega}_0$ and $r-3$ angular rates relative to body 0 about the gimbal axes at the joints. By summing equation (2.15) over all n bodies, three equations free of $\bar{T}_{\lambda j}^C$ result. The additional $r-3$ equations necessary are obtained by using the fact that the constraint torque at a joint is orthogonal to each of the gimbal axes at that joint. Therefore, equation (2.15) can be summed over all bodies to one side of a joint, j , to isolate $\bar{T}_{\lambda j}^C$ at that joint. Taking the scalar product of this sum with each of the gimbal axes, \hat{g}_i , of the joint yields equations equal in number to the degrees of freedom at the joint, all free of $\bar{T}_{\lambda j}^C$. Repeating this for all system joints yields $r-3$ equations free of constraint torques to complete the required set of r equations. Hooker [7] shows the result of this procedure applied to equation (2.8). When applied to equation (2.15), the result is

$$\begin{bmatrix} a_{00} & \bar{a}_{01} & \bar{a}_{02} & \dots & \bar{a}_{0,r-3} \\ \bar{a}_{10} \\ \vdots \\ \bar{a}_{r-3,0} \end{bmatrix} \begin{bmatrix} \dot{\bar{\omega}}_0 \\ \ddots \\ \ddot{\gamma}_1 \\ \ddots \\ \ddot{\gamma}_2 \\ \ddots \\ \ddot{\gamma}_{r-3} \end{bmatrix} = \quad (2.16)$$

$$\begin{aligned} & \sum_{\lambda} \bar{E}_{\lambda}^* - \sum_{\lambda} \sum_{\mu \neq \lambda} m_{\mu} \bar{\mathcal{L}}_{\lambda\mu} \times [\ddot{D}_{\lambda\mu}^R + 2\bar{\omega}_{\lambda} \times \dot{D}_{\lambda\mu}^R] + \sum_{\mu} \sum_{\lambda \neq \mu} \bar{D}_{\lambda\mu} \times m_{\mu} [\ddot{D}_{\mu\lambda}^R + 2\bar{\omega}_{\mu} \times \dot{D}_{\mu\lambda}^R] \\ & \hat{g}_1 \cdot \{ \sum_{\lambda} \epsilon_{1\lambda} \bar{E}_{\lambda}^* - \sum_{\lambda} \epsilon_{1\lambda} \sum_{\mu \neq \lambda} m_{\mu} \bar{\mathcal{L}}_{\lambda\mu} \times [\ddot{D}_{\lambda\mu}^R + 2\bar{\omega}_{\lambda} \times \dot{D}_{\lambda\mu}^R] \\ & + \sum_{\lambda} \epsilon_{1\lambda} \sum_{\mu \neq \lambda} \bar{D}_{\lambda\mu} \times m_{\mu} [\ddot{D}_{\mu\lambda}^R + 2\bar{\omega}_{\mu} \times \dot{D}_{\mu\lambda}^R] \} \\ & \vdots \\ & \hat{g}_{r-3} \cdot \{ \sum_{\lambda} \epsilon_{r-3,\lambda} \bar{E}_{\lambda}^* - \sum_{\lambda} \epsilon_{r-3,\lambda} \sum_{\mu \neq \lambda} m_{\mu} \bar{\mathcal{L}}_{\lambda\mu} \times [\ddot{D}_{\lambda\mu}^R + 2\bar{\omega}_{\lambda} \times \dot{D}_{\lambda\mu}^R] \\ & + \sum_{\lambda} \epsilon_{r-3,\lambda} \sum_{\mu \neq \lambda} \bar{D}_{\lambda\mu} \times m_{\mu} [\ddot{D}_{\mu\lambda}^R + 2\bar{\omega}_{\mu} \times \dot{D}_{\mu\lambda}^R] \} \end{aligned}$$

where

$$a_{00} = \sum_{\lambda} \sum_{\mu} \phi_{\lambda\mu}, \text{ a dyadic,} \quad (2.17)$$

$$\bar{a}_{0k} = \sum_{\lambda} \sum_{\mu} \epsilon_{k\mu} \phi_{\lambda\mu} \cdot \hat{g}_k, \text{ a vector,} \quad (2.18)$$

$$\bar{a}_{i0} = \hat{g}_i \cdot \sum_{\lambda} \sum_{\mu} \epsilon_{i\lambda} \phi_{\lambda\mu}, \text{ a vector,} \quad (2.19)$$

$$a_{ik} = \hat{g}_i \cdot \sum_{\lambda} \sum_{\mu} \epsilon_{i\lambda} \epsilon_{k\mu} \phi_{\lambda\mu} \cdot \hat{g}_k, \text{ a scalar,} \quad (2.20)$$

$$\bar{E}_{\lambda}^* = \bar{E}_{\lambda} - \sum_{\mu} \phi_{\lambda\mu} \cdot \sum_k \epsilon_{k\mu} \dot{\gamma}_k \hat{g}_k, \quad (2.21)$$

$$\text{and } \epsilon_{i\mu} = \begin{cases} 1, & \text{if } \hat{g}_i \text{ belongs to a joint anywhere} \\ & \text{on the chain of bodies connecting} \\ & \text{body } \mu \text{ and the reference body.} \\ 0, & \text{otherwise (e.g. } \mu = 0 \text{).} \end{cases} \quad (2.22)$$

Equation (2.16) is a second order matrix differential equation. To propagate system orientation with respect to an external frame, r additional first order differential equations are required. Three of these are usually Euler angle rate equations, and the remaining $r-3$ equations are

$$\frac{d}{dt} \gamma_i = \dot{\gamma}_i. \quad (2.23)$$

Joint motions with respect to the bodies they connect must also be specified in terms of $\dot{\mathcal{L}}_{\lambda\mu}^R$ and $\ddot{\mathcal{L}}_{\lambda\mu}^R$. Then equation (2.5) is twice differentiated to compute $\ddot{D}_{\lambda\mu}^R$ and $\ddot{D}_{\lambda\mu}^R$ required for equation (2.16). The same is required where $\dot{\mathcal{L}}_{\mu\lambda}^R$ and $\ddot{\mathcal{L}}_{\mu\lambda}^R$ are considered.

2.4 Two-Body Equations for the Capture Problem

Specializing equation (2.16) to the two-body system of the capture problem is straightforward and is presented in detail here as an example of the Hooker [7] procedure applied to equation (2.15). Referring back to Figure 1, the OMV is body 0 and the target satellite is body 1. The two-degree-of-freedom joint allows rotations γ_1 about gimbal axis \hat{g}_1 , a unit vector in the \hat{e}_1 direction, and γ_2

about gimbal axis \hat{g}_2 , a unit vector in the \hat{n}_3 direction.

The angular velocities of the two bodies are written as

$$\bar{\omega}_0 = \omega_{01} \hat{e}_1 + \omega_{02} \hat{e}_2 + \omega_{03} \hat{e}_3 \quad (2.24)$$

and

$$\bar{\omega}_1 = \bar{\omega}_0 - \dot{\gamma}_1 \hat{g}_1 + \dot{\gamma}_2 \hat{g}_2. \quad (2.25)$$

Equation (2.15) for body 0 is

$$\begin{aligned} \phi_{00} \cdot \dot{\bar{\omega}}_0 + \phi_{01} \cdot \dot{\bar{\omega}}_1 &= \bar{E}_0 + \bar{T}_{01}^C \\ &- m_1 \bar{x}_{01} \times (\ddot{\bar{D}}_{01}^R + 2\bar{\omega}_0 \times \dot{\bar{D}}_{01}^R) \end{aligned} \quad (2.26)$$

and for body 1 is

$$\begin{aligned} \phi_{10} \cdot \dot{\bar{\omega}}_0 + \phi_{11} \cdot \dot{\bar{\omega}}_1 &= \bar{E}_1 + \bar{T}_{11}^C \\ &+ \bar{D}_{10} \times m(\ddot{\bar{D}}_{01}^R + 2\bar{\omega}_0 \times \dot{\bar{D}}_{01}^R). \end{aligned} \quad (2.27)$$

Summing equations (2.26) and (2.27) eliminates the constraint torques since $\bar{T}_{01}^C = -\bar{T}_{11}^C$, so the result is

$$\begin{aligned} (\phi_{00} + \phi_{10}) \cdot \dot{\bar{\omega}}_0 + (\phi_{01} + \phi_{11}) \cdot \dot{\bar{\omega}}_1 &= \\ \bar{E}_0 + \bar{E}_1 - m_1 \bar{x}_{01} \times (\ddot{\bar{D}}_{01}^R + 2\bar{\omega}_0 \times \dot{\bar{D}}_{01}^R) \\ + \bar{D}_{10} \times m(\ddot{\bar{D}}_{01}^R + 2\bar{\omega}_0 \times \dot{\bar{D}}_{01}^R). \end{aligned} \quad (2.28)$$

Equation (2.25) must be differentiated with respect to

time and substituted into equation (2.28), so

$$\dot{\bar{\omega}}_1 = \dot{\bar{\omega}}_0 - \ddot{\gamma}_1 \hat{g}_1 - \dot{\gamma}_1 \dot{\hat{g}}_1 + \ddot{\gamma}_2 \hat{g}_2 + \dot{\gamma}_2 \dot{\hat{g}}_2 . \quad (2.29)$$

Substituting into equation (2.28) yields

$$\begin{aligned} & (\phi_{00} + \phi_{01} + \phi_{10} + \phi_{11}) \cdot \dot{\bar{\omega}}_0 + (\phi_{01} + \phi_{11}) \cdot (-\ddot{\gamma}_1 \hat{g}_1 + \ddot{\gamma}_2 \hat{g}_2) = \\ & \bar{E}_0 + \bar{E}_1 - (\phi_{01} + \phi_{11}) \cdot (-\dot{\gamma}_1 \dot{\hat{g}}_1 + \dot{\gamma}_2 \dot{\hat{g}}_2) \\ & - m_1 \bar{\mathcal{L}}_{01} \times (\ddot{\bar{D}}_{01}^R + 2\bar{\omega}_0 \times \dot{\bar{D}}_{01}^R) \\ & + \bar{D}_{10} \times m(\ddot{\bar{D}}_{01}^R + 2\bar{\omega}_0 \times \dot{\bar{D}}_{01}^R) . \end{aligned} \quad (2.30)$$

Applying equations (2.17), (2.18), (2.21), and (2.22) to equation (2.30) yields

$$a_{00} = \phi_{00} + \phi_{01} + \phi_{10} + \phi_{11} \quad , \quad 3 \times 3, \quad (2.31)$$

$$\bar{a}_{01} = (\phi_{01} + \phi_{11}) \cdot \hat{g}_1 \quad , \quad 3 \times 1, \quad (2.32)$$

$$\bar{a}_{02} = (\phi_{01} + \phi_{11}) \cdot \hat{g}_2 \quad , \quad 3 \times 1, \quad (2.33)$$

$$\bar{E}_0^* = \bar{E}_0 - \phi_{01} \cdot (-\dot{\gamma}_1 \dot{\hat{g}}_1 + \dot{\gamma}_2 \dot{\hat{g}}_2) , \quad (2.34)$$

$$\text{and} \quad \bar{E}_1^* = \bar{E}_1 - \phi_{11} \cdot (-\dot{\gamma}_1 \dot{\hat{g}}_1 + \dot{\gamma}_2 \dot{\hat{g}}_2) . \quad (2.35)$$

At this point equation (2.30) with equations (2.31) through (2.35) gives three of the five equations required to describe the motion of the two-body system. The other two equations are obtained from equation (2.27) by using

the fact that \bar{T}_{11}^C is orthogonal to both \hat{g}_1 and \hat{g}_2 . Taking the scalar product of \hat{g}_1 and \hat{g}_2 with equation (2.27) after substituting for $\dot{\omega}_1$ yields

$$\begin{aligned} & \hat{g}_1 \cdot [(\phi_{10} + \phi_{11}) \cdot \dot{\omega}_0 + \phi_{11} \cdot (-\ddot{\gamma}_1 \hat{g}_1 + \ddot{\gamma}_2 \hat{g}_2) \\ & - \bar{E}_1^* - \bar{D}_{10} \times m(\ddot{D}_{01}^R + 2\bar{\omega}_0 \times \dot{D}_{01}^R)] = 0 \end{aligned} \quad (2.36)$$

and

$$\begin{aligned} & \hat{g}_2 \cdot [(\phi_{10} + \phi_{11}) \cdot \dot{\omega}_0 + \phi_{11} \cdot (-\ddot{\gamma}_1 \hat{g}_1 + \ddot{\gamma}_2 \hat{g}_2) \\ & - \bar{E}_1^* - \bar{D}_{10} \times m(\ddot{D}_{01}^R + 2\bar{\omega}_0 \times \dot{D}_{01}^R)] = 0 \end{aligned} \quad (2.37)$$

Applying equations (2.19), (2.20), and (2.22) yields the following terms which appear in equations (2.36) and (2.37):

$$\bar{a}_{10} = \hat{g}_1 \cdot (\phi_{10} + \phi_{11}) , \quad 1 \times 3, \quad (2.38)$$

$$\bar{a}_{20} = \hat{g}_2 \cdot (\phi_{10} + \phi_{11}) , \quad 1 \times 3, \quad (2.39)$$

$$a_{11} = \hat{g}_1 \cdot \phi_{11} \cdot \hat{g}_1 , \quad (2.40)$$

$$a_{12} = \hat{g}_1 \cdot \phi_{11} \cdot \hat{g}_2 , \quad (2.41)$$

$$a_{21} = \hat{g}_2 \cdot \phi_{11} \cdot \hat{g}_1 , \quad (2.42)$$

$$\text{and} \quad a_{22} = \hat{g}_2 \cdot \phi_{11} \cdot \hat{g}_2 . \quad (2.43)$$

All that remains is to rewrite equations (2.30), (2.36) and (2.37) in matrix form, which finally gives

$$\begin{bmatrix} a_{00} & \bar{a}_{01} & \bar{a}_{02} \\ \bar{a}_{10} & a_{11} & a_{12} \\ \bar{a}_{20} & a_{21} & a_{22} \end{bmatrix} \begin{bmatrix} \dot{\omega}_{01} \\ \dot{\omega}_{02} \\ \dot{\omega}_{03} \\ -\ddot{\gamma}_1 \\ \ddot{\gamma}_2 \end{bmatrix} = \begin{bmatrix} \bar{E}_0^* + \bar{E}_1^* - m_1 \bar{L}_{01} \times (\ddot{D}_{01}^R + 2\bar{\omega}_0 \times \dot{D}_{01}^R) \\ + \bar{D}_{10} \times m (\ddot{D}_{01}^R + 2\bar{\omega}_0 \times \dot{D}_{01}^R) \\ \hat{g}_1 \cdot [\bar{E}_1^* + \bar{D}_{10} \times m (\ddot{D}_{01}^R + 2\bar{\omega}_0 \times \dot{D}_{01}^R)] \\ \hat{g}_2 \cdot [\bar{E}_1^* + \bar{D}_{10} \times m (\ddot{D}_{01}^R + 2\bar{\omega}_0 \times \dot{D}_{01}^R)] \end{bmatrix}, \quad (2.44)$$

the matrix differential equation for the motion of the two-body system in the capture problem with the joint moveable on body 0.

As previously mentioned, the above derivation yields a method to determine the constraint torque on the joint. Equation (2.27) can be rewritten as

$$\begin{aligned} \bar{T}_{11}^C = & \phi_{10} \cdot \dot{\omega}_0 + \phi_{11} \cdot \dot{\omega}_1 - \bar{E}_1 \\ & - \bar{D}_{10} \times m (\ddot{D}_{01}^R + 2\bar{\omega}_0 \times \dot{D}_{01}^R). \end{aligned} \quad (2.45)$$

All quantities on the right hand side of equation (2.45) are known by way of the integration of equation (2.44) and the five kinematical equations. Therefore, the constraint torque can be calculated directly from equation (2.45) in the process of propagating the system motion through numerical integration as Hooker [7] has shown.

2.5 Joint Constraint Force Equation

The constraint force on the joint in the capture problem is calculated by a method similar to that for the constraint torque in that Newton's equation for body 0 or

body 1 is used in conjunction with equation (2.44) and the kinematic equations. Rewriting Newton's equation in terms of the variables in the capture problem is helpful however. Since gravitational effects are to be ignored, equation (2.1) can be written for body 0 as

$$\bar{F}'_0 + \bar{F}^H_{01} = m_0 \ddot{\bar{r}}_0, \quad (2.46)$$

where \bar{r}_0 is the vector from the system center of mass to the center of mass of body 0. From the definition of the center of mass given by Greenwood [8],

$$\bar{r}_0 = \frac{m_1}{m} (\bar{\mathcal{L}}_{10} - \bar{\mathcal{L}}_{01}) = \frac{m_1}{m} \bar{\mathcal{L}}. \quad (2.47)$$

Then

$$\begin{aligned} \ddot{\bar{r}}_0 = \frac{m_1}{m} (\ddot{\bar{\mathcal{L}}}^R + 2\bar{\omega}_0 \times \dot{\bar{\mathcal{L}}}^R + \dot{\bar{\omega}}_0 \times \bar{\mathcal{L}} \\ + \bar{\omega}_0 \times (\bar{\omega}_0 \times \bar{\mathcal{L}})), \end{aligned} \quad (2.48)$$

where $\bar{\mathcal{L}}$ is written in and differentiated in the \hat{e} basis.

Substituting back into equation (2.46) yields

$$\begin{aligned} \bar{F}^H_{01} = -\bar{F}'_0 + \frac{m_0 m_1}{m} (\ddot{\bar{\mathcal{L}}}^R + 2\bar{\omega}_0 \times \dot{\bar{\mathcal{L}}}^R + \dot{\bar{\omega}}_0 \times \bar{\mathcal{L}} \\ + \bar{\omega}_0 \times (\bar{\omega}_0 \times \bar{\mathcal{L}})), \end{aligned} \quad (2.49)$$

which can be solved for \bar{F}^H_{01} since all required quantities are available from equation (2.44) and the kinematic equations.

The component of the constraint force, \bar{F}_{01}^H , in the direction of joint motion is the force required to move the joint. However, equation (2.49) confirms that the joint motion, contained in $\bar{\mathcal{Z}}$ and its time derivatives, is not simply forced by \bar{F}_{01}^H and \bar{F}_0' . The joint acceleration is also a function of the time derivatives of the angular rates. Furthermore, from equation (2.44) the time derivatives of the angular rates are functions of the joint acceleration. Consequently, the joint motion must be specified to propagate the system attitude motion.

2.6 Equation Verification

The equations derived in the previous two sections were checked against the known results of various test cases. Equation (2.44), the two-body system attitude equation, was verified first by two cases in which the right hand side was known to be zero: first, the post-docking configuration of the capture problem with no control forces or torques acting and the joint position fixed and second, the final spin-stabilized configuration after capture with no control forces or torques and the joint position fixed on the \hat{e}_3 axis. In these same two cases the constraint torque and force on the joint were also known to be zero, so equation (2.45) for the constraint torque and equation (2.49) for the constraint force could also be verified. Equation (2.44) was further verified by numerical integration from several initial conditions and with either no

control forces and torques acting or with only internal control torques acting. In all of these cases system angular momentum about the system center of mass must be conserved, which was observed in the computer results.

The angular momentum calculated above had to account for joint motion specified in each case. The expression used for that calculation is derived here from first principles. Designating \bar{H}_{cm} as the system angular momentum about the system center of mass and writing both inertia dyadics and all vectors in the \hat{e} basis, the definition of system angular momentum from Greenwood [8] is applied, giving

$$\bar{H}_{cm} = \phi_0 \bar{\omega}_0 + \phi_1 \bar{\omega}_1 + \bar{r}_0 \times m_0 \dot{\bar{r}}_0 + \bar{r}_1 \times m_1 \dot{\bar{r}}_1. \quad (2.50)$$

\bar{r}_0 was previously defined by equation (2.47) as the vector from the system center of mass to the center of mass of body 0. \bar{r}_1 is similarly defined for body 1 as

$$\bar{r}_1 = -\frac{m_0}{m} (\bar{\mathcal{L}}_{10} - \bar{\mathcal{L}}_{01}) = -\frac{m_0}{m} \bar{\mathcal{L}}. \quad (2.51)$$

Substituting equations (2.47) and (2.51) into equation (2.50) and combining terms gives

$$\begin{aligned} \bar{H}_{cm} = & \phi_0 \bar{\omega}_0 + \phi_1 \bar{\omega}_1 \\ & + (\bar{\mathcal{L}}_{10} - \bar{\mathcal{L}}_{01}) \times \frac{m_0 m_1}{m} (\dot{\bar{\mathcal{L}}}_{10} - \dot{\bar{\mathcal{L}}}_{01}). \end{aligned} \quad (2.52)$$

Since all vectors are written in the \hat{e} basis, $\dot{\bar{\mathcal{L}}}_{10}$ and $\dot{\bar{\mathcal{L}}}_{01}$

must be computed as

$$\dot{\bar{\mathcal{L}}}_{\lambda\mu} = \dot{\bar{\mathcal{L}}}_{\lambda\mu}^R + \bar{\omega}_0 \times \bar{\mathcal{L}}_{\lambda\mu} . \quad (2.53)$$

$\dot{\bar{\mathcal{L}}}_{01}^R$ is not zero when the joint is moving relative to body 0.
 $\dot{\bar{\mathcal{L}}}_{10}^R$ is independent of joint motion but does depend on $\dot{\gamma}_1$.

2.7 Conclusion

By tracing the derivation of the equations of motion of a multi-body satellite given by Hooker and Margulies [6] and Hooker [7], the effects of their assumptions were found that restricted the application of their equations to configurations in which joints were fixed in position relative to the bodies they connect. The changes to their equations that account for joint motion were shown in equations (2.15) and (2.16). From these new equations was derived equation (2.44), which describes the attitude motion of the two-body system of Figure 1 with the joint moveable on the surface of the OMV (body 0). A method for computing the constraint torque and force on the joint from equations (2.44), (2.45), and (2.49) was also indicated. These results were checked by comparison with known motions from simple initial conditions.

CHAPTER 3

CAPTURE BY CONTINUOUS OPEN
LOOP OPTIMAL CONTROL

3.1 Introduction

In this chapter the methods of classical optimal control theory are used to derive control histories that detumble the target satellite. The optimal control problem is nonlinear and cannot be solved in closed form, so a numerical method is employed. The problem is structured to be compatible with the numerical method by considering only those cases in which the final absolute orientation of the OMV is unspecified. Results are obtained for a case in which the controls are free and for cases in which control constraints are applied. The results are compared and discussed to show that capture is possible with very reasonable control profiles and that the constraint loads on the joint cause no undue structural requirements or undue control requirements to move the joint during capture. Furthermore, the solutions are seen not to be diminished by leaving the final absolute orientation of the OMV unspecified.

3.2 The Optimal Control Problem

The capture problem, as an open loop optimal control problem, is to drive the OMV-target system from the

given initial state to the prescribed final state in a specified time interval while minimizing the integral performance index,

$$P.I. = \frac{1}{2} \int_{t_0}^{t_f} \left[\sum_{i=1}^n u_i^2 \right] dt . \quad (3.1)$$

The u_i 's represent the system controls, which must be defined. Since there are five rotational degrees of freedom in the two-body system, five controls are selected, an external thruster torque applied about each axis of the OMV and an internal torque applied about each of the two gimbal axes at the joint. No control variable is associated with joint translation because the velocity and acceleration profiles are precomputed to satisfy the desired final joint position.

Using fundamental optimal control theory, Bryson and Ho [11], the system dynamic and kinematic equations are adjoined as constraints to the integral performance index with Lagrange multipliers or costate variables. After defining the system Hamiltonian, the optimality conditions, by way of the Pontryagin principle, are applied, which transform the original minimization problem to an equivalent two-point-boundary-value-problem (TPBVP) in the state and costate variables. For the most general case of this capture problem there are 20 independent differential equations defining the TPBVP in terms of 10 each independent states and costates.

The capture problem here can be suitably cast for an algorithm recently developed by Pereyra [12], which solves the TPBVP directly. The Pontryagin principle can then be applied to the solution to solve for the five control histories. Therefore, the TPBVP is derived next to provide the inputs required by the algorithm.

3.3 The Two-Point-Boundary-Value-Problem (TPBVP)

To follow the procedure given above for deriving the TPBVP, a more compact form of equation (2.44) describing the system dynamics is desired. First, the 5 x 5 matrix on the left hand side of equation (2.44) is defined as the matrix A. Next, the five element vector on the right hand side of equation (2.44) is defined as \bar{F}^* . Finally, by letting

$$[\dot{\omega}_{01} \ \dot{\omega}_{02} \ \dot{\omega}_{03} \ -\ddot{\gamma}_1 \ \ddot{\gamma}_2] = [\dot{x}_1 \ \dot{x}_2 \ \dot{x}_3 \ -\dot{x}_4 \ \dot{x}_5] = \dot{\bar{x}} \quad (3.2)$$

equation (2.44) can be written as

$$A\dot{\bar{x}} = \bar{F}^* \quad (3.3)$$

However, reference to equations (2.11), (2.21), and (2.44), with the fact that the gimbal axes at the joint are orthogonal, shows that \bar{F}^* can be decomposed into a sum of two vectors, the control vector \bar{u} and a vector \bar{F} consisting of the remaining terms in \bar{F}^* . Therefore, equation (3.3) is written as

all but one of the elements were derived, and these were verified at a selected point in the state and costate space by using a numerical differentiation technique. Agreement to at least eight significant figures was always achieved. The complexity of the last partial derivative, $\partial \dot{\lambda}_6 / \partial \gamma_1$, and the accuracy achieved above led to using the numerical method for this one derivative to complete the Jacobian.

Turning now to the results of the three selected cases, Figures 2 through 7 summarize Case 1 in which all five controls are unconstrained. In referring to these figures and the others that follow note that

$$[\omega_{01} \ \omega_{02} \ \omega_{03} \ \dot{\gamma}_1 \ \dot{\gamma}_2 \ \gamma_1 \ u_1 \ u_2 \ u_3 \ u_4 \ u_5] =$$

$$[W1 \ W2 \ W3 \ G1D \ G2D \ G1 \ T1 \ T2 \ T3 \ TG1 \ TG2] \ .$$

The Case 1 solution was achieved with a grid of 87 points. The minimum value of the performance index was computed to be 2.335. Figure 2, showing the histories of the components of the OMV angular velocity, indicates that the OMV angular velocity vector remains very nearly aligned with the body fixed \hat{e}_3 axis during capture. Therefore, the OMV remains virtually in a state of pure spin about the \hat{e}_3 axis during capture, which confirms that specifying the final orientation of the OMV is not necessary. Consequently,

Of the two approaches offered by the algorithm to solve the TPBVP's, the manual method of solving a sequence of problems, varying the initial state of the system, was selected for its ease of programming. For the case of unconstrained controls, the sequence of initial conditions used is shown in Table 4, all of which represent free spin and precession of the target and pure spin of the OMV about the \hat{e}_3 axis. The solution grid for each problem was used as the initial estimate of the solution for the next problem. For the cases of constrained controls, the free control solution for the initial conditions of Table 3 was used as the initial solution estimate. To verify the computer code, a simple linear problem was solved first and checked against the analytical solution.

TABLE 4
Sequence of Initial Conditions

γ_1	$\dot{\gamma}_2$	ω_{03}
0.017 rad	-0.002 rad/sec	-0.019 rad/sec
0.087 rad	-0.004 rad/sec	-0.048 rad/sec
0.087 rad	-0.009 rad/sec	-0.096 rad/sec
0.175 rad	-0.009 rad/sec	-0.097 rad/sec
0.349 rad	-0.009 rad/sec	-0.102 rad/sec
(20°)	(-0.5°/sec)	(-5.8°/sec)

Since the Jacobian matrix is critical to the algorithm, some discussion of its derivation, coding, and verification is important. For the capture problem the Jacobian is a 12 x 12 matrix. Analytical expressions for

TABLE 2

System Mass Properties

	<u>Mass</u>	<u>I₁</u>	<u>I₂</u>	<u>I₃</u>
Target Spacecraft	1000 kg	1000 kg-m ²	1000 kg-m ²	1100 kg-m ²
OMV	4500 kg	6400 kg-m ²	6400 kg-m ²	11800 kg-m ²

TABLE 3

Initial Conditions

$$\omega_{01} = 0.0$$

$$\omega_{02} = 0.0$$

$$\omega_{03} = -0.102 \text{ rad/sec}$$

$$\dot{\gamma}_1 = 0.0$$

$$\dot{\gamma}_2 = -0.009 \text{ rad/sec}$$

$$\gamma_1 = 0.349 \text{ rad}$$

$$\bar{L}_{01} \cdot \hat{e}_1 = 0.0 \text{ meters}$$

$$\bar{L}_{01} \cdot \hat{e}_2 = -0.599 \text{ meters}$$

$$\bar{L}_{01} \cdot \hat{e}_3 = 0.62 \text{ meters}$$

} Joint Position

$$\dot{\bar{L}}_{01}^R = (0.002 \text{ meters/sec}) \hat{e}_2 \quad \text{Joint Velocity}$$

$$\ddot{\bar{L}}_{01}^R = 0.0 \text{ meters/sec}^2 \quad \text{Joint Acceleration}$$

$$\bar{L}_{10} = (1.75 \text{ meters}) \hat{n}_3$$

(3.28) and the control constraint is

$$u_4 - k_1 \gamma_1 - k_2 \dot{\gamma}_1 = 0. \quad (3.30)$$

Changes to two of the costate equations follow directly, and μ and the other four controls are found again from equation (3.14) written as

$$[u_1 \ u_2 \ u_3 \ u_4 \ u_5] + {}_1\bar{\lambda}_5^T A^{-1} + [0 \ 0 \ 0 \ \mu \ 0] = 0. \quad (3.31)$$

The Jacobian matrix is further changed from the previous case since $\dot{\lambda}_4$ and $\dot{\lambda}_6$ are functions of μ , and γ_1 and $\dot{\gamma}_1$ appear explicitly in the control driving the state equations of the reduced twelfth order system.

3.7 Results

Applying the algorithm described in section 3.5 to the TPBVP's for the case of unconstrained controls and the two cases of constrained controls produces the results presented here for a two-body system with the mass properties and initial conditions of Tables 2 and 3. The final time is chosen to be 300 seconds, and the joint translational velocity is chosen as the constant required to move the joint from its initial position to the \hat{e}_3 axis in that time. Solution accuracy is controlled by setting the relative error tolerance used by the algorithm to the desired level, 1.0×10^{-6} for all cases.

control constraints are adjoined to the performance index, equation (3.12), with Lagrange multipliers. The resulting Hamiltonian is

$$H = \frac{1}{2} \bar{u}^T \bar{u} + \bar{\lambda}^T \begin{bmatrix} A^{-1} \bar{F} + A^{-1} \bar{u} \\ x_4 \\ x_5 \end{bmatrix} + \bar{v}^T [C_1 \bar{u}] + \bar{\mu}^T [{}_1 \bar{u}_3 - {}_1 \bar{C}_3] , \quad (3.28)$$

where $\bar{\lambda}$ is a three element vector of Lagrange multipliers and \bar{C} is a three element vector of the constant thruster torques. The same necessary conditions apply; they are equations (3.14), (3.16), and (3.17). The TPBVP reduces to a system of 12 differential equations as before with the same costate differential equations. The state equations are driven by a different control vector from equation (3.14) given by

$$[C_1 \ C_2 \ C_3 \ u_4 \ u_5] + {}_1 \bar{v}_5^T A^{-1} + [\mu_1 \ \mu_2 \ \mu_3 \ 0 \ 0] = 0 , \quad (3.29)$$

which also determines \bar{v} . The Jacobian maxtrix is changed only in the quadrant, ${}_1 \dot{x}_6 / {}_1 \bar{v}_6$, since the costate equations are unchanged and the control constraints are not functions of the states.

For the case in which u_4 is represented as a torsional spring and damper, \bar{v} becomes a scalar in equation

The results of a successful run of the algorithm are in the form of a grid. The differential equations are discretized and solved at program selected points between t_0 and t_f , so the solution grid contains the converged values of the states and costates at those same points. The control histories can then be computed using equation (3.15). Equations (2.45) and (2.49) also can be applied over the grid to solve for the histories of the constraint torque and constraint force on the joint.

3.6 Capture With Control Constraints

To this point a method has been developed to find unconstrained, continuous, optimal, open loop controls that solve the capture problem. Implementing these controls is another matter, so the advantages of simplifying the control system by way of control constraints need to be considered against the resulting increase in the cost of capture. One realistic control constraint is to require the thruster torques about the axes of the \hat{e} basis to be constants during the capture. A second constraint might be to require the torque about gimbal axis 1 to be proportional to the angle, γ_1 , and the angular rate, $\dot{\gamma}_1$, representing a torsional spring and damper.

The method of adjoining these control constraints to the optimal control problem is described by Bryson and Ho [11]. In the case of constant thruster torques, the

$$J = \begin{bmatrix} \frac{\partial \dot{\bar{x}}_6}{\partial \bar{x}_6} & \frac{\partial \dot{\bar{x}}_6}{\partial \bar{\lambda}_6} \\ \frac{\partial \dot{\bar{\lambda}}_6}{\partial \bar{x}_6} & \frac{\partial \dot{\bar{\lambda}}_6}{\partial \bar{\lambda}_6} \end{bmatrix} \quad (3.27)$$

Computer storage requirements are manageable for a twelfth order system, and single precision computations are adequate since a relative error tolerance is used in the convergence test.

The algorithm offers two approaches to solving nonlinear problems. One approach is to attack the nonlinear problem directly. The other is a continuation method by which the boundary conditions and nonlinear terms in the differential equations are multiplied by a factor of ϵ . The algorithm advances ϵ from zero to one and solves a sequence of problems using the previous solution as the initial solution estimate for the new problem. With $\epsilon = 0$ the problem should be simple, linear if possible. With $\epsilon = 1$ the original problem should be recovered. If only the boundary conditions are parameterized, the continuation method is simply an automated version of the first method, which can be applied to a sequence of problems, each with different boundary conditions from the previous problem, using the previous solution as the initial estimate for the new problem.

TABLE 1
State Boundary Conditions

	t_o	t_f
ω_{01}	0.0	0.0
ω_{02}	0.0	0.0
ω_{03}	specified	free
$\dot{\gamma}_1$	0.0	0.0
$\dot{\gamma}_2$	specified	0.0
γ_1	specified	0.0

Allowing ω_{03} to be free at t_f requires that $\lambda_3(t_f)$ be zero, giving the twelfth boundary condition required to solve the TPBVP.

3.5 Solving the Reduced Order TPBVP

Having reduced the TPBVP to a nonlinear system of 12 independent differential equations, solution can be attempted by a discretization method. The algorithm to be employed is based on that developed by Pereyra [12]. Finite difference methods convert the differential equations into a higher order nonlinear system of algebraic-transcendental equations to be solved simultaneously using a Newton iteration. As inputs the algorithm requires the system of differential equations forming the TPBVP, the boundary conditions, and the nonsingular Jacobian matrix of equation (3.27), which is used in the Newton iteration.

the Hamiltonian, equations (3.12) and (3.13). Consequently, the equations for $\dot{\bar{\lambda}}$ also become independent of \bar{v} , $\bar{\beta}$, and Ω .

Leaving the final value of x_7 (γ_2) unspecified yields a similar result. The symmetry of the target makes the Hamiltonian independent of x_7 which gives

$$\dot{\lambda}_7 = 0 \quad (3.22)$$

and

$$\lambda_7 = \text{Constant} . \quad (3.23)$$

But $\lambda_7(t_f)$ is zero since $x_7(t_f)$ is free; therefore, $\lambda_7(t)$ is zero.

The TPBVP is now reduced to a system of 12 independent differential equations in six state and six costate variables, which is summarized as follows:

$$\dot{\bar{x}} = A^{-1}\bar{F} + A^{-1}\bar{u} , \quad (3.24)$$

$$\dot{\bar{x}}_6 = x_4 , \quad (3.25)$$

and

$${}_1\dot{\bar{\lambda}}_6 = - {}_1\bar{\lambda}_6^T \begin{bmatrix} A^{-1}\bar{F} + A^{-1}\bar{u} \\ x_4 \quad {}_1\bar{x}_6 \end{bmatrix} , \quad (3.26)$$

where equation (3.15) is used to substitute for \bar{u} after the indicated partial differentiation is performed. The state boundary conditions to be considered are summarized in Table 1.

further complicating factors. The special numerical treatment required of these two equations outlined by Junkins and Turner [13] means that this capture problem is not well posed for conventional numerical methods for solving TPBVP's. In particular, the constant in equation (3.21) is unknown. Furthermore, the two dependent equations in the system of 22 equations of the TPBVP cause the Jacobian matrix of the system to be singular. But a nonsingular Jacobian is required for the Newton iteration used by advanced shooting methods and discretization methods for solving TPBVP's. Therefore, a simplification is sought to reduce the dimension of the problem and eliminate the two dependent equations from the TPBVP.

3.4 The Reduced Order TPBVP

The general TPBVP can be reduced to a system of 12 independent differential equations by selecting the boundary conditions at the final time so that the equations for $\bar{\beta}$ and \bar{v} , as well as those for x_7 and its associated costate, λ_7 , can be ignored. Noting that the equations for $\dot{\bar{x}}$ are independent of $\bar{\beta}$ suggests leaving $\bar{\beta}$ unspecified at t_f , equivalent to leaving the final orientation of the OMV unspecified. Doing so effectively ignores the kinematics of the OMV, so the associated equations and the vector \bar{v} can be removed from the augmented performance index and

TPBVP. Junkins and Turner [13] point out, though, that equations (3.8) and (3.20) are equivalent and write

$$\sum_{i=1}^4 v_i^2 = \text{Constant}. \quad (3.21)$$

Therefore, as with \bar{p} , only three of the equations for \bar{v} are independent, so there are in fact only 20 independent equations in the TPBVP.

Twenty boundary conditions are required to solve the TPBVP with two others determined from equations (3.11) and (3.21). The 11 state variables are generally specified at the initial time, t_0 , and some or all of them specified at the final time, t_f . For those state variables unspecified at t_f , their associated costate variables must be zero at t_f , except for \bar{v} which must satisfy equation (3.21) as shown by Vadali, et al. [14], since the performance index is not a function of the final state.

Solving this TPBVP numerically is a very formidable task. While Junkins and Turner [13] have treated the optimal control of a rigid body with 12 independent equations forming the TPBVP, moving forward to treat systems of rigid bodies is not a trivial step. Even with a two-body system, the state equations are much more complex, and the costate equations become equally so. The dimensionality increase has obvious impacts on computer storage requirements, and the two dependent equations in the TPBVP are

$$\bar{u}^T = -[\bar{\lambda}_5^T] A^{-1}, \quad (3.15)$$

meaning that the control vector, \bar{u} , is a function of the matrix, A , and the first five elements of the vector, $\bar{\lambda}$.

Further conditions require that

$$\dot{\bar{\lambda}}^T = [\dot{\lambda}_1, \dot{\lambda}_2, \dot{\lambda}_3, -\dot{\lambda}_4, \dot{\lambda}_5, \dot{\lambda}_6, \dot{\lambda}_7] = -H_x \quad (3.16)$$

and

$$\dot{\bar{v}}^T = -H_{\beta} \quad (3.17)$$

Therefore,

$$\dot{\bar{\lambda}}^T = -\bar{\lambda}^T \begin{bmatrix} A^{-1}\bar{F} + A^{-1}\bar{u} \\ x_4 \\ x_5 \end{bmatrix}_{1\bar{x}_7} - \bar{v}^T [\Omega \quad \bar{\beta}]_{1\bar{x}_7}, \quad (3.18)$$

and

$$\dot{\bar{v}}^T = -\bar{v}^T \Omega, \quad (3.19)$$

or

$$\dot{\bar{v}} = \Omega \bar{v} \quad (3.20)$$

since Ω is skew symmetric. Substituting for \bar{u} from equation (3.15) in the state equations (3.5), (3.6), (3.7), and (3.8) and in the costate equations (3.18) and (3.20) gives the nonlinear system of 22 ordinary, first-order, differential equations in the states and costates that form the

However, as Junkins and Turner [13] point out, only three of the Euler parameter equations are independent since $\bar{\beta}$ is constrained by the equation

$$\sum_{i=0}^3 \bar{\beta}_i^2 = 1 . \quad (3.11)$$

The TPBVP can now be derived by first writing the augmented performance index,

$$\begin{aligned} \text{P.I.} = \int_{t_0}^{t_f} \left\{ \frac{1}{2} \bar{u}^T \bar{u} + \bar{\lambda}^T \begin{bmatrix} A^{-1} \bar{F} + A^{-1} \bar{u} - \dot{\bar{x}} \\ x_4 - \dot{x}_6 \\ x_5 - \dot{x}_7 \end{bmatrix} \right. \\ \left. + \bar{v}^T [\Omega \bar{\beta} - \dot{\bar{\beta}}] \right\} dt , \end{aligned} \quad (3.12)$$

where $\bar{\lambda}$ and \bar{v} are seven and four element (costate) vectors respectively. Next, the Hamiltonian, H , is extracted from equation (3.12) and is written as

$$H = \frac{1}{2} \bar{u}^T \bar{u} + \bar{\lambda}^T \begin{bmatrix} A^{-1} \bar{F} + A^{-1} \bar{u} \\ x_4 \\ x_5 \end{bmatrix} + \bar{v}^T [\Omega \bar{\beta}] . \quad (3.13)$$

Applying the Pontryagin principle,

$$H_u = 0 , \quad (3.14)$$

gives the optimal control as

$$A\dot{\bar{x}} = \bar{F} + \bar{u} \quad (3.4)$$

or equivalently as

$$\dot{\bar{x}} = A^{-1}\bar{F} + A^{-1}\bar{u} , \quad (3.5)$$

where the existence of A^{-1} is guaranteed in this case.

A set of kinematic equations to determine the orientation of the two-body system relative to the fixed $\hat{i}, \hat{j}, \hat{k}$ reference frame in Figure 1 is also required. The orientation of the target with respect to the OMV is given by integrating

$$\dot{\gamma}_1 = \dot{x}_6 = x_4 \quad (3.6)$$

and

$$\dot{\gamma}_2 = \dot{x}_7 = x_5 . \quad (3.7)$$

The Euler parameters are used to determine the orientation of the OMV. In the notation of Junkins and Turner [13], the Euler parameter variational equations are

$$\dot{\bar{\beta}} = \Omega \bar{\beta} , \quad (3.8)$$

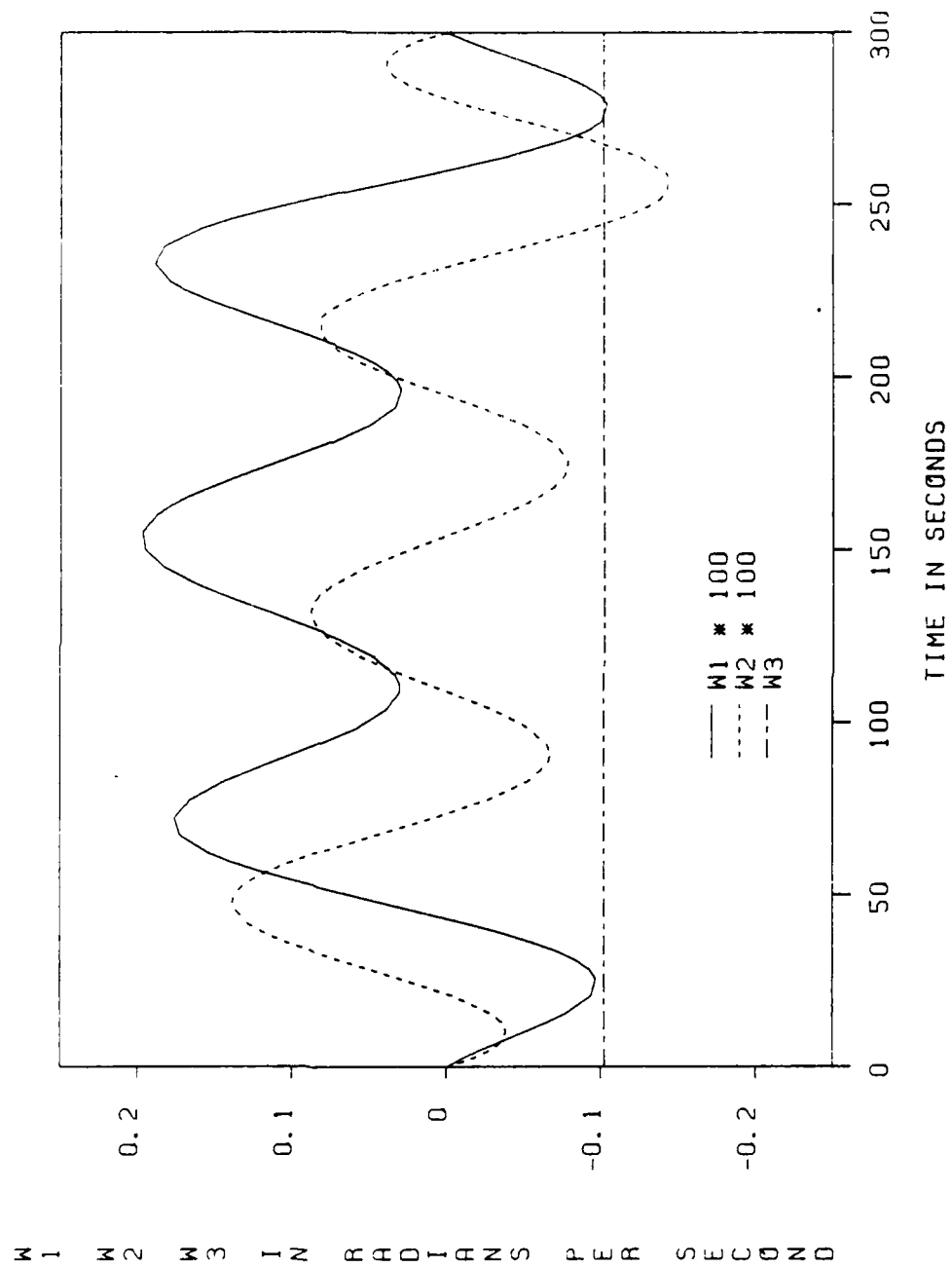
where

$$\bar{\beta}^T = [\beta_0 \ \beta_1 \ \beta_2 \ \beta_3] \quad (3.9)$$

and

$$\Omega = \frac{1}{2} \begin{bmatrix} 0 & -x_1 & -x_2 & -x_3 \\ x_1 & 0 & x_3 & -x_2 \\ x_2 & -x_3 & 0 & x_1 \\ x_3 & x_2 & -x_1 & 0 \end{bmatrix} . \quad (3.10)$$

Figure 2. Body 0 Angular Rate Histories (Case 1)



reducing the TPBVP from a system of 20 differential equations to 12 is clearly justified. The very nearly constant behavior of ω_{03} in Figure 2 is the result of scaling. Small fluctuations in ω_{03} can be seen in the actual output, and at 300 seconds ω_{03} is -0.101 rad/sec. Figure 3 shows the smooth behavior of γ_1 and $\dot{\gamma}_2$ in decreasing from their initial values to zero at 300 seconds. Figure 4 shows that $\dot{\gamma}_1$ remains very small during capture and, along with Figure 2, suggests that optimal capture should be a quite benign process. Figures 5 and 6, showing the external and internal control torques, are encouraging in that the magnitudes of all controls appear not to impose excessive requirements on the control system or to require much longer time intervals for capture. In Figure 7 FC is the magnitude of the joint constraint force on the OMV, and TC is the dot product of the joint constraint torque on the OMV with the constraint axis, which forms a dextral set with \hat{g}_1 and \hat{g}_2 . Figure 7 indicates that the constraint loads at the joint should not require a prohibitively massive or stiff structure to link the OMV and target. Also in Figure 7 the component of FC in the \hat{e}_2 direction, F2, is the force required to maintain the constant joint velocity during capture and also appears to pose no excessive control requirement.

Case 2 considers the external torques on the OMV, T_1 , T_2 , and T_3 , to be constant during capture. Their

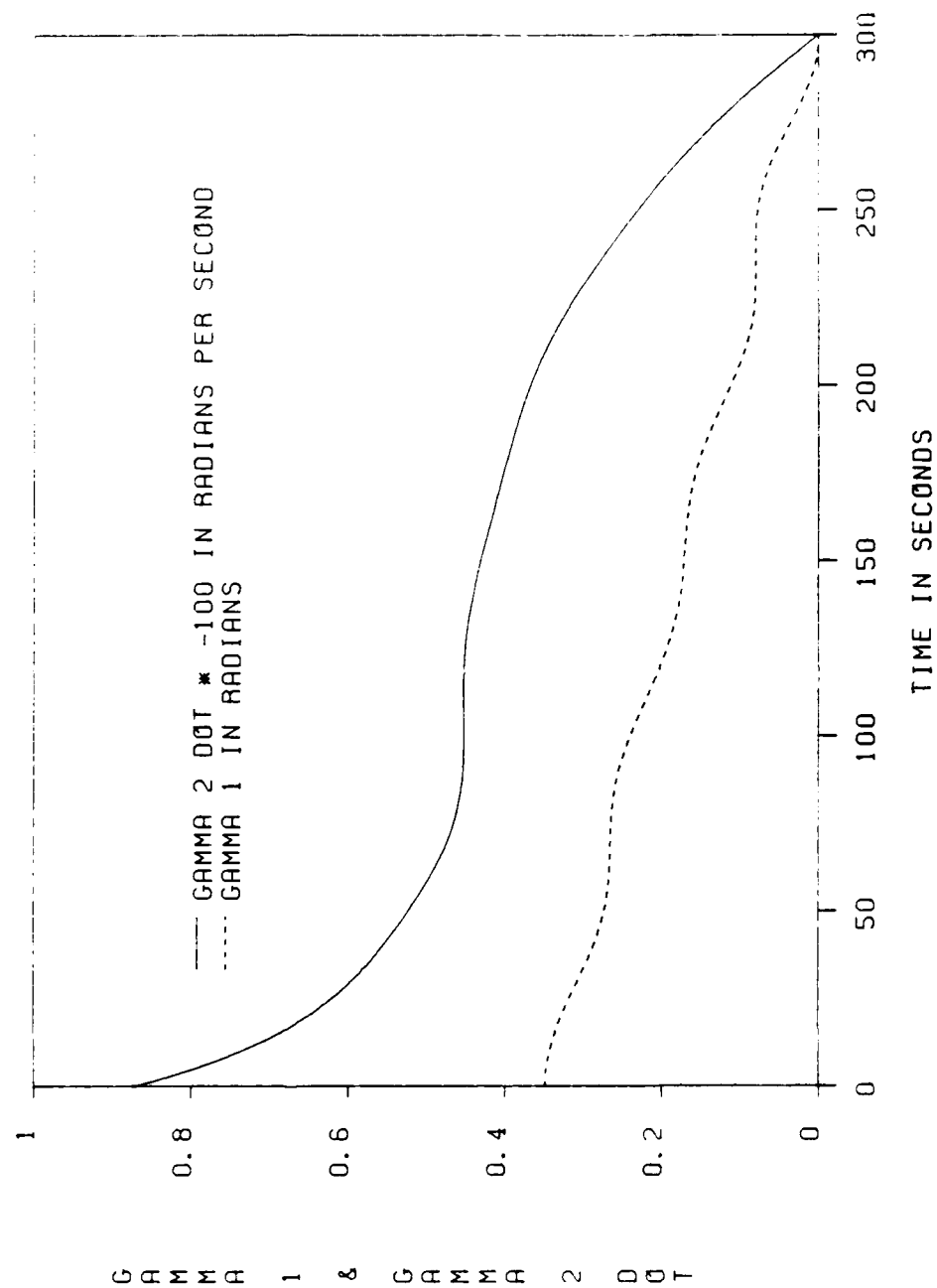
Figure 3. Body 1 γ_1 and $\dot{\gamma}_2$ Histories (Case 1)

Figure 4. Body 1 $\dot{\gamma}_1$ History (Case 1)

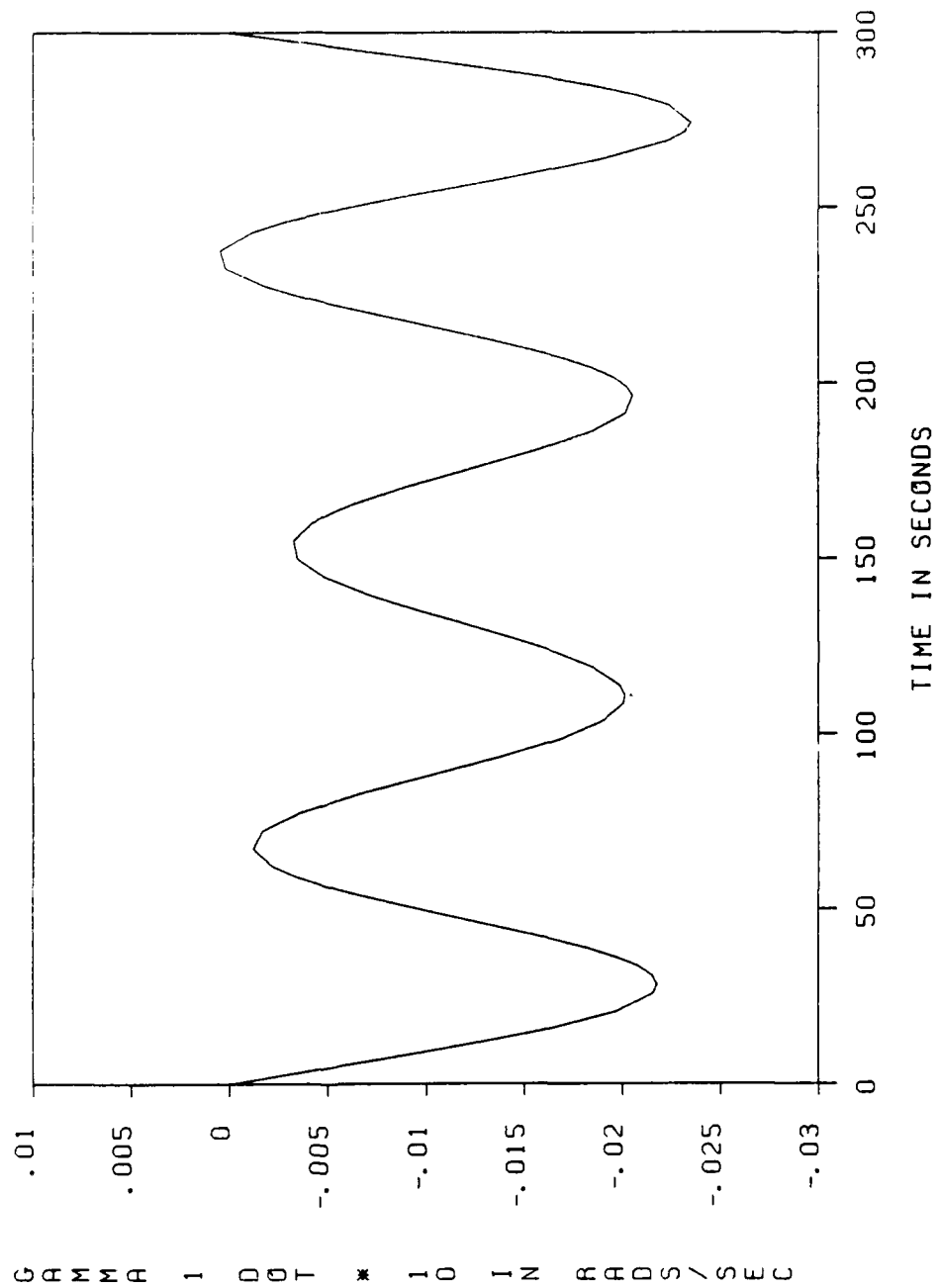


Figure 5. External Torque Histories (Case 1)

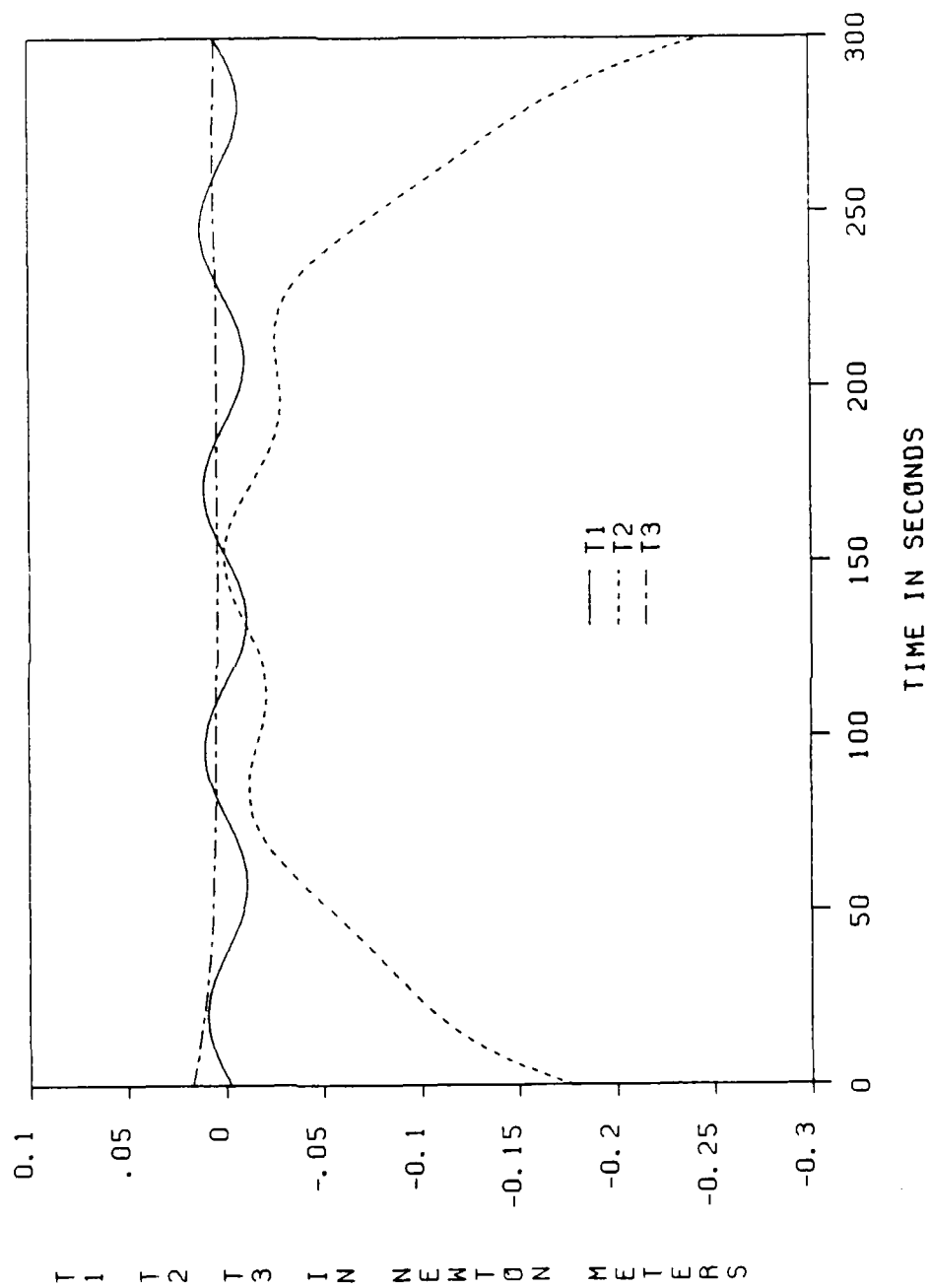


Figure 6. Internal Torque Histories (Case 1)

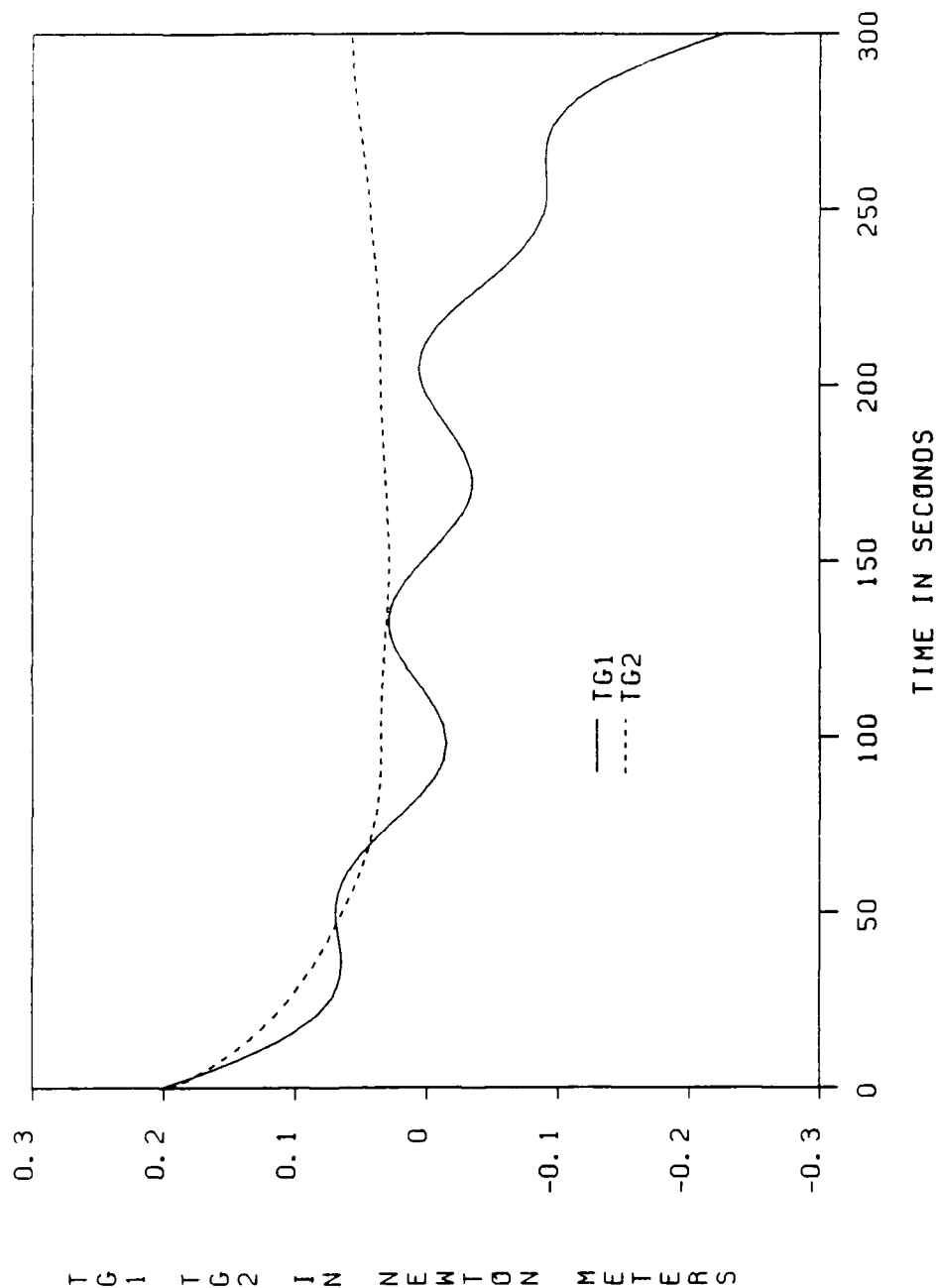
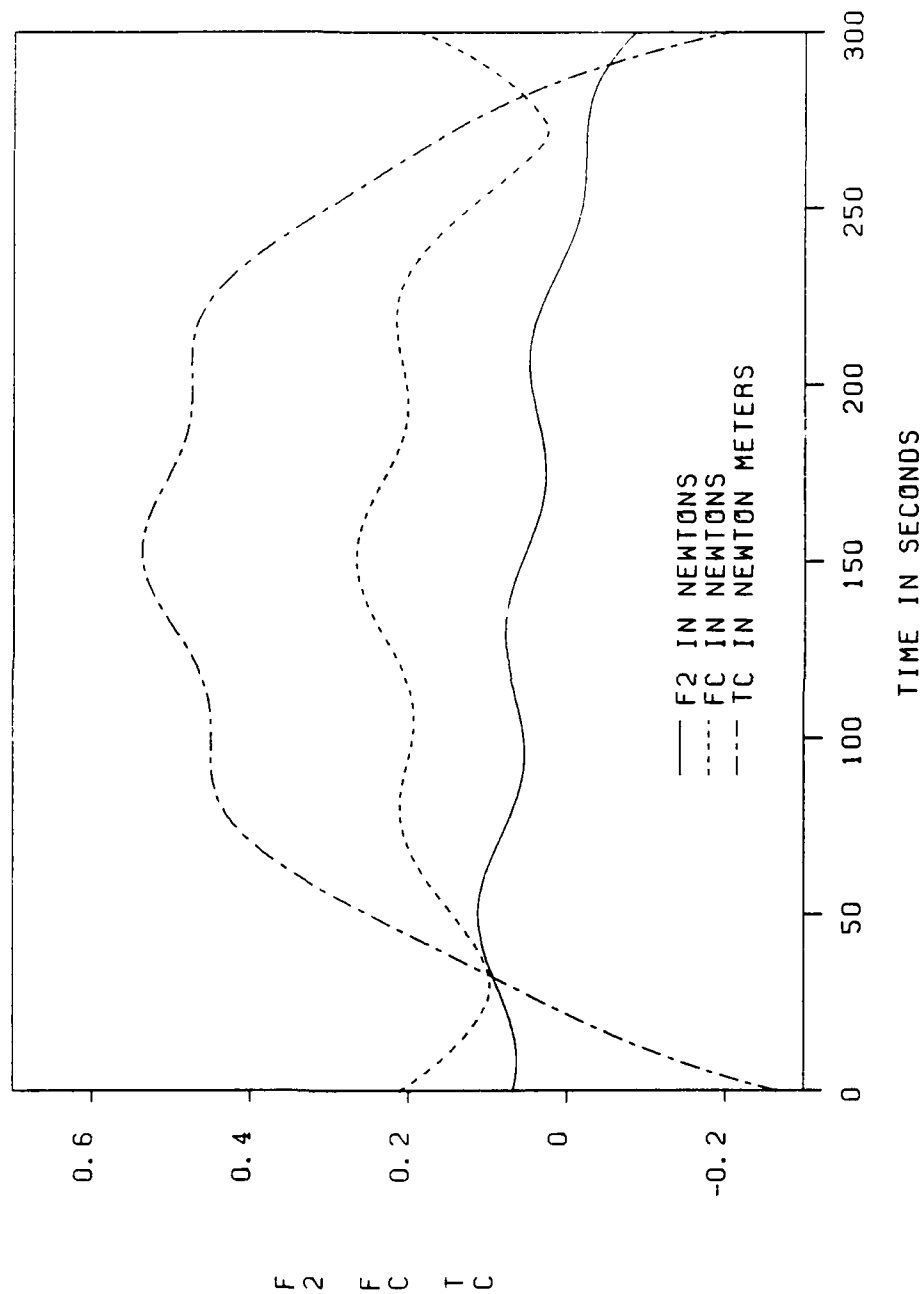


Figure 7. Constraint Load Histories (Case 1)



assigned values are $T_1 = 0.0$, $T_2 = -0.07$, and $T_3 = 0.011$ Newton-meters. The final grid size remained at 87, and the performance index was computed to be 3.066. Figures 8 through 12 summarize Case 2. Except for the external torques, comparing the figures of Case 2 with the corresponding figures of Case 1 shows little difference in the histories of the states, controls, and constraint loads. The increase in the performance index is the most immediate quantitative difference between the two cases, while the Case 2 figures show only small changes in the last third of the capture. Of significance is the fact that capture is possible with one component of the external torque set to zero, which raises the question of what minimum control configuration is required from controllability considerations.

In Case 3 the internal torque, T_{G1} , is assumed to be produced by a torsional spring and damper. The torque constraint is chosen as $T_{G1} = u_4 = 0.57 \gamma_1 + 100.0 \dot{\gamma}_1$. The final grid size was again 87, and the performance index was 4.108. Case 3 is summarized in Figures 13 through 18. From Figures 14 and 18 the behaviors of γ_1 , $\dot{\gamma}_2$, and the constraint loads are seen to be only slightly changed from Case 1. The other Case 3 figures, however, show more significant changes in the motion and torque histories. In particular, as T_{G1} goes to zero at 300 seconds, the magnitudes of T_1 and T_2 increase significantly to achieve

Figure 8. Body 0 Angular Rate Histories (Case 2)

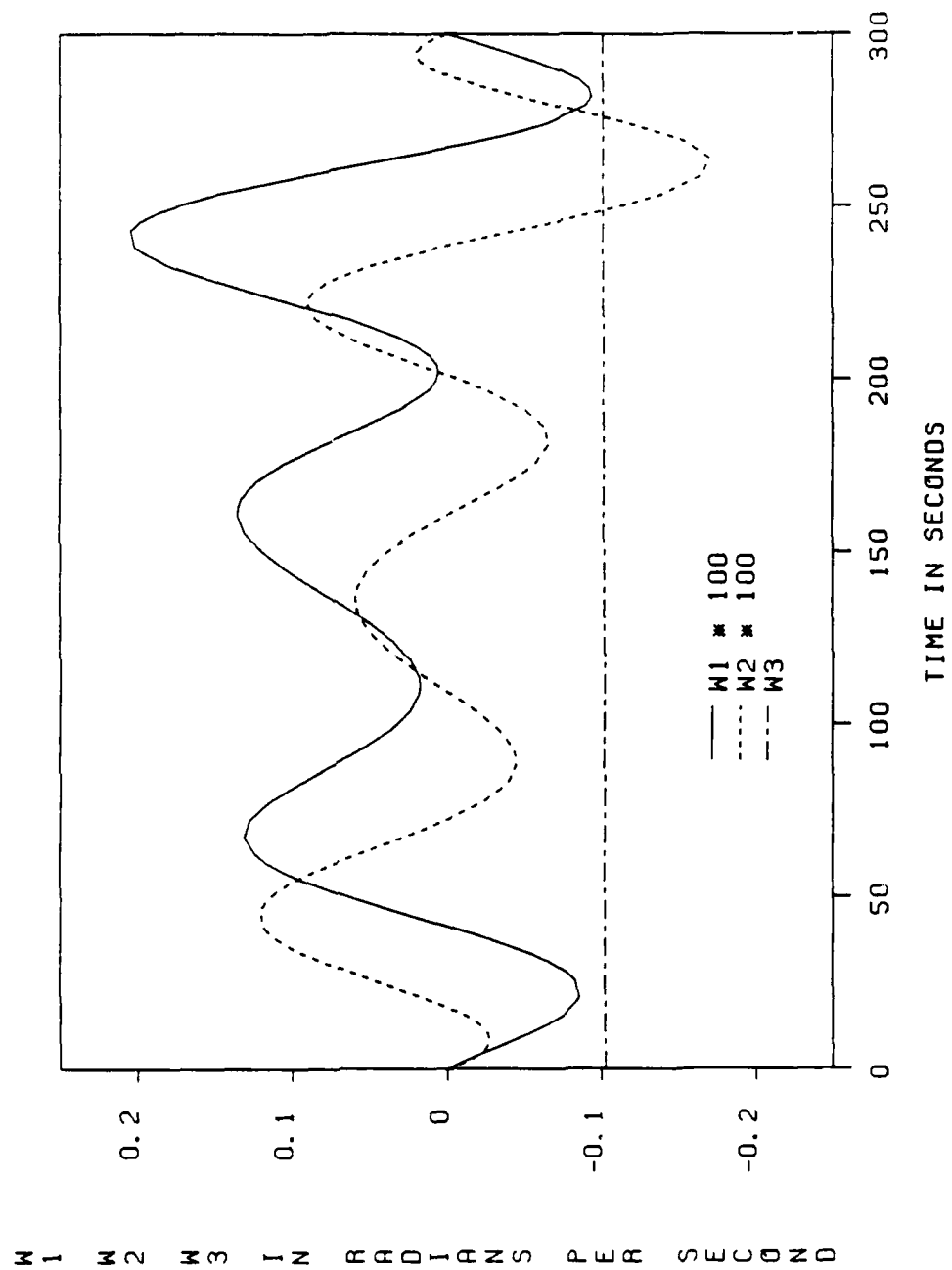


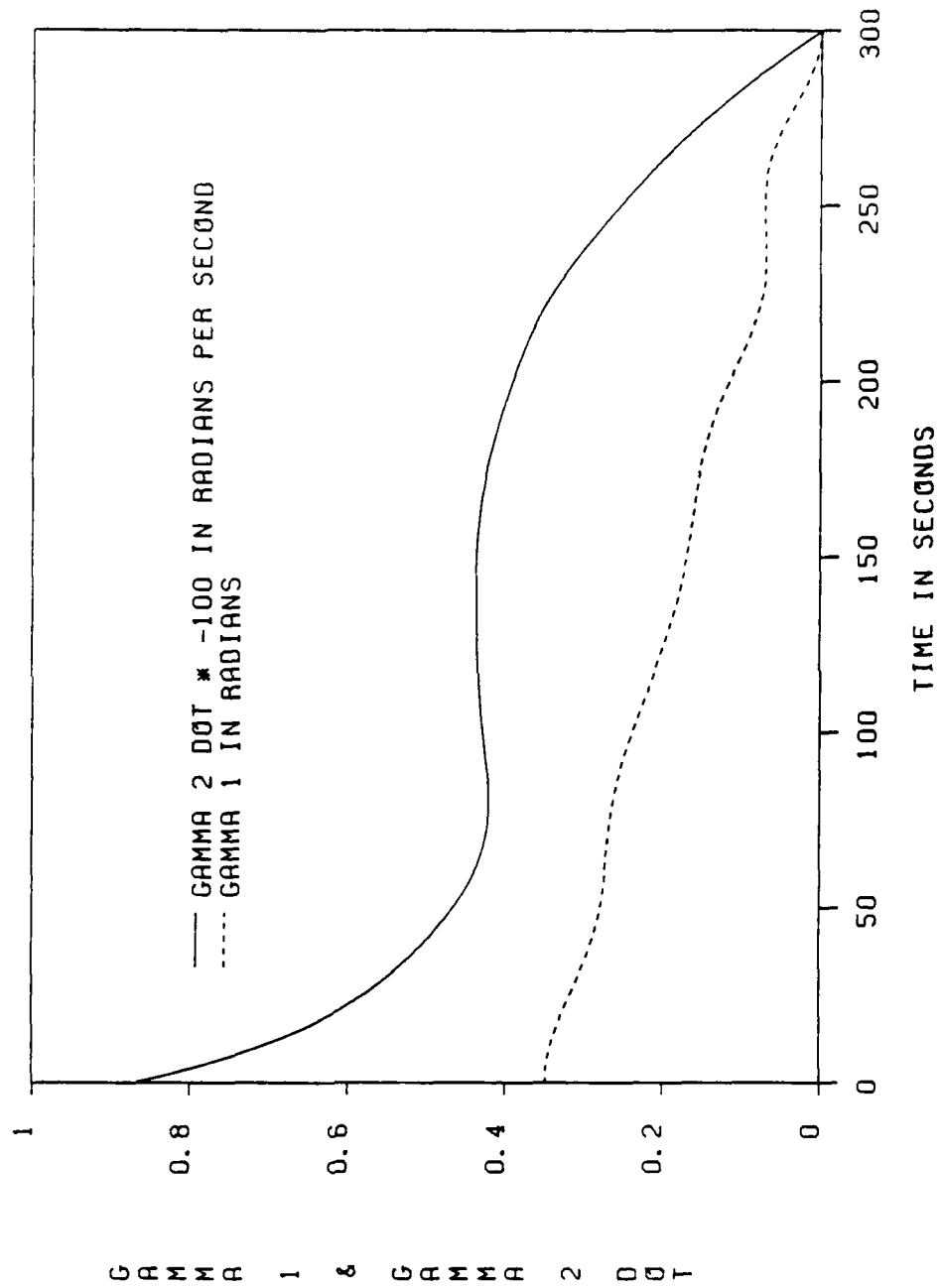
Figure 9. Body 1 γ_1 and $\dot{\gamma}_2$ Histories (Case 2)

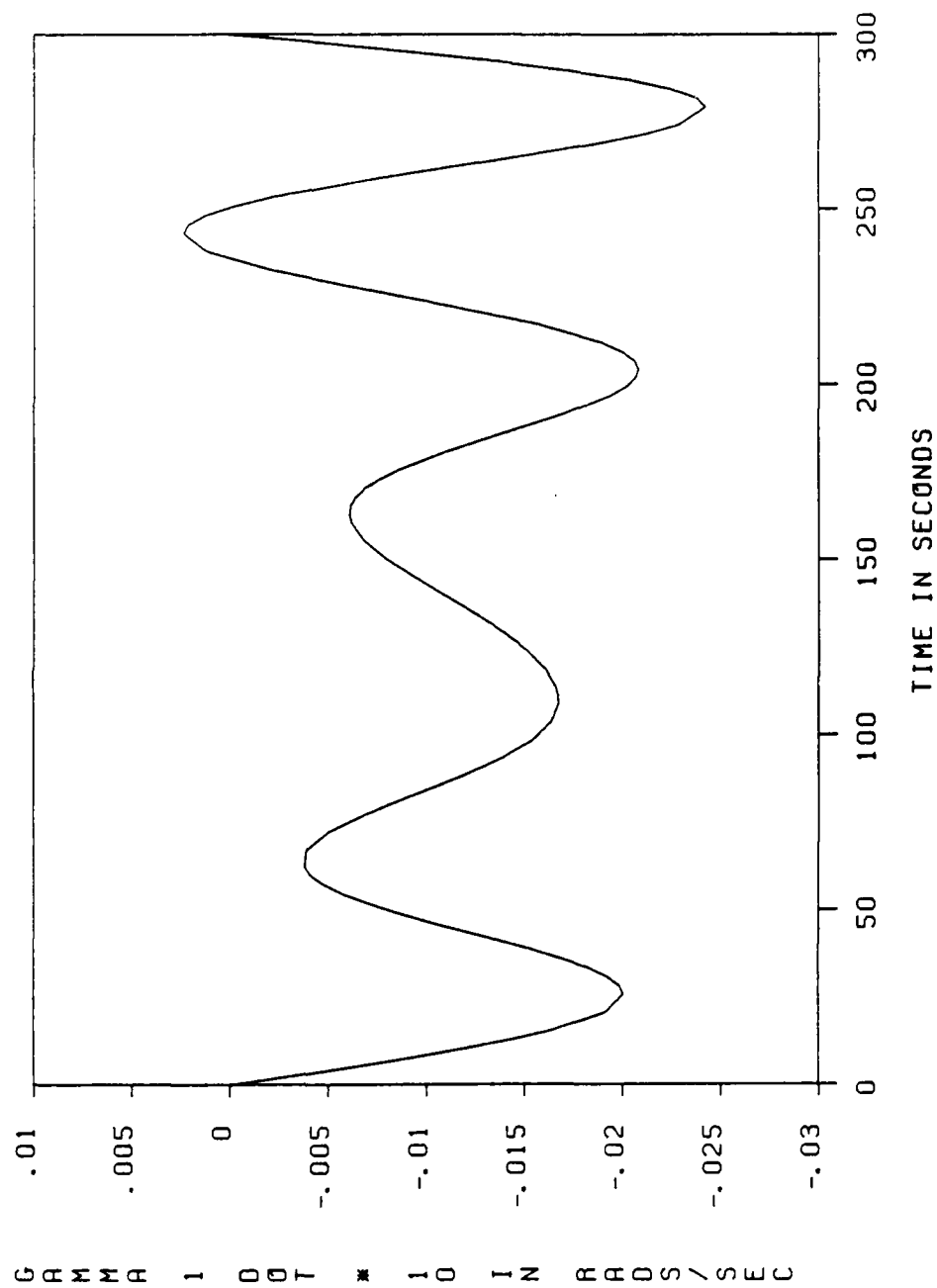
Figure 10. Body 1 $\dot{\gamma}_1$ History (Case 2)

Figure 11. Internal Torque Histories (Case 2)

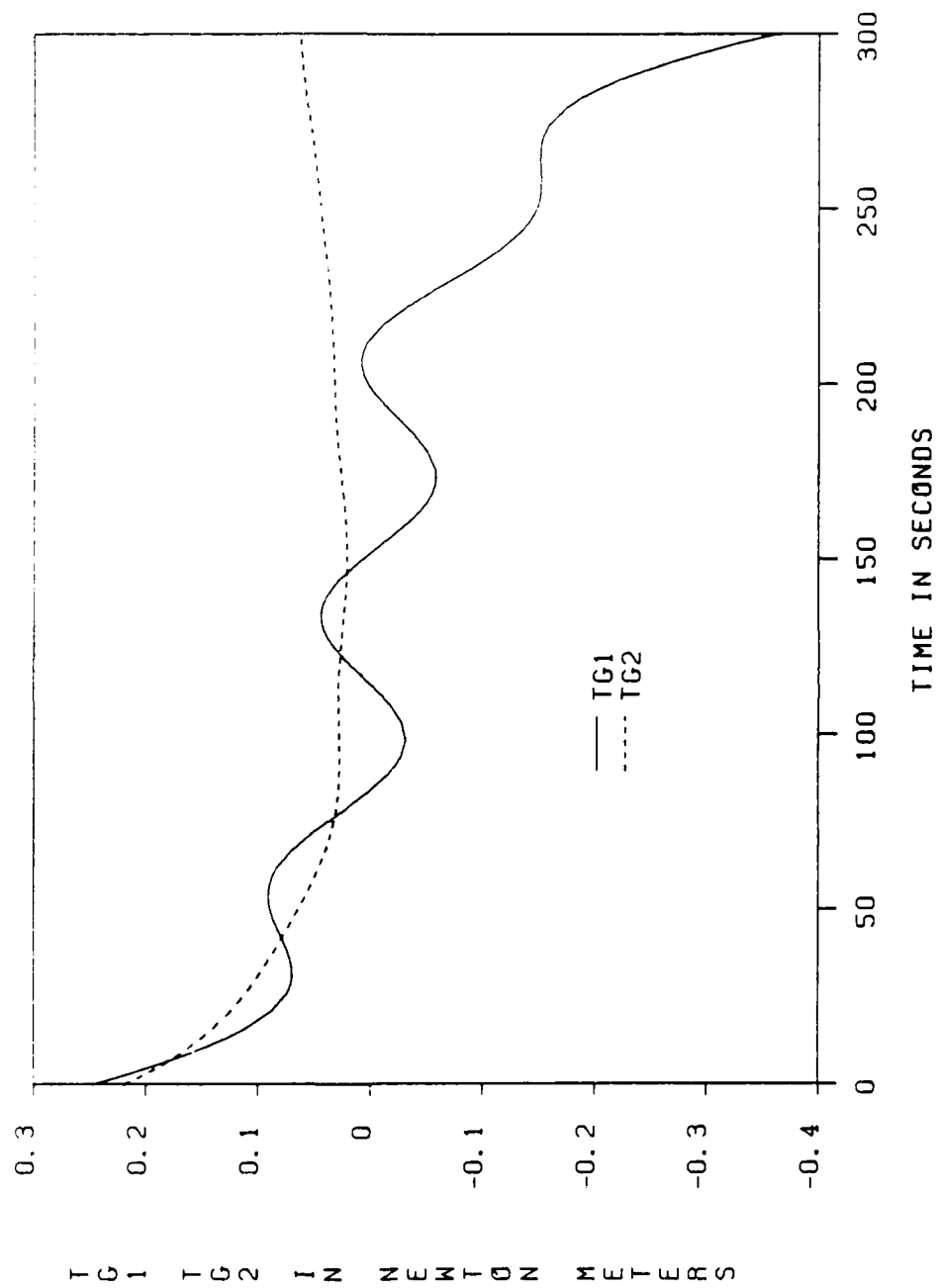


Figure 12. Constraint Load Histories (Case 2)

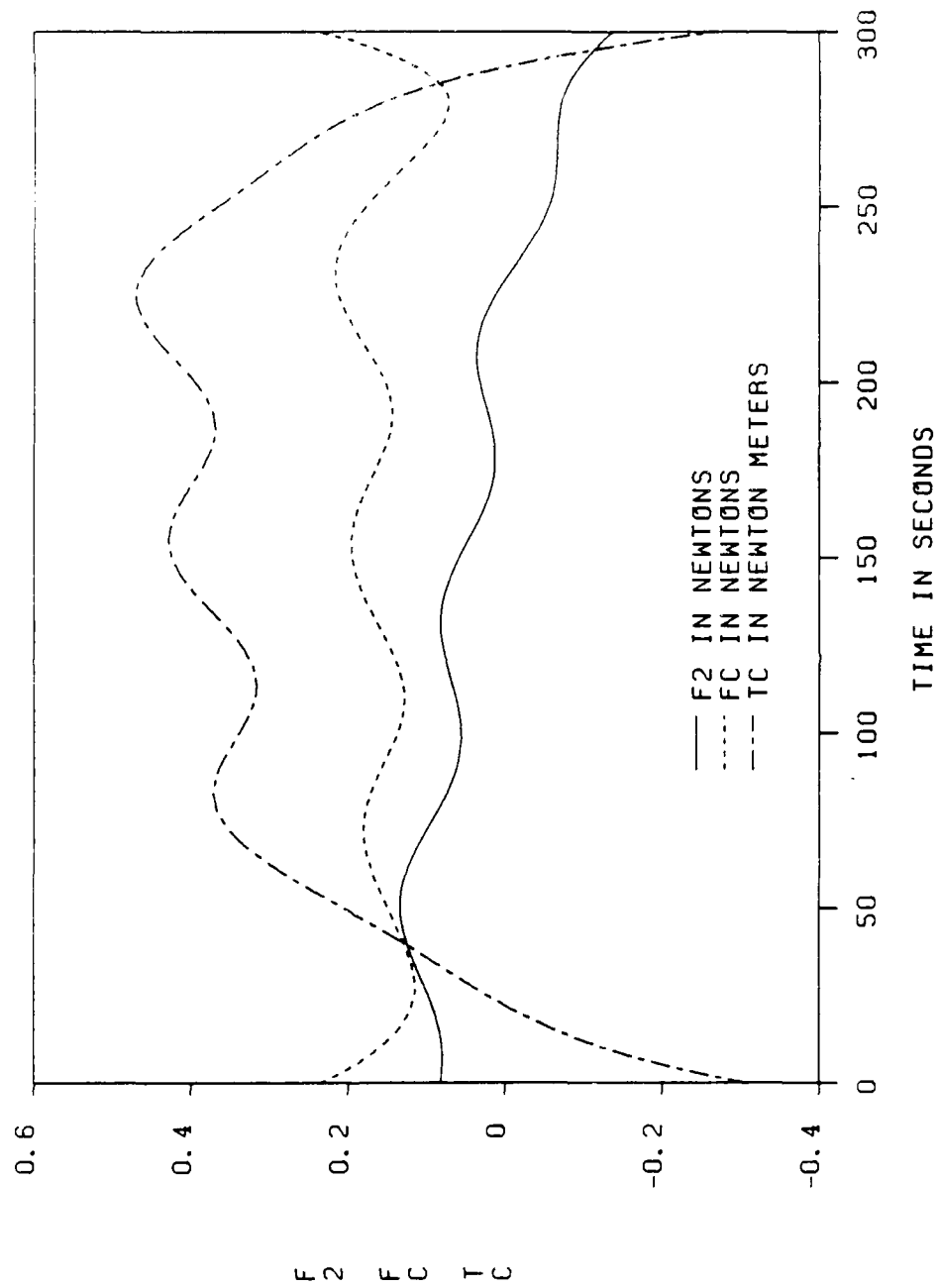
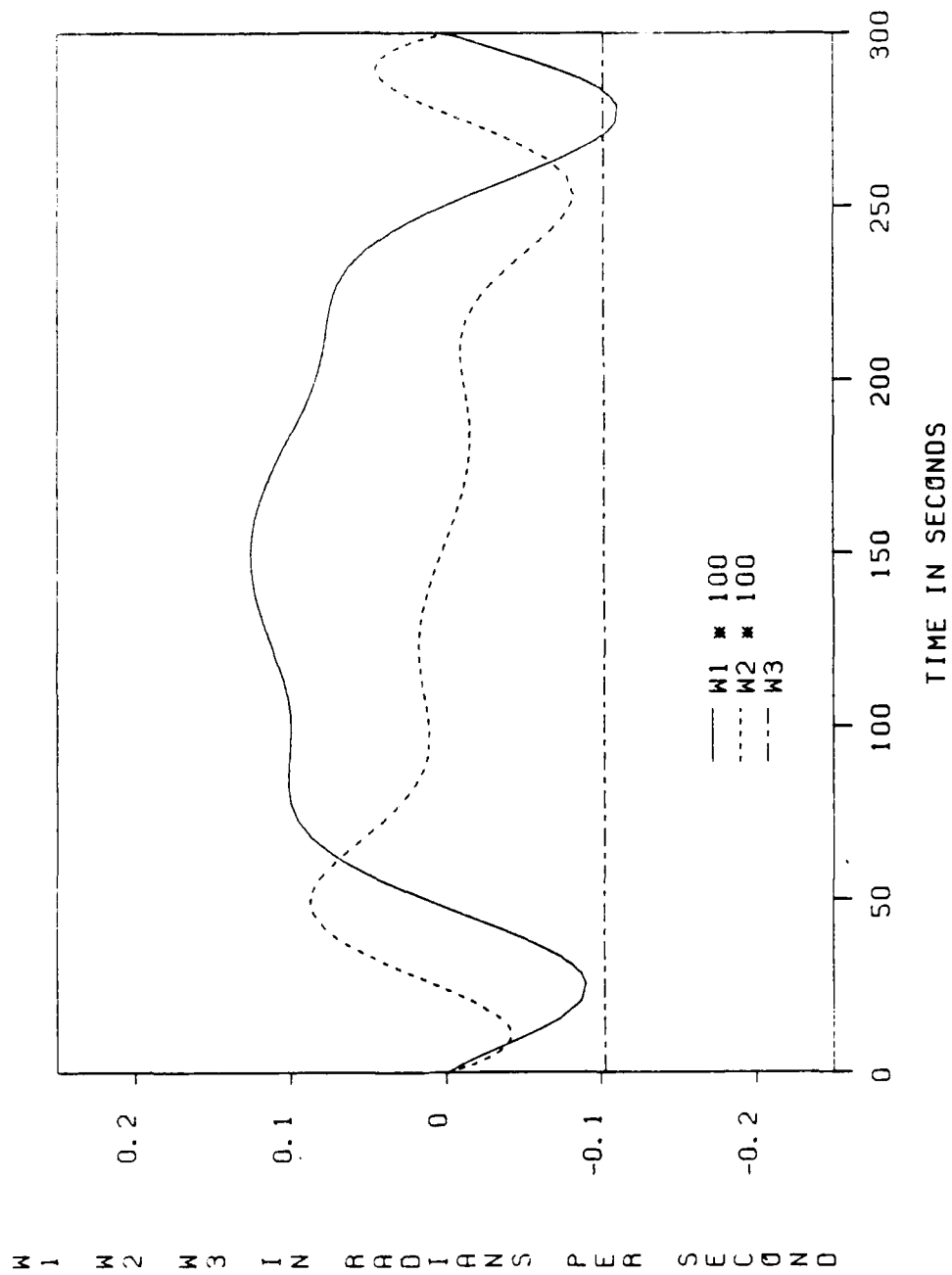


Figure 13. Body 0 Angular Rate Histories (Case 3)



$$\dot{\bar{x}} = [0 \ 0 \ 0 \ k_4 x_6 \ 0]^T - B \bar{x} \quad (4.14)$$

$$x_6 = x_4$$

$$\dot{\bar{y}} = D \bar{y} .$$

Then with $B_{33} = 0$, $\dot{x}_3 = 0$, so x_3 remains constant at its initial value. Furthermore, if capture is initiated with $x_1 = 0$ and $x_2 = 0$ as in Table 1, then x_1 and x_2 remain zero throughout capture, and the OMV is always in a state of constant spin about the \hat{e}_3 axis.

Implementing the control law given by equation (4.13) requires k_4 and the remaining four diagonal elements of B to be specified. To keep control forces small, large displacements of the target center of mass from the \hat{e}_3 axis must be avoided. Specifying the three constants of the matrix, D , in the system, (4.14), in conjunction with k_4 and B_{44} can establish joint motion that closely follows the decay of x_6 to control the position of the target center of mass.

4.4 Results

To compute state, feedback control, and constraint load histories, the system, (4.14), was integrated forward for 300 seconds from the initial conditions of Table 3 for ${}_1\bar{x}_6$ and y_1 . y_2 and y_3 were initialized to zero. The remaining system constants were selected as follows:

Then substituting from the system, (4.4), yields

$$\begin{aligned} \dot{V} = & \bar{x}^T [A^{-1}\bar{F} + A^{-1}\bar{u}] + k_4 x_6 x_4 + \bar{y}^T D^T R \bar{y} \\ & + \bar{y}^T R D \bar{y} . \end{aligned} \quad (4.11)$$

However, if D is already specified as negative definite, the familiar Liapunov equation can be written,

$$D^T R + R D = -Q , \quad (4.12)$$

where Q is a positive definite matrix. To make \dot{V} at least negative semidefinite, choose

$$\bar{u} = -\bar{F} + A[0 \ 0 \ 0 \ k_4 x_6 \ 0]^T - AB\bar{x} . \quad (4.13)$$

If the matrix, B , is positive definite, \dot{V} is negative semidefinite in x_6 . Furthermore, if B is diagonal and B_{33} is zero, \dot{V} is negative semidefinite in x_3 and x_6 . Then from the above lemma the system, (4.4), with the control, \bar{u} , of equation (4.13) is asymptotically stable with respect to the largest invariant set contained in the x_3, x_6 plane. However, any nonzero x_6 results in a nonzero u_4 and, consequently, a nonzero \dot{x}_4 . Therefore, the largest invariant set contained in the x_3, x_6 plane is the x_3 axis, which represents the spin-stabilized equilibrium if ω_{03} does not go to zero.

Substituting for \bar{u} in the system, (4.4), results in a linear system written as

$$\Omega_d = \{ {}_1\bar{x}_6, \bar{y} : V({}_1\bar{x}_6, \bar{y}) \leq d \}$$

is bounded. Suppose that V is bounded below over the set Ω_d and that $\dot{V}({}_1\bar{x}_6, \bar{y}) \leq 0$ for all ${}_1\bar{x}_6$ and \bar{y} in Ω_d . Let S denote the subset of Ω_d defined by

$$S = \{ {}_1\bar{x}_6, \bar{y} \in \Omega_d : \dot{V}({}_1\bar{x}_6, \bar{y}) = 0 \} ,$$

and let M be the largest invariant set of the system, (4.4), contained in S . Then, whenever

$${}_1\bar{x}_6(0), \bar{y}(0) \in \Omega_d,$$

the solution of the system, (4.4), approaches M as $t \rightarrow \infty$." Note that $V({}_1\bar{x}_6, \bar{y})$ is not required to be positive definite and that any solution trajectory of the system, (4.4), constitutes an invariant set.

Using this lemma a nonlinear feedback control law can be derived for the two-body system of the capture problem. Take as a candidate Liapunov function

$$V = \frac{1}{2} \bar{x}^T I \bar{x} + \frac{1}{2} k_4 x_6^2 + \bar{y}^T R \bar{y} \quad (4.8)$$

$$\text{with } \bar{x}^T = [x_1 \ x_2 \ x_3 \ -x_4 \ x_5] , \quad (4.9)$$

where I is the identity matrix, k_4 is a positive constant, and R is a positive definite constant matrix. Differentiating this positive definite V with respect to time gives

$$\dot{V} = \bar{x}^T I \dot{\bar{x}} + k_4 x_6 \dot{x}_6 + \dot{\bar{y}}^T R \bar{y} + \bar{y}^T R \dot{\bar{y}} . \quad (4.10)$$

4.3 Global Asymptotic Stability by Nonlinear Feedback Control

For continuous nonlinear autonomous systems such as that described by the system of equations, (4.4), the Liapunov direct method for establishing the global asymptotic stability of an equilibrium point is stated from Theorem 6.7.2 of Meirovitch [16] as follows:

"If there exists for the system, (4.4), a positive (negative) definite function $V(\bar{x}_6, \bar{y})$ whose total time derivative $\dot{V}(\bar{x}_6, \bar{y})$ is negative (positive) definite along every trajectory of (4.4), then the trivial solution is asymptotically stable."

The trivial solution is, of course, the equilibrium point, and the control vector, \bar{u} , is now considered to be a vector function of \bar{x}_6 and \bar{y} . However, applying the above theorem to the equilibrium point of the capture problem can lead to situations in which $\dot{V}(\bar{x}_6, \bar{y})$ is only semi-definite, so a weaker sufficient condition is required.

An extension of the Liapunov direct method through LaSalle's Theorem for autonomous and periodic systems is developed by Vidyasagar [15]. One of the steps to LaSalle's Theorem is given as lemma 81, which provides the required stability condition for the capture problem. Stated here for the autonomous system, (4.4), lemma 81 is as follows:

"Let $V(\bar{x}_6, \bar{y})$ be continuously differentiable, and suppose that for some $d > 0$, the set

$$\begin{array}{c} 9 \times 1 \\ \begin{bmatrix} \dot{\bar{x}} \\ \cdot \\ x_6 \\ \cdot \\ y_1 \\ \cdot \\ y_2 \\ \cdot \\ y_3 \end{bmatrix} \end{array} = \begin{array}{c} 9 \times 9 \\ \begin{bmatrix} [A^{-1}\bar{F}]^E \bar{x}_6 & [A^{-1}\bar{F}]^E \bar{y} \\ 0 & 0 & 0 & 1 & 0 & 0 & 0 & 0 & 0 \\ 0 & 0 & 0 & 0 & 0 & 0 & 0 & 1 & 0 \\ 0 & 0 & 0 & 0 & 0 & 0 & 0 & 0 & 1 \\ 0 & 0 & 0 & 0 & 0 & 0 & -k_3 & -k_2 & -k_1 \end{bmatrix} \end{array} \begin{array}{c} 9 \times 1 \\ \begin{bmatrix} \bar{x} \\ x_6 \\ y_1 \\ y_2 \\ y_3 \end{bmatrix} \end{array} + \begin{array}{c} 9 \times 5 \quad 5 \times 1 \\ \begin{bmatrix} [A^{-1}]^E \bar{u} \\ 0 & 0 & 0 & 0 & 0 \\ 0 & 0 & 0 & 0 & 0 \\ 0 & 0 & 0 & 0 & 0 \\ 0 & 0 & 0 & 0 & 0 \end{bmatrix} \bar{u} \end{array} \quad (4.7)$$

where superscript E implies that the indicated quantities are evaluated at equilibrium after any indicated partial differentiation. The system, (4.7), is suitably formulated as a linear control problem. Controllability is assured because a control is provided for each of the five degrees of freedom in the system. Therefore, a control vector, \bar{u} , as a linear function of the nine states can be found to make the equilibrium point asymptotically stable.

The details of deriving a particular linear feedback control, \bar{u} , and quantifying it are not carried out here because of the local nature of the stability that results. Establishing global asymptotic stability requires Liapunov's direct method applied to the nonlinear system with the linear control law. The difficulty here is that with the selected coordinate system a clear path to conclusive analytic results is not apparent. However, the Liapunov direct method leads to global asymptotic stability if nonlinear feedback control is considered.

$$\dot{\bar{\mathcal{L}}}_{01}^R \cdot \hat{e}_2 = y_2 , \quad (4.2)$$

$$\text{and } \ddot{\bar{\mathcal{L}}}_{01}^R \cdot \hat{e}_2 = y_3 , \quad (4.3)$$

an autonomous system results by writing

$$\dot{\bar{x}} = A^{-1}\bar{F} + A^{-1}\bar{u}$$

$$\dot{x}_6 = x_4$$

$$\begin{bmatrix} \dot{y}_1 \\ \dot{y}_2 \\ \dot{y}_3 \end{bmatrix} = \begin{bmatrix} 0 & 1 & 0 \\ 0 & 0 & 1 \\ -k_3 & -k_2 & -k_1 \end{bmatrix} \begin{bmatrix} y_1 \\ y_2 \\ y_3 \end{bmatrix} = D \bar{y} \quad (4.4)$$

The matrix, A , is now a function of y_1 , and the vector, \bar{F} , is a function of the vector, \bar{y} . The equilibrium point of interest is

$$[x_1 \ x_2 \ x_3 \ x_4 \ x_5 \ x_6] = [0 \ 0 \ C \ 0 \ 0 \ 0] \quad (4.5)$$

$$\text{and } [y_1 \ y_2 \ y_3] = [0 \ 0 \ 0] , \quad (4.6)$$

where C is some constant. A simple translation in x_3 brings the equilibrium point to the origin.

The system of equations, (4.4), can be linearized about the desired equilibrium giving

4.2 Linear Feedback Control About an Equilibrium Point

The Liapunov indirect method as described by Vidyasagar [15] is often used to design a linear feedback control law such that an equilibrium point of a nonlinear system is locally asymptotically stable. The system equations are linearized about the equilibrium point to set up a linear control problem. If controllability conditions are met, linear feedback can be found by various methods such that the equilibrium point for the linearized system is asymptotically stable. Then, invoking the results of the Liapunov indirect method, the same linear feedback can be applied to the nonlinear system assuring the asymptotic stability of the equilibrium point in some neighborhood of that point.

Looking now at the capture problem, the system equations (3.5) and (3.6) are nonautonomous because the matrix, A , and the vector, \bar{F} , are functions of the joint motion, which is a prescribed function of time. However, since the equilibrium point of interest is the spin-stabilized state with the joint at rest on the \hat{e}_3 axis in Figure 1, the joint motion can be prescribed in terms of three additional states to form an autonomous system when adjoined to equations (3.5) and (3.6). Letting

$$\bar{\mathcal{L}}_{01} \cdot \hat{e}_2 = y_1, \quad (4.1)$$

CHAPTER 4

CAPTURE BY CONTINUOUS NONLINEAR FEEDBACK CONTROL

4.1 Introduction

The capture problem can also be solved by a feedback control approach in which the control vector, \bar{u} , is a function of the system state variables. In this chapter Liapunov stability theory is employed to derive feedback control laws which result in an asymptotic approach to the final desired spin-stabilized state. Liapunov's indirect or first method leads to a linear feedback control law which guarantees the local asymptotic stability of the spin-stabilized equilibrium. Global asymptotic stability is achieved through a nonlinear feedback control law derived from Liapunov's direct or second method and its extension through LaSalle's theorem. This nonlinear control law is applied to the two-body system of Figure 1 in an initial state of free spin and precession of the target and free spin of the OMV. Numerical results are presented to show state, control, and constraint load histories during capture. The motion during capture is seen to be very benign, and the controls and constraint loads seem to be within very manageable bounds.

the specified final state. On the other hand, different constants in the torque constraint might yield a lower cost.

3.8 Conclusions

Using an optimal control approach, continuous open loop controls have been produced that detumble the target satellite. The capture process has been seen to be very benign with no significant change in the attitude of the spinning OMV while the two-body system was driven to a final spin-stabilized state. When the five system controls were unconstrained, only very moderate internal (joint) and external (thruster) torque magnitudes were required for a very reasonable capture time of 300 seconds. Even with various control constraints, control magnitudes were reasonable, and the attitude of the OMV remained virtually undisturbed. In all cases the constraint loads at the joint indicate no requirement for a prohibitively massive or stiff structure to link the two bodies. Furthermore, only small forces are required to translate the joint with the desired constant velocity.

Figure 18. Constraint Load Histories Case 3)

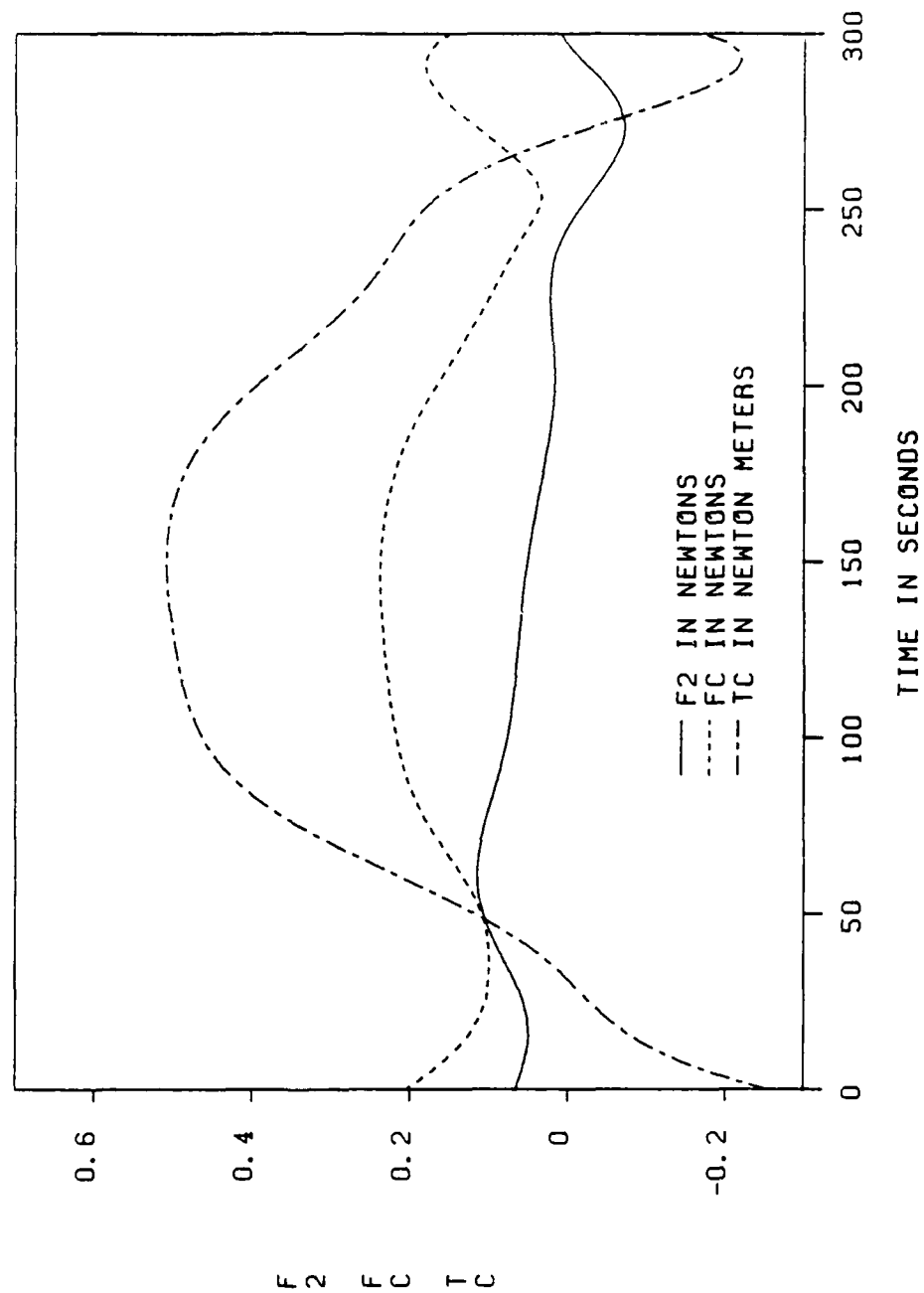


Figure 17. Internal Torque Histories (Case 3)

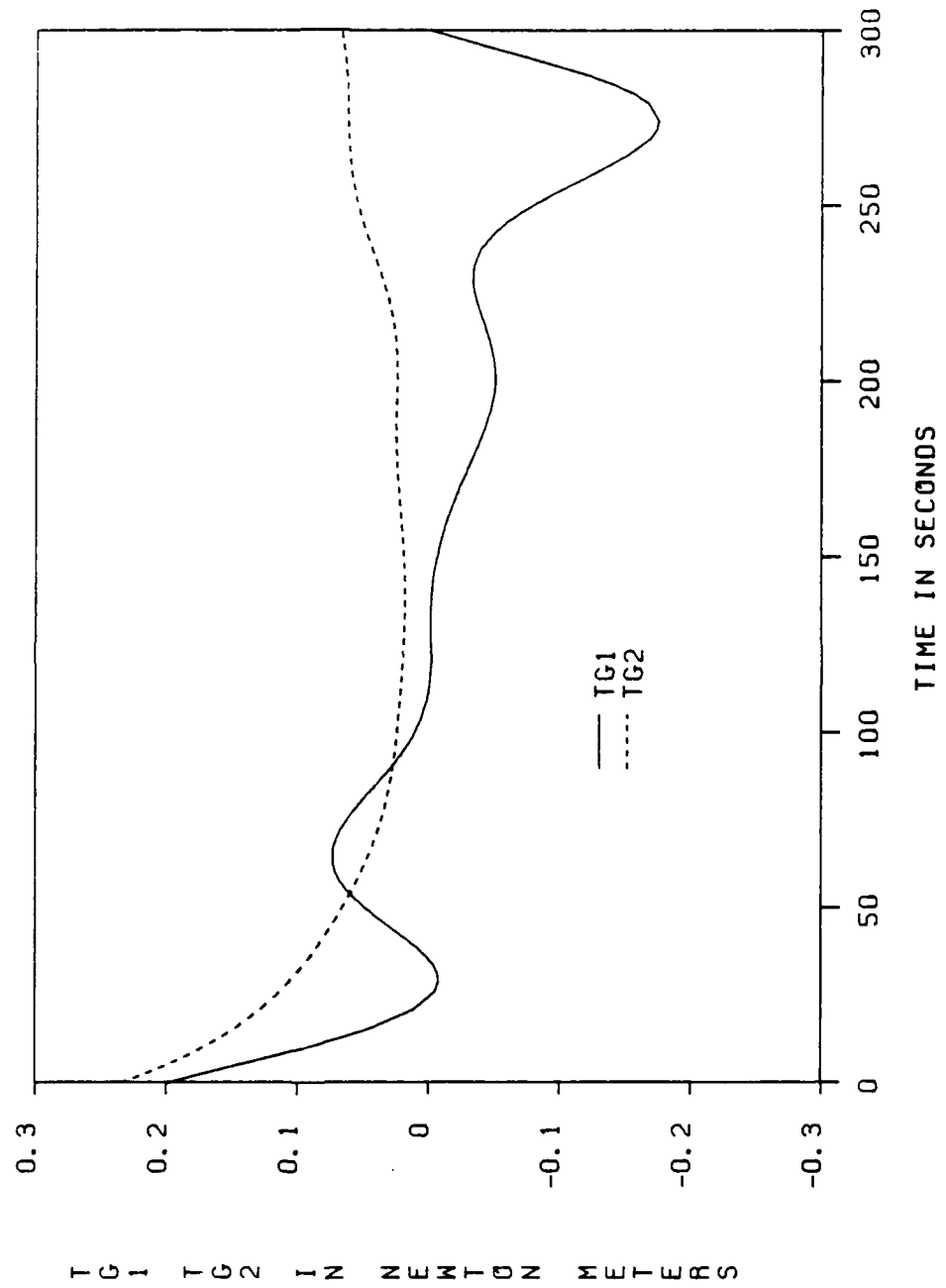


Figure 16. External Torque Histories (Case 3)

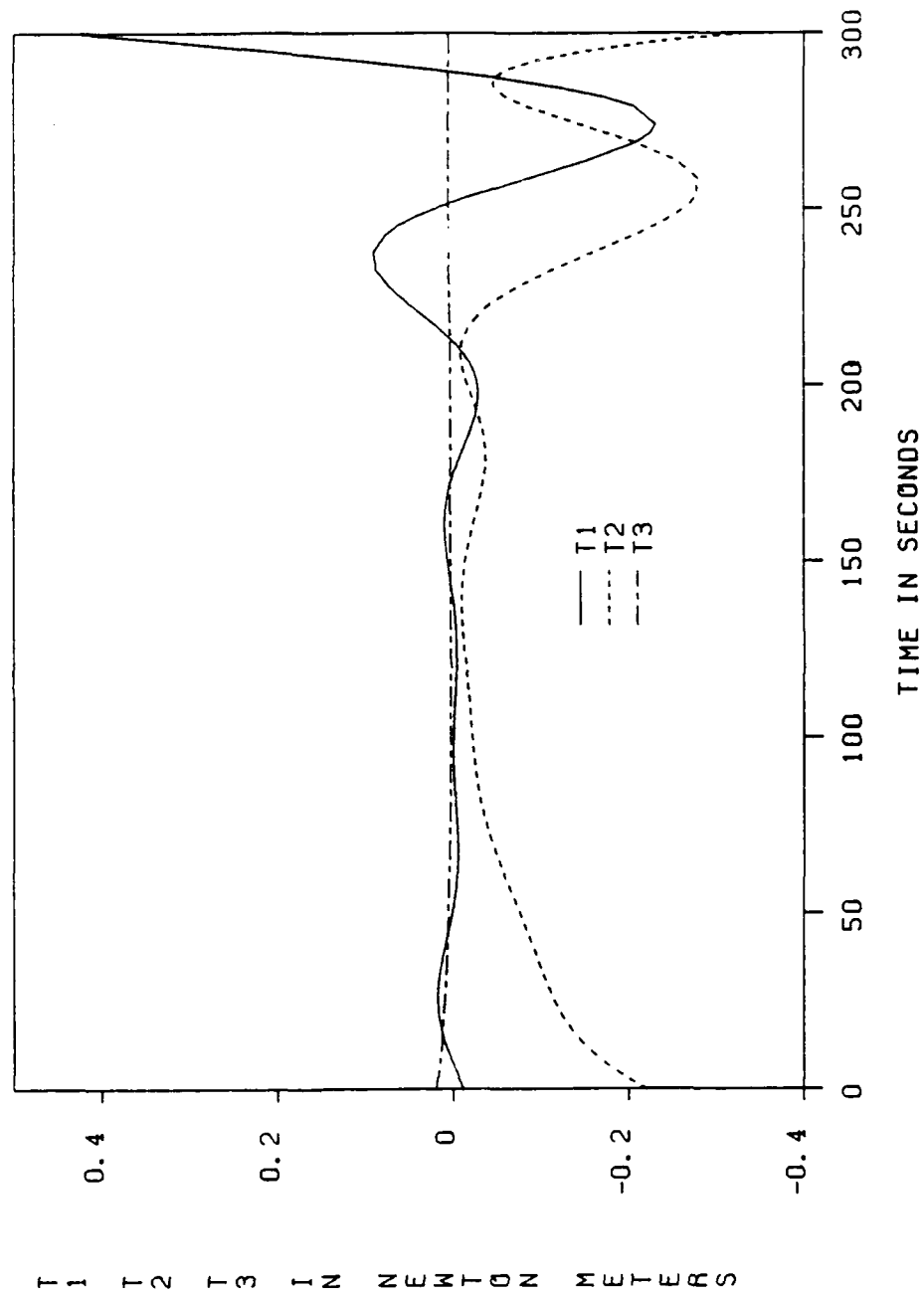


Figure 15. Body 1 $\dot{\gamma}_1$ History (Case 3)

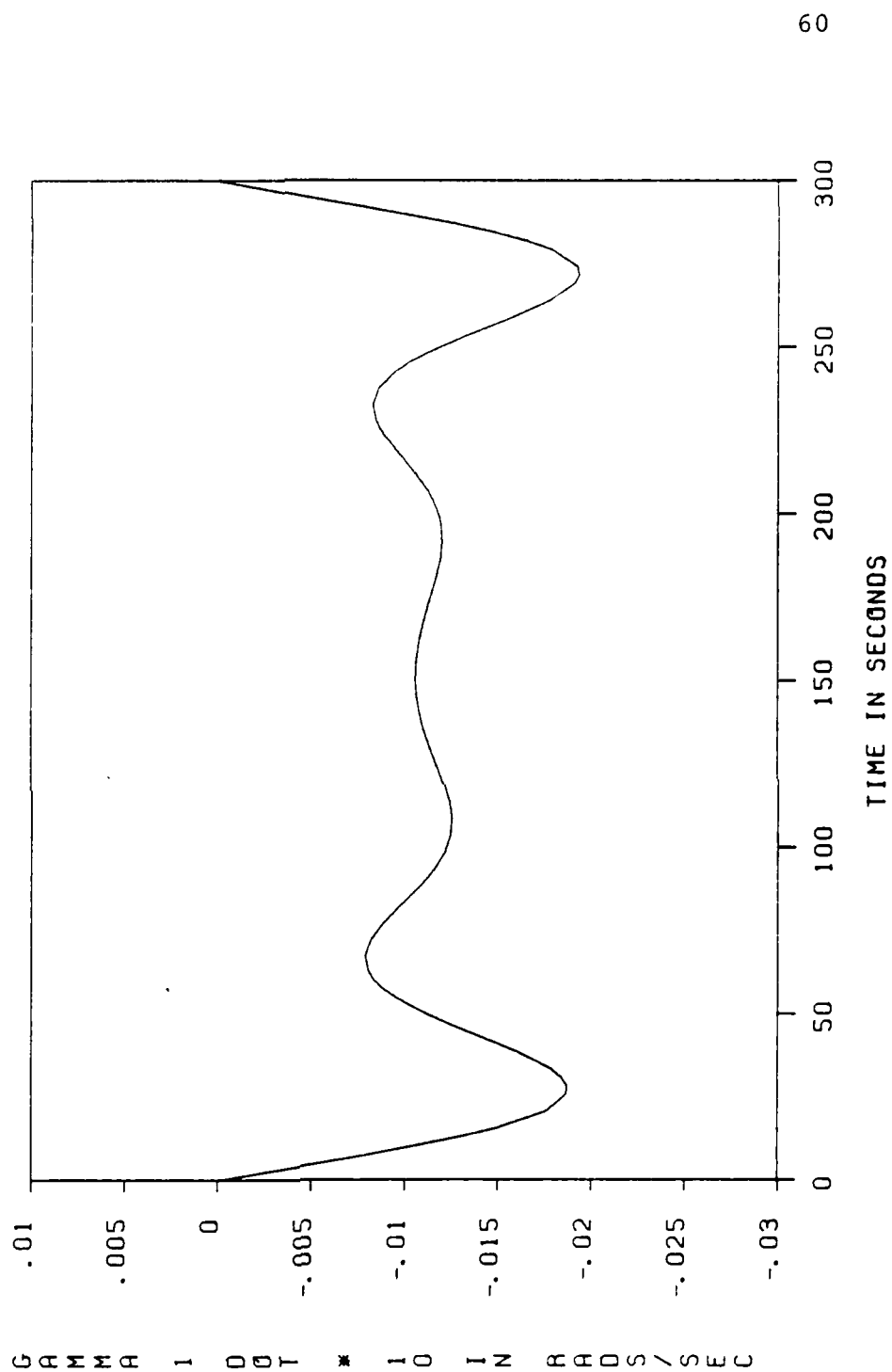
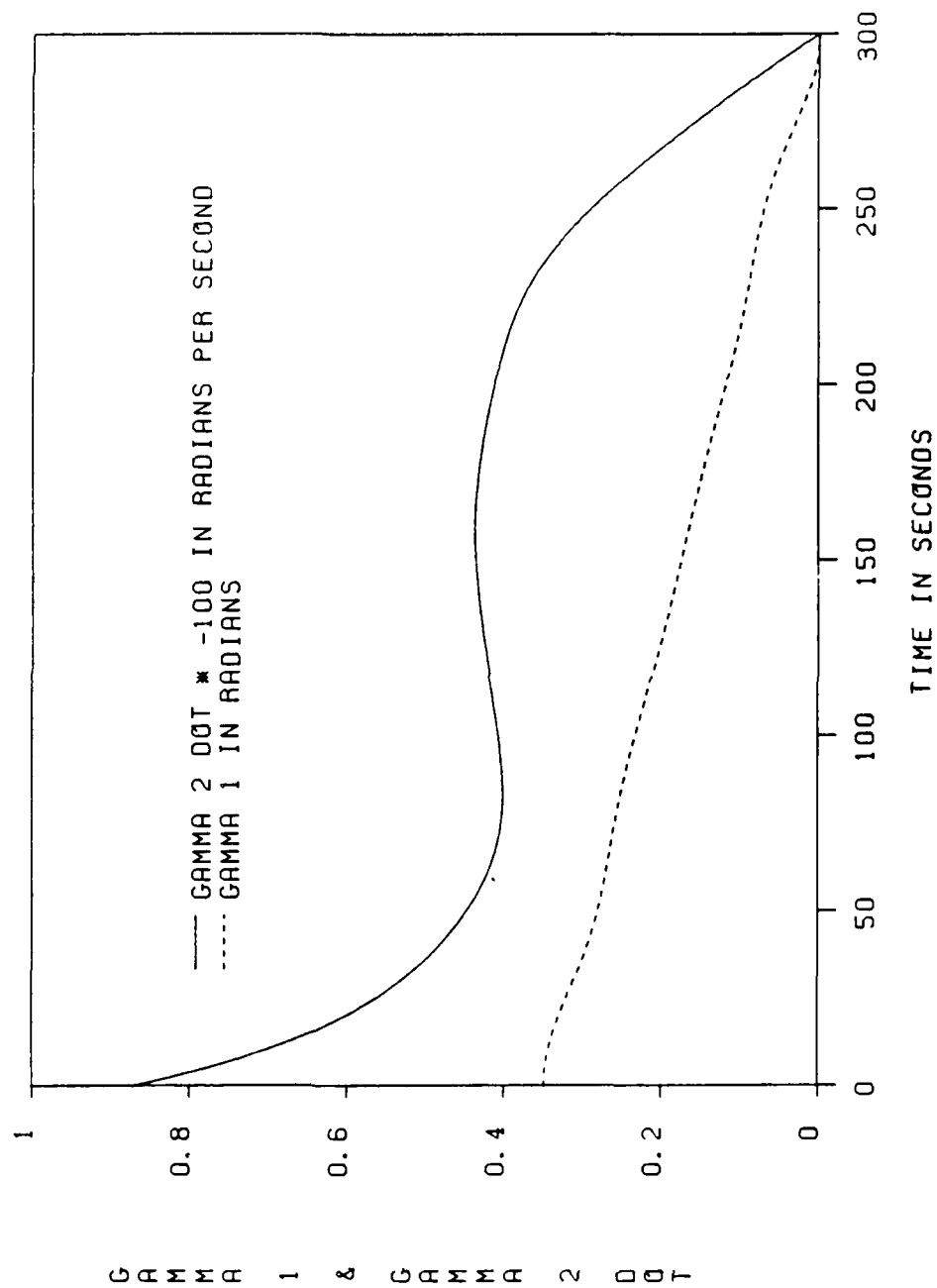


Figure 14. Body 1 γ_1 and $\dot{\gamma}_2$ Histories (Case 3)

$$k_4 = 0.001225 \quad (4.15)$$

$$B = \begin{bmatrix} +0.046 & 0 & 0 & 0 & 0 \\ 0 & +0.046 & 0 & 0 & 0 \\ 0 & 0 & 0.0 & 0 & 0 \\ 0 & 0 & 0 & +0.07 & 0 \\ 0 & 0 & 0 & 0 & +0.02 \end{bmatrix} \quad (4.16)$$

$$D = \begin{bmatrix} 0 & 1 & 0 \\ 0 & 0 & 1 \\ -0.000064 & -0.0048 & -0.12 \end{bmatrix} . \quad (4.17)$$

B_{44} and k_4 critically damped the x_4 , x_6 system giving two equal eigenvalues of -0.035 . The matrix, D , resulted by specifying three equal eigenvalues, -0.04 . Consequently, both x_6 and y_1 were reduced to 0.05% of their initial values in 300 seconds. While x_4 rose to a peak value of -0.0045 radians per second, both x_4 and x_5 were reduced at 300 seconds to values less than 0.5% of their peak values. The values of x_1 , x_2 , and x_3 were constant.

The histories of the system, (4.14), states, \bar{y} , x_4 , x_5 , and x_6 , are shown in Figures 19 through 21. Figure 19 plots the joint motion histories corresponding to \bar{y} . Figures 20 and 21 plot the histories of x_4 , x_5 , and x_6 , which correspond as before to $\dot{\gamma}_1$, $\dot{\gamma}_2$, and γ_1 respectively. The joint velocity and $\dot{\gamma}_1$ both remain quite

Figure 19. Joint Motion Histories (Feedback)

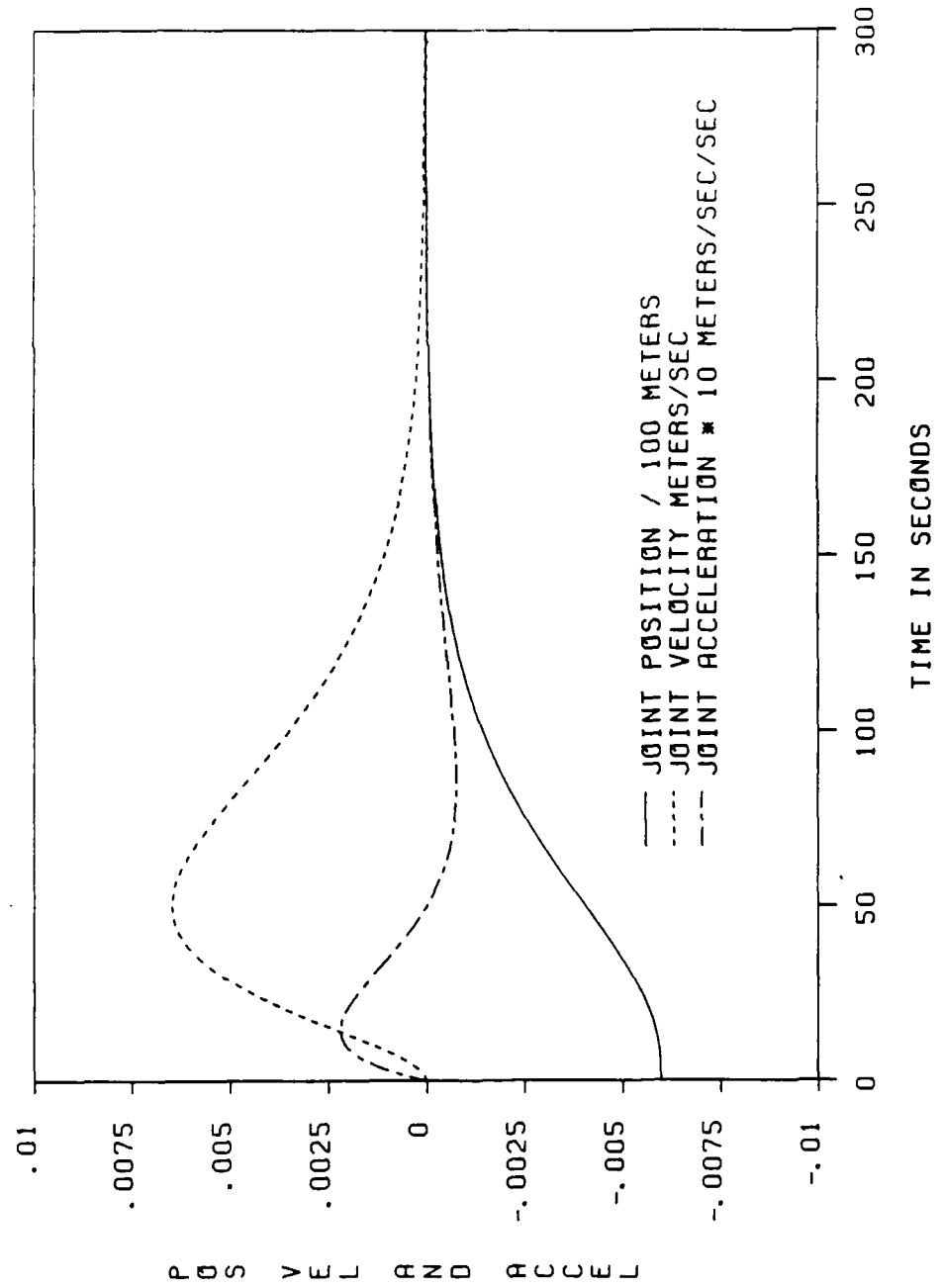


Figure 20. Body 1 γ_1 and $\dot{\gamma}_2$ Histories (Feedback)

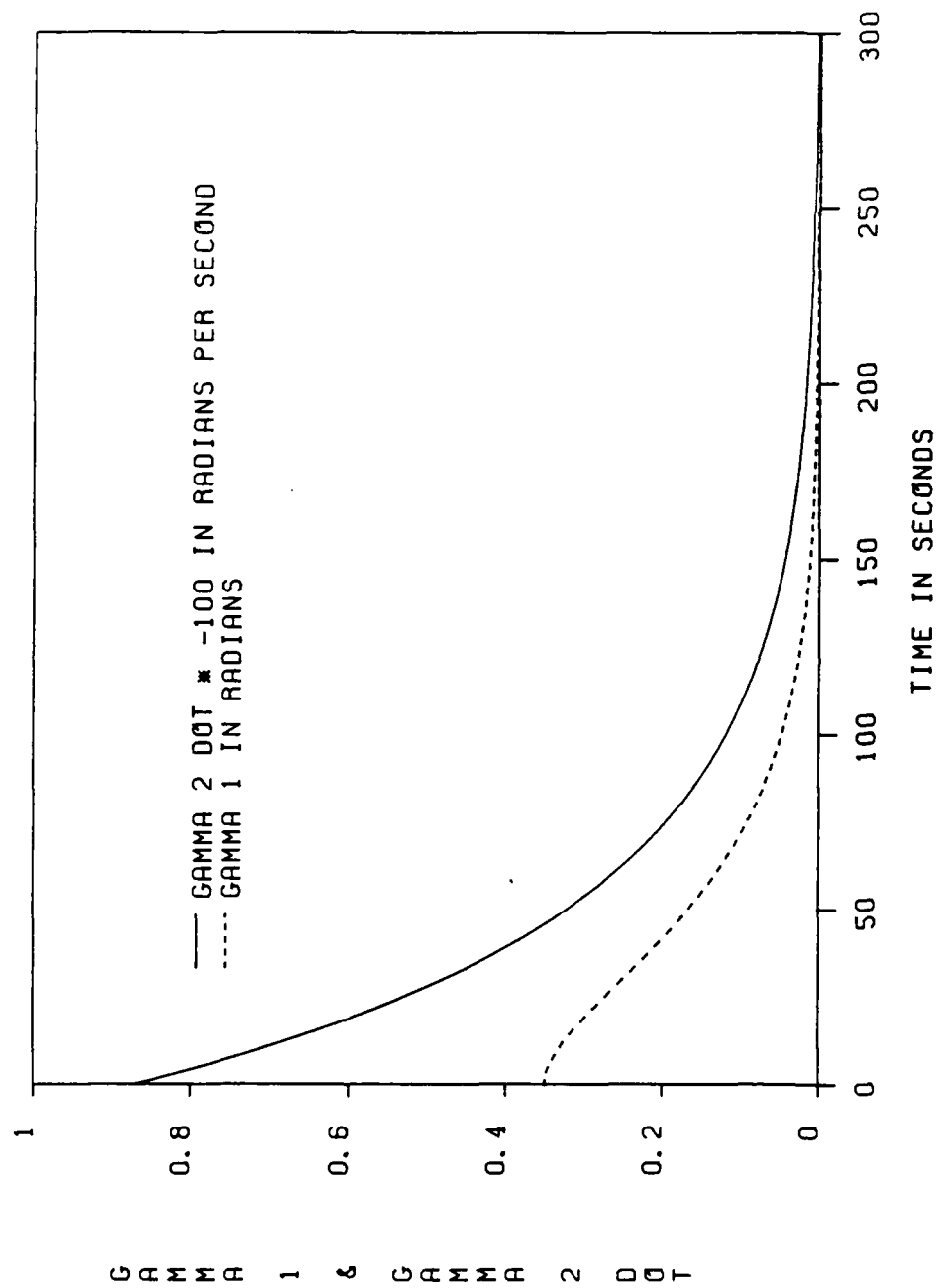
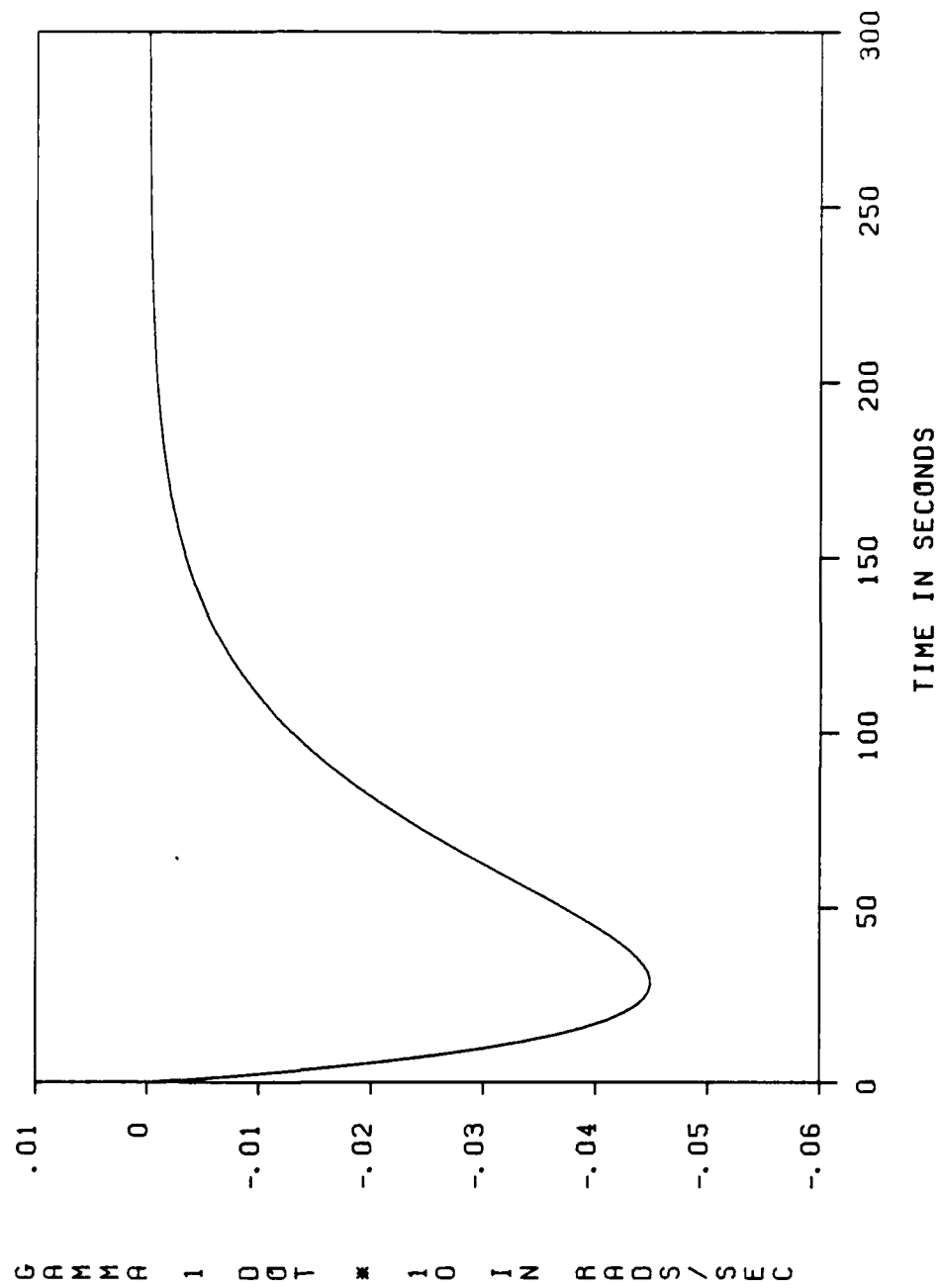


Figure 21. Body 1 $\dot{\gamma}_1$ History (Feedback)

GRAMMA 1 DOT * 10 IN RAD/SEC

small over the 300 second interval. Maximum joint velocity of 0.0065 meters per second is achieved at 49 seconds while $\dot{\gamma}_1$ peaks at -0.0045 radians per second at 28 seconds.

At each integration step the control vector, \bar{u} , was computed from equation (4.13), and the constraint torque and constraint force were computed from equations (2.45) and (2.49) with inputs from the system, (4.14). The component of the constraint force in the \hat{e}_2 direction again gave the force required to move the joint. The five control histories are shown in Figures 22 and 23. T1 and TG1 are seen to have similar profiles. T3 and TG2 oppose each other in sign but otherwise differ primarily only in the first 50 seconds. When the performance index, equation (3.1) is applied to these control histories a value of 386.74 results. The constraint loads, as defined in Chapter 3, are shown in Figure 24.

4.5 Summary and Conclusions

The Liapunov stability theory has been applied to the two-body system of the capture problem to develop a nonlinear feedback control law which results in global asymptotic stability of the X_3 (ω_{03}) axis of the system state space. The control law contains no linear terms but does transform the original nonlinear dynamic system

Figure 22. External Torque Histories (Feedback)

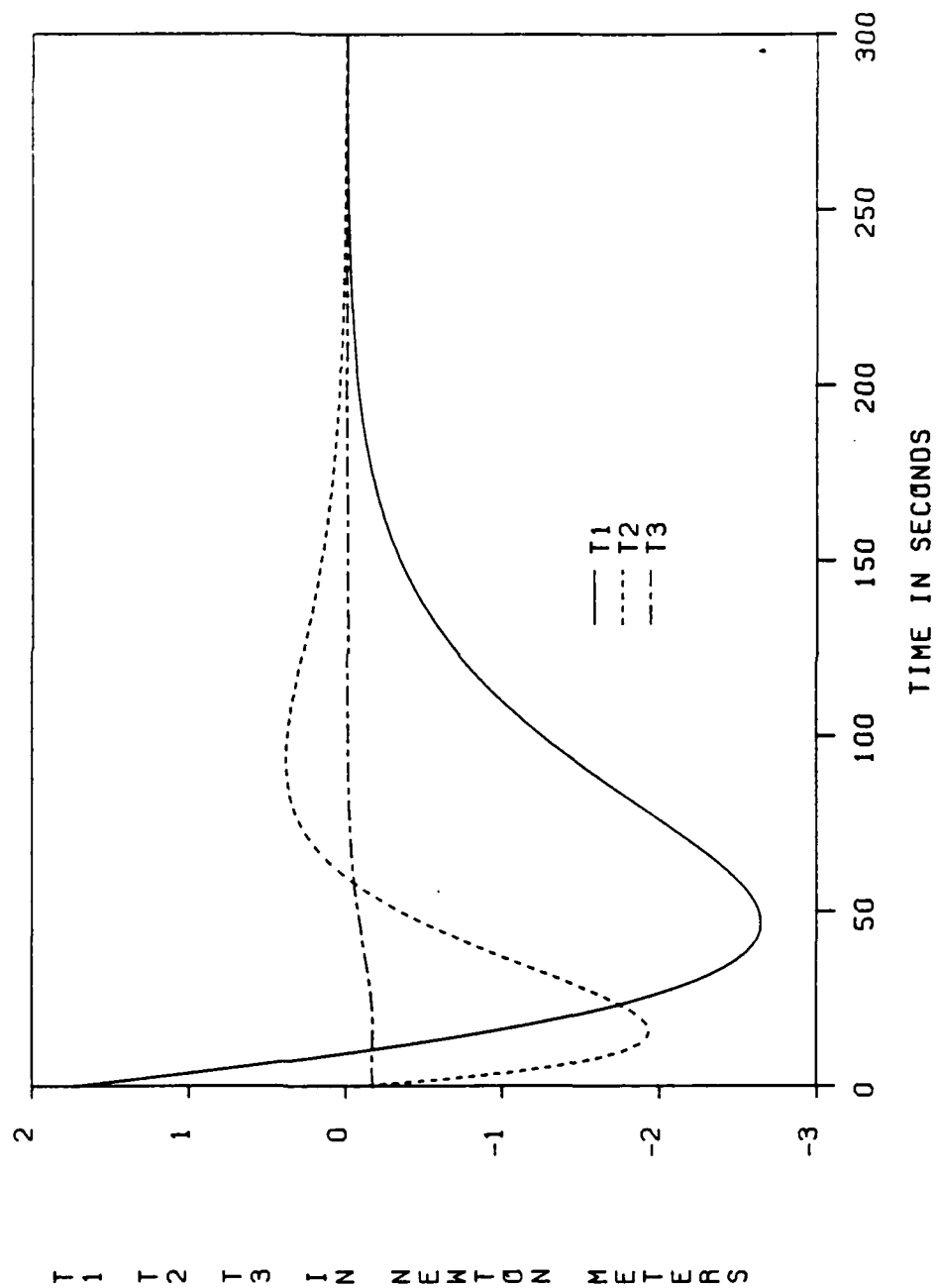


Figure 23. Internal Torque Histories (Feedback)

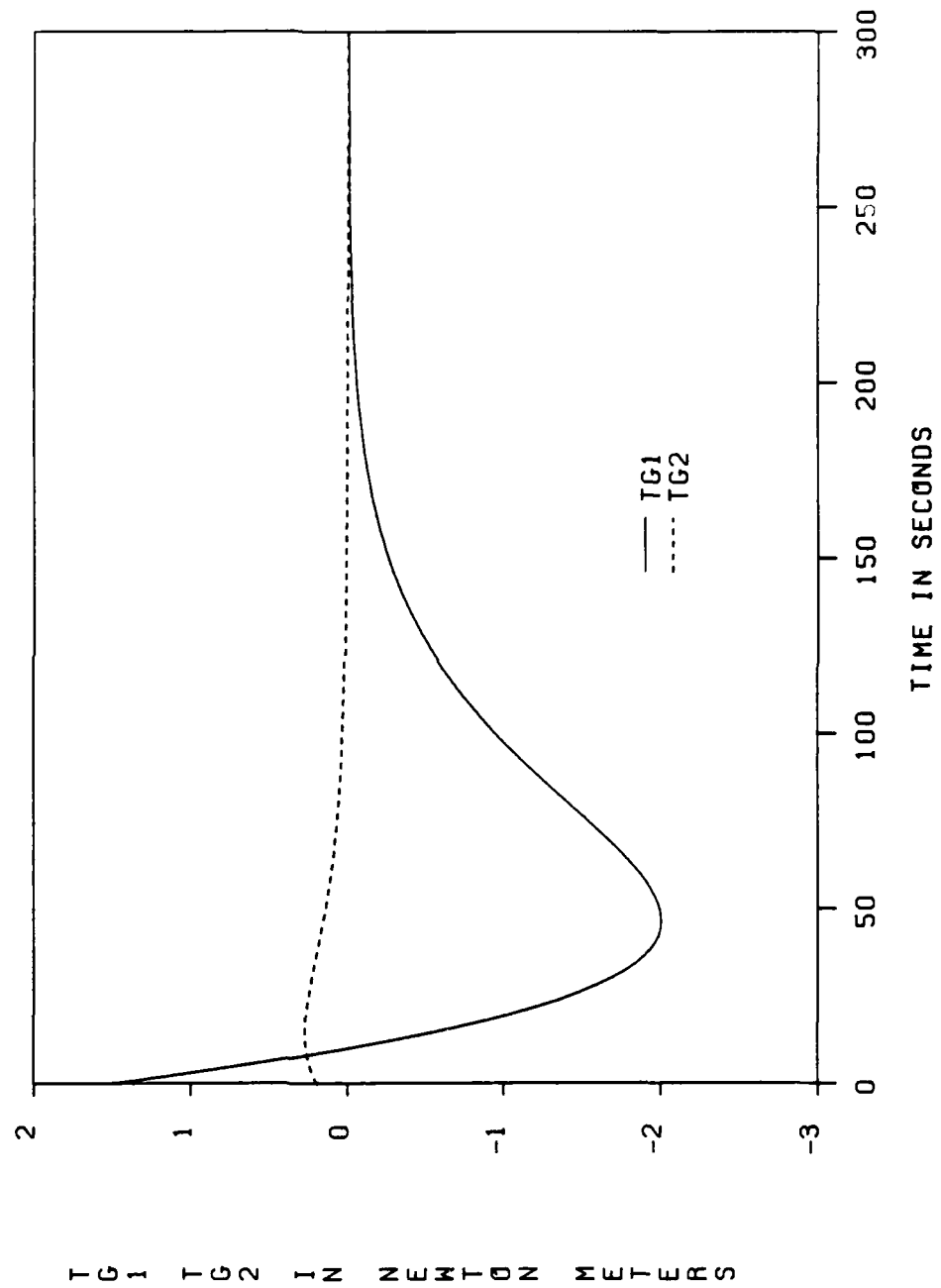
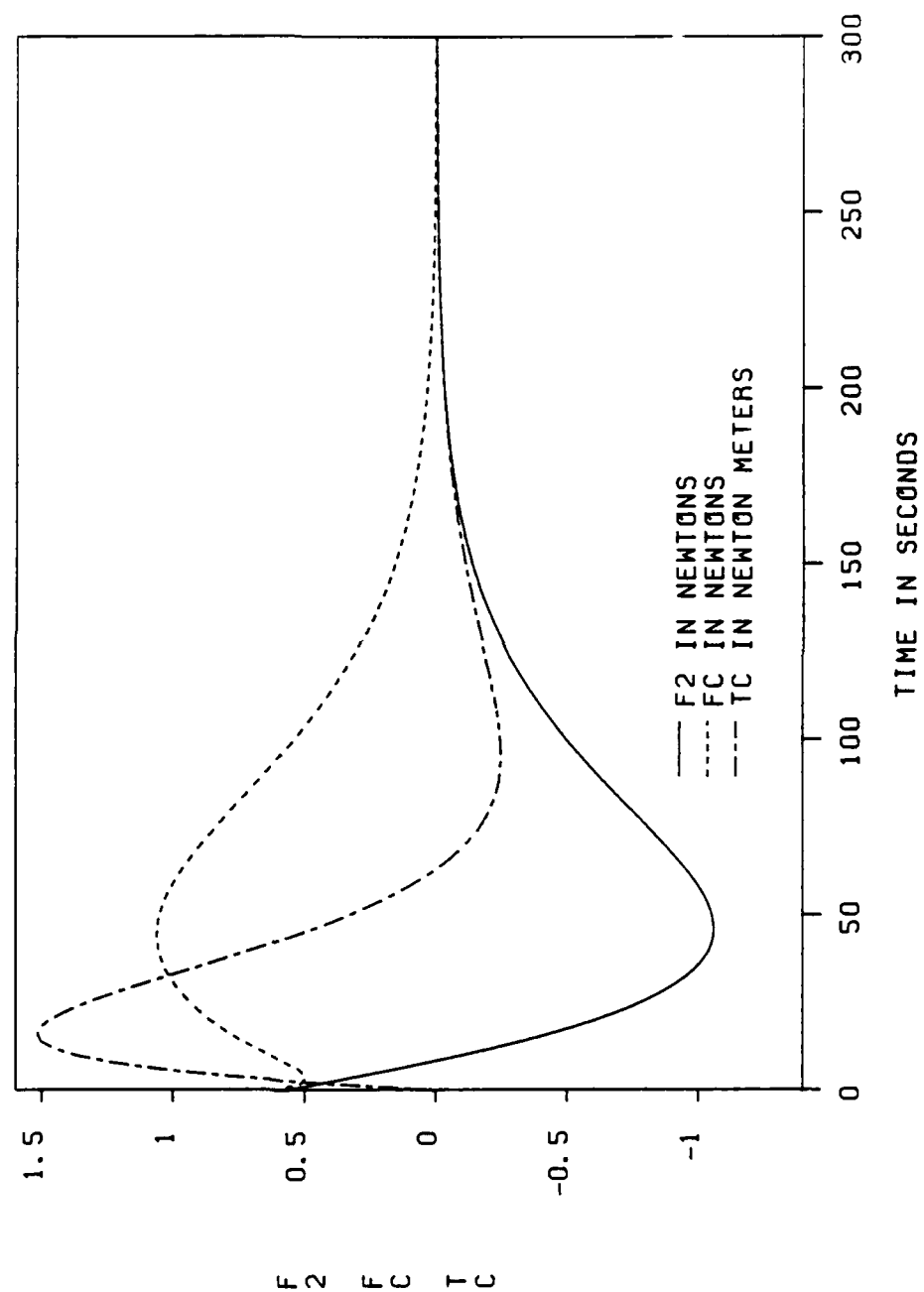


Figure 24. Constraint Load Histories (Feedback)



into a linear system, which is easily analyzed. As an example the free parameters of the control law were specified to produce desired system response. Profiles of the states, controls, and constraint loads were developed by numerical integration of the resulting linear system over a 300 second interval. While peak control torques and constraint loads do not appear excessive, they directly depend on the specified parameters in the control law. Consequently, these peaks can be reduced by appropriately respecifying the control system gains.

With this same feedback control law, the motion of the two-body system was seen to be very benign. From initial conditions of free spin and precession of the target and free spin of the OMV, the attitude of the OMV and its spin rate do not change during capture. The cone angle of the target decays as a second order linear system while the target's spin rate decays as a first order linear system. The joint moves to the \hat{e}_3 axis on the OMV as a third order linear system, which is specified to coordinate joint motion with cone angle decay. Consequently, the complete system motion is easily visualized, and the final orientation of the system can be deduced without formal use of a complementary set of kinematic equations for the OMV.

CHAPTER 5

CONTROL SCHEME COMPARISONS AND CONCLUSIONS

5.1 Introduction

Two control strategies have been developed to solve the remote orbital capture problem proposed in Chapter 1. Optimal control theory was employed in Chapter 3 to solve for continuous open loop controls. Liapunov stability theory was used in Chapter 4 to derive continuous feedback controls. Numerical examples of both strategies have shown that the motion of the two-body system is very benign during capture.

In this chapter the numerical examples of both control strategies are compared, and an example of using both strategies in a sequence is presented. Significant details of the previous chapters are reviewed, and some conclusions are drawn. To close, several directions for future work are suggested.

5.2 Control Scheme Comparisons

The numerical examples of open loop and feedback control contain significant differences. Most significant is that open loop controls drive the two-body system to the specified final state exactly in the specified time while the feedback controls give only an asymptotic approach to that state. Second, the joint motion on the OMV

is specified differently in the two examples. Consequently, the objective of the comparison is limited to forming some idea of the ranges of the control torque and constraint load magnitudes that can occur with different control strategies.

Table 5 shows the ranges of control torque and constraint load magnitudes that occurred in the numerical examples of unconstrained open loop control and feedback control. Both examples considered a 300 second maneuver time. In the case of feedback control, all states were reduced to within 0.5% of equilibrium values from peak values. Significant differences in the required control torque magnitudes can be seen except for TG2. On the other hand, the ranges of the constraint load magnitudes, F2, FC, and TC, show smaller variations. But no attempt was made to limit the ranges of the control torque and constraint load magnitudes. To the contrary, only a simple scheme of selecting free parameters in the control law was considered to obtain the desired dynamic response of the two-body system. Even so, the resulting forces and torques do not appear prohibitive from control or structural considerations. As a final comparison recall that the cost of capture, as measured by the performance index, equation (3.1), was 2.335 for unconstrained open loop control and 386.74 for feedback control. While this seems

TABLE 5

Control and Constraint Load Ranges for Unconstrained
Optimal Open Loop Control and Feedback Control*

	Open Loop	Feedback
T1 (newton-meters)	-0.012 to +0.013	-2.65 to +1.74
T2 (newton-meters)	-0.246 to +0.001	-1.94 to +0.39
T3 (newton-meters)	+0.0049 to +0.0173	-0.19 to 0.00
TG1 (newton-meters)	-0.23 to +0.21	-2.01 to +1.50
TG2 (newton-meters)	+0.028 to +0.200	0.00 to +0.28
F2 (newtons)	-0.86 to +0.12	-1.07 to +0.58
FC (newtons)	+0.024 to +0.270	0.00 to +1.07
TC (newton-meters)	-0.27 to +0.54	-0.25 to +1.52

$$*[u_1 \ u_2 \ u_3 \ u_4 \ u_5] = [T1 \ T2 \ T3 \ TG1 \ TG2]$$

TC = Dot product of constraint torque with constraint axis

FC = Magnitude of constraint force

F2 = Component of constraint force in \hat{e}_2 direction

to indicate a clear advantage for open loop control, the cost of feedback control could be very sensitive to the choice of gains in the control law and the system describing the joint motion.

While the ranges of the control magnitudes for the two examples are quite different, the motions of the two-body system under the two control schemes are very similar. With open loop control the OMV very nearly maintains a state of pure spin about its axis of maximum moment of inertia. With feedback control, because of the initial conditions, no deviation from the state of pure spin results. In both cases the target cone angle and spin rate relative to the OMV are smoothly eliminated as the connecting joint moves to the \hat{e}_3 axis on the OMV. A final spin-stabilized configuration results with either control scheme.

5.3 Capture by an Open Loop Control to Feedback Control Sequence

Open loop control cannot achieve the specified final state exactly because of the presence of small system errors. On the other hand, feedback control derived by the Liapunov method can bring the two-body system arbitrarily close to the desired final state in a fixed time, though perhaps at much greater cost. Therefore, a switch during capture from open loop control to feedback control might be considered. An example can be constructed using the case of unconstrained optimal open loop control where

a switch is made to feedback control after approximately 290 seconds of the nominal 300 second maneuver. From the solution grid of the TPBVP, the state of the two-body system at 289.655 seconds is given in Table 6. Allowing an additional 130 seconds for nonlinear feedback control, the free parameters of equation (4.13) are specified as follows:

$$k_4 = 0.00855625$$

$$B = \begin{bmatrix} +0.046 & & & & \\ & +0.046 & & & 0 \\ & & 0.0 & & \\ & & & +0.185 & \\ 0 & & & & +0.02 \end{bmatrix} .$$

The joint motion, as defined by the system, (4.4), is specified by three equal eigenvalues of -0.11.

This example of switching from open loop to feedback control is constructed to achieve a slightly different response from that in the previous example of feedback control. Here the joint position and γ_1 overshoot their equilibrium values by 0.0021 meters and 0.0010 radians respectively. However, relative to their values at 289.655 seconds, they return to within 0.01% of equilibrium after 130 seconds of feedback control. The values of B_{11} , B_{22} , and B_{55} are arbitrarily left unchanged from the previous

AD-A151 967

OPTIMAL OPEN LOOP AND NONLINEAR FEEDBACK CONTROL FOR
REMOTE ORBITAL CAPTURE(U) AIR FORCE INST OF TECH
WRIGHT-PATTERSON AFB OH J W WIDHALM 1985

2/2

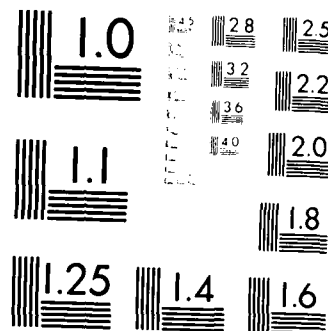
UNCLASSIFIED

AFIT/CI/NR-85-32D

F/G 22/1

NL





MICROCOPY RESOLUTION TEST CHART
NATIONAL BUREAU OF STANDARDS-1963-A

TABLE 6

System State Summary for the Open Loop-Feedback Case

	289.655 seconds (termination of optimal control)	419.655 seconds (termination of feedback control)
ω_{01}	-0.00061651 rad/sec	-0.000001559 rad/sec
ω_{02}	0.00039625 rad/sec	0.000001002 rad/sec
ω_{03}	-0.10128 rad/sec	-0.10128 rad/sec
$\dot{\gamma}_1$	-0.0013204 rad/sec	0.0000000417 rad/sec
$\dot{\gamma}_2$	-0.00057541 rad/sec	-0.00004274 rad/sec
γ_1	0.0068254 rad	-0.000000496 rad
$\bar{L}_{01} \cdot \hat{e}_2$	-0.020639 meters	0.00000095 meters
$\dot{\bar{L}}_{01}^R \cdot \hat{e}_2$	0.0019951 meters/sec	-0.0000000895 meters/sec
$\ddot{\bar{L}}_{01}^R \cdot \hat{e}_2$	0.0 meters/sec ²	0.0000000083 meters/sec ²

example of feedback.

To generate state, control, and constraint load histories, the system, (4.14), can be integrated forward for 130 seconds. The control vector, \bar{u} , can be computed from equation (4.13), and the constraint loads, from equations (2.45) and (2.49) as before. Linking these histories with those for optimal open loop control results in composite histories for the 419.655 second interval. The system states at the terminal time, 419.655 seconds are shown in Table 6.

Figures 25 through 30 show the composite histories of the states, controls, and constraint loads for the 419.655 second interval. The transition of four of the states to exponential decay is clearly shown. The spin rate, ω_{03} , is constant over the last 130 seconds since $B_{33} = 0$. The sixth state, γ_1 , also decays exponentially, but scaling prevents its depiction. The decay of the controls and constraint loads is also clear, but more apparent are the sudden changes which occur at the switching point. Modifying the system response might bring the feedback controls closer to the open loop controls at the switch.

A related control strategy would be to allow the optimal controller to execute completely its precomputed control histories, and then reduce any residual errors with feedback control. Finally, the joint would be locked

Figure 25. Body 0 Angular Rate Histories (Composite)

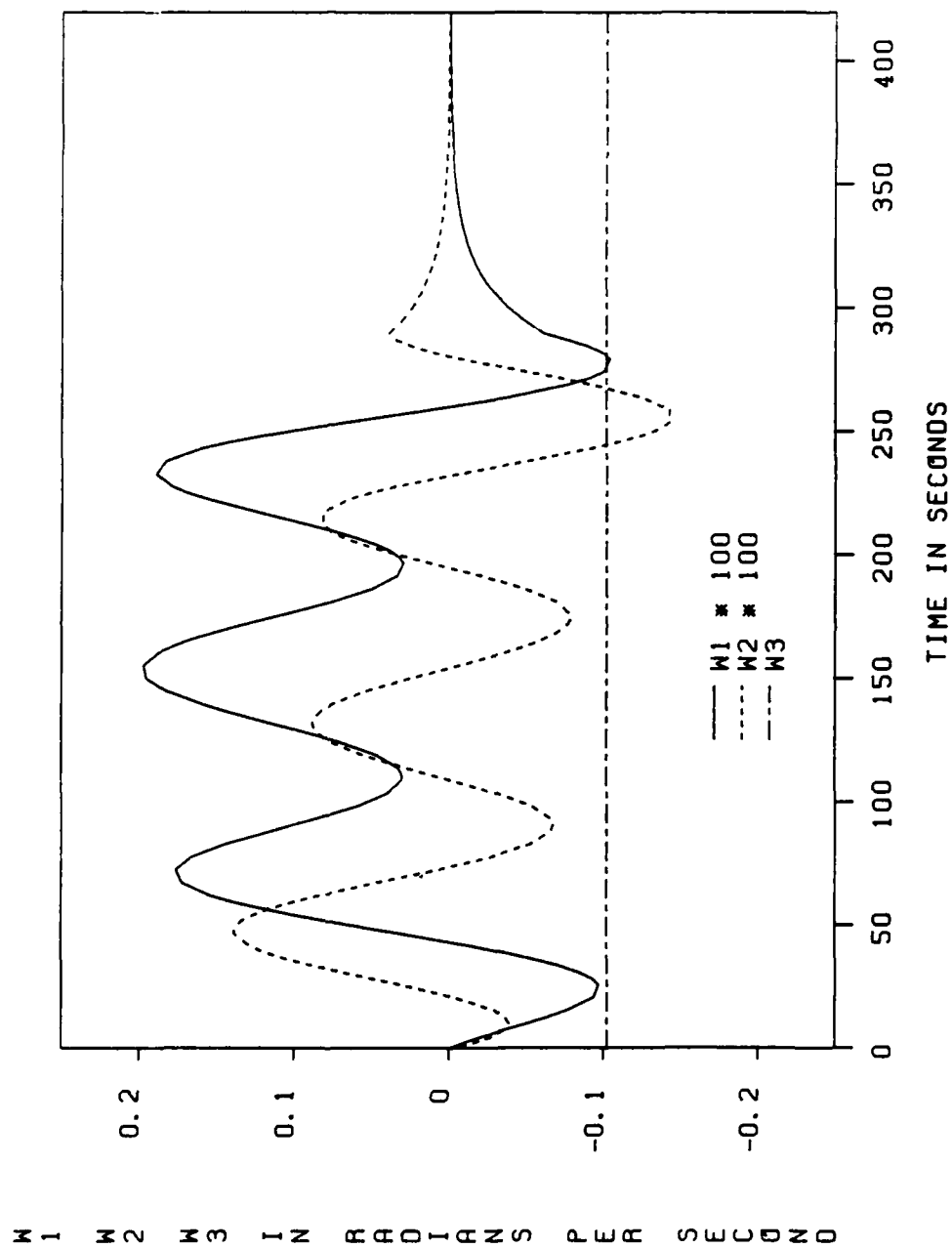


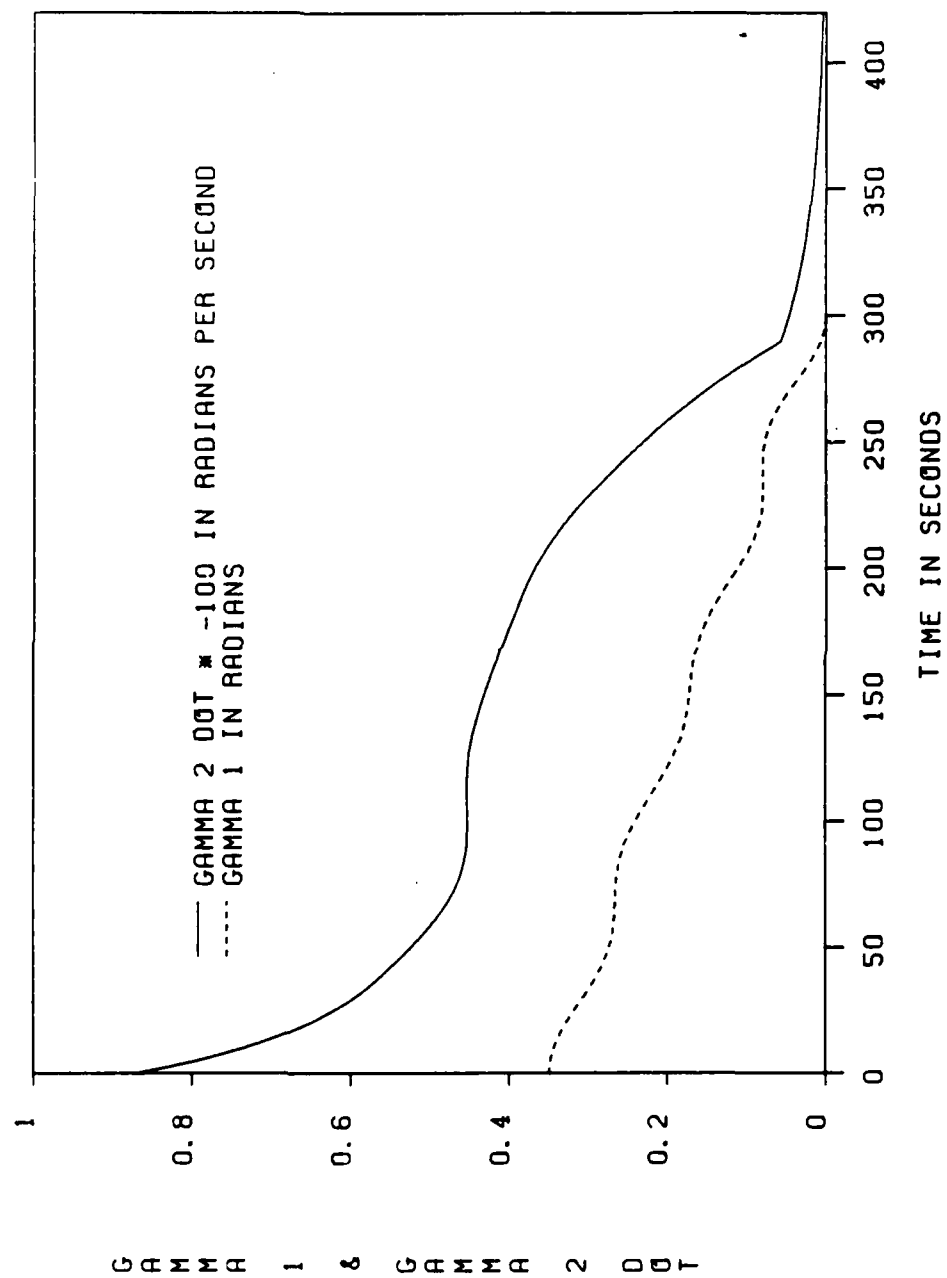
Figure 26. Body 1 γ_1 and $\dot{\gamma}_2$ Histories (Composite)

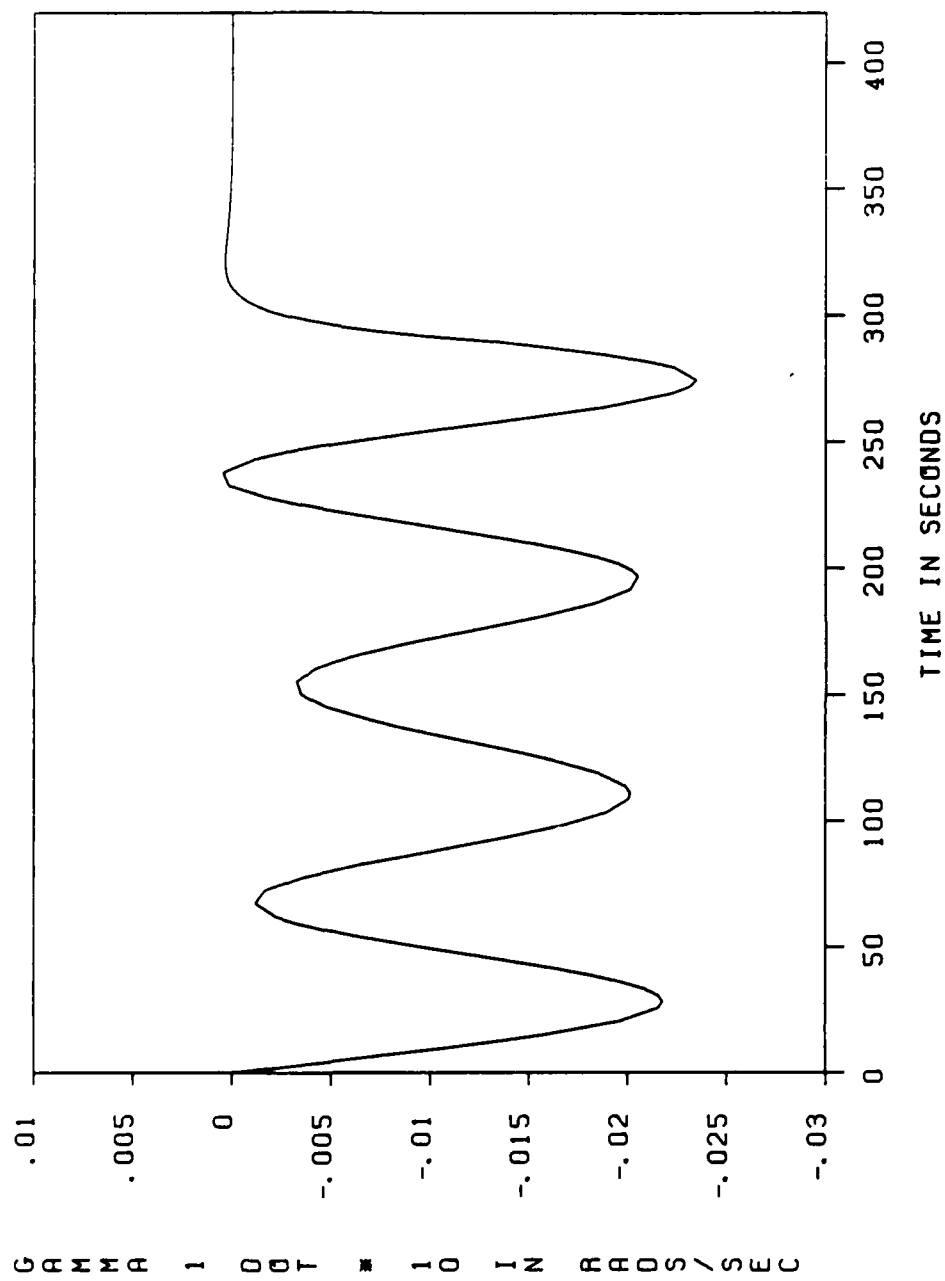
Figure 27. Body 1 $\dot{\gamma}_1$ History (Composite)

Figure 28. External Torque Histories (Composite)

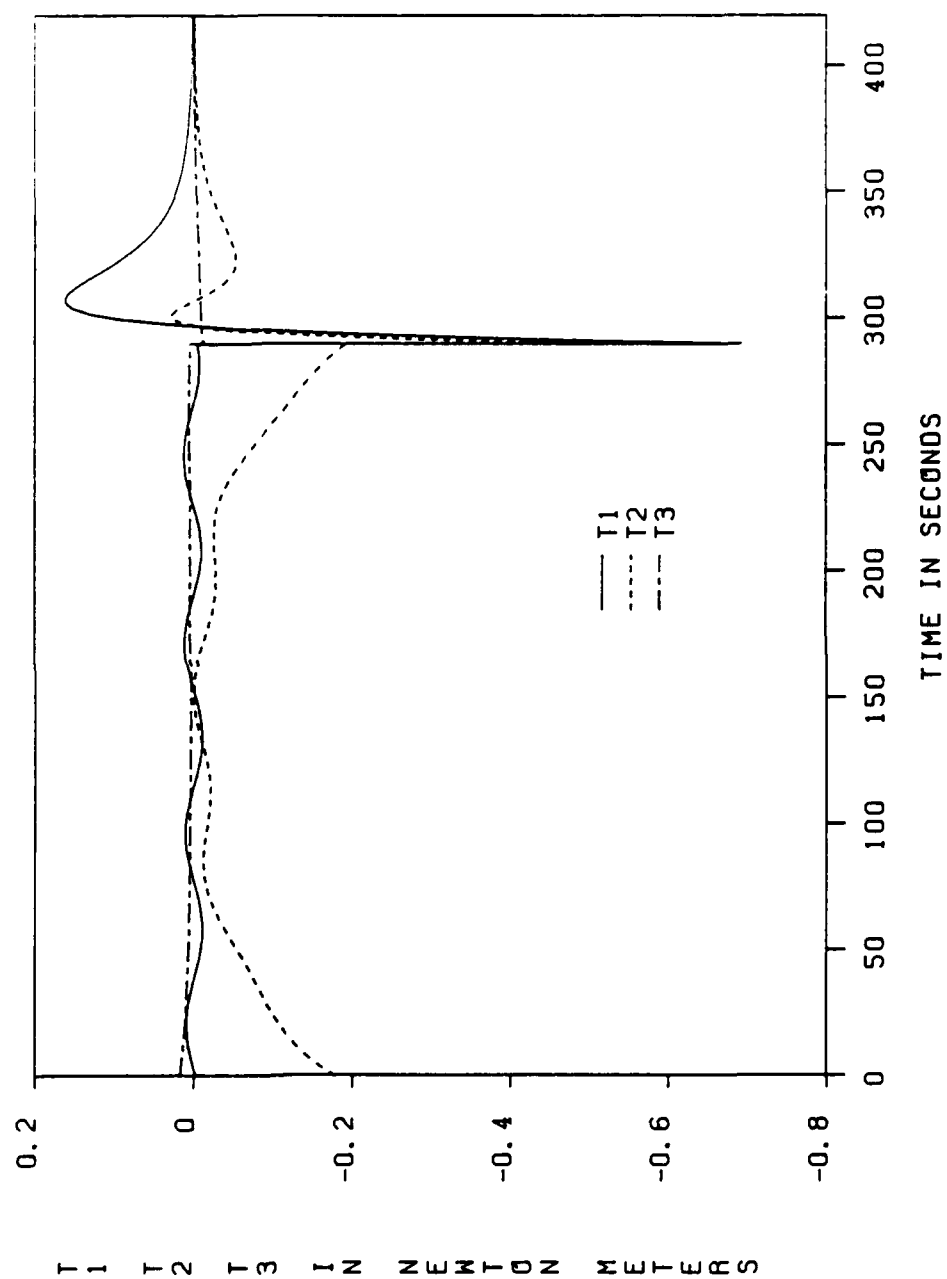


Figure 29. Internal Torque Histories (Composite)

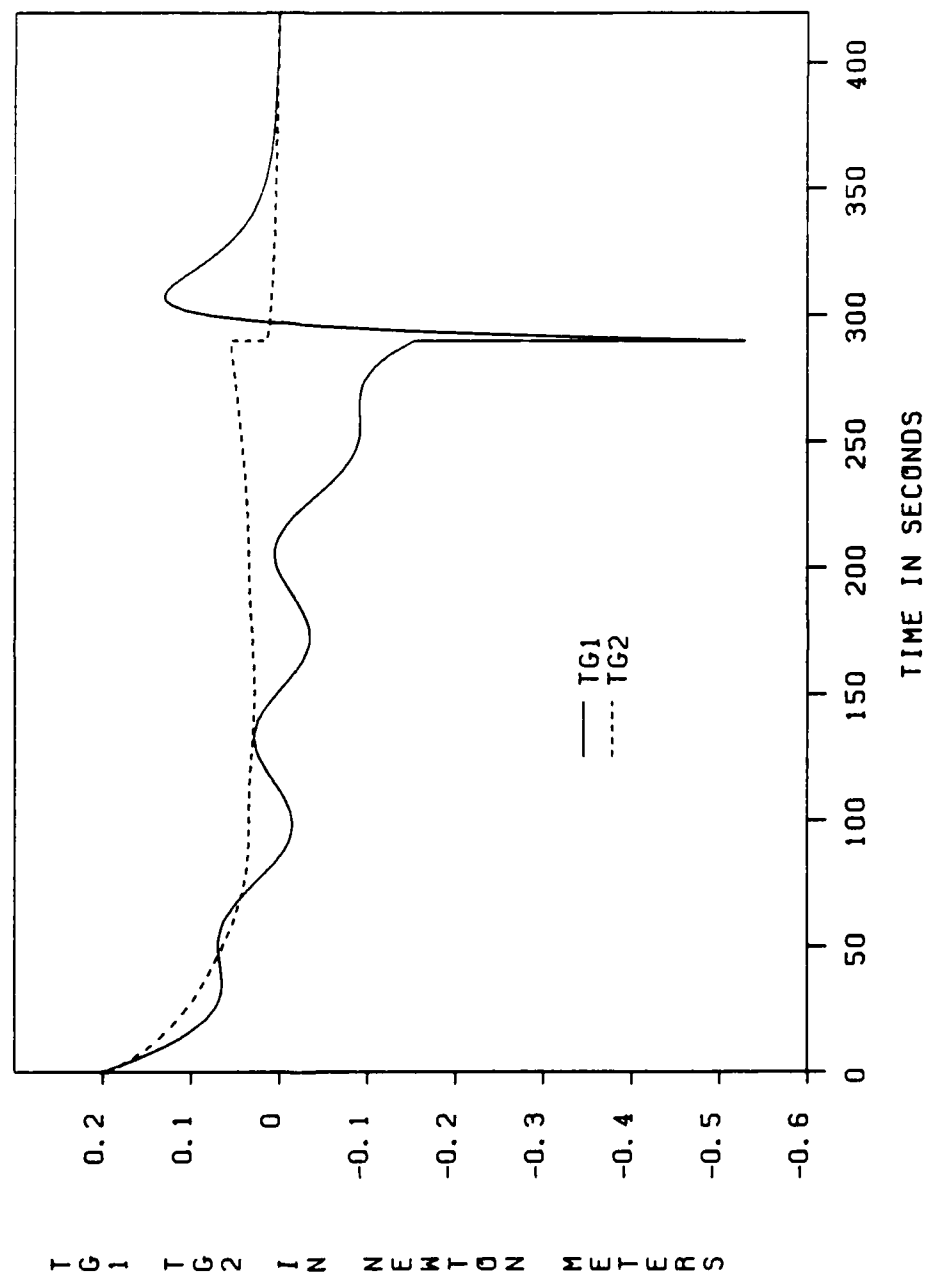
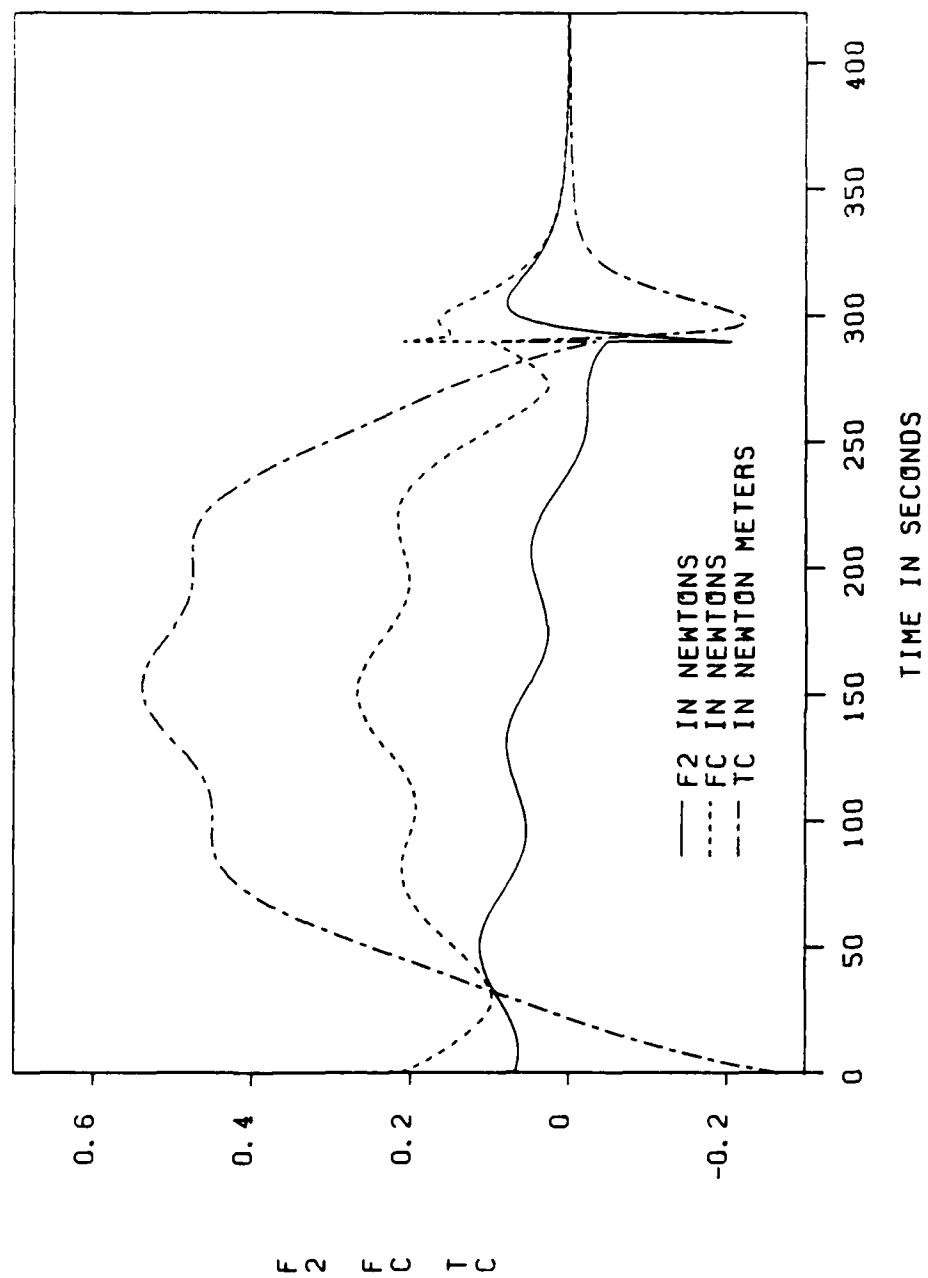


Figure 30. Constraint Load Histories (Composite)



to give a single, spin-stabilized, rigid body. From the example above, the system state of 289.655 seconds could be considered the state actually achieved after 300 seconds of open loop control. Then the same 130 seconds of additional feedback control from the example would result in the system state given in Table 6 for 419.655 seconds. In this case, however, the total maneuver time would be 430 seconds. The control cost of this strategy from equation (3.1) is the open loop cost plus the feedback cost, which would be $2.335 + 1.400 = 3.735$. Therefore, if feedback control should prove to be impractical for the complete capture maneuver, this dual control strategy might be a good compromise.

5.4 Summary and Conclusions

The problem of remote orbital capture has been addressed from a more realistic approach than others found in the literature. Previous work has not effectively considered the requirement to control the absolute motion of the two-body system as relative motion between the two bodies is eliminated. Here a control problem based on the coupled dynamics of a two-body system was considered. Eulerian-based equations of motion were derived which accounted for a novel concept: The joint connecting the two bodies is allowed to translate along the surface of one of the bodies. Derivation of these equations was

motivated by interest in a very specific capture problem, that of detumbling a freely spinning and precessing axially symmetric statellite by a spinning axially symmetric retriever spacecraft. This initial configuration is dynamically stable, and joint motion on the surface of the retriever spacecraft makes possible a final spin-stabilized configuration. The Eulerian-based equations of motion allow internal and external torques on the two-body system to be specified, so the capture problem became one of finding control profiles or control laws to drive the two-body system to a spin-stabilized final state.

Since the posed capture problem is nonlinear, optimal control theory was employed first to solve for open loop control profiles. Optimal control theory had not been applied previously to this type of multi-body problem, but difficulties were expected from results of optimal control of single rigid bodies. In particular, the problem in which the final orientation of the two-body system is completely specified is very difficult to solve numerically because the kinematic Euler parameter equations are not independent. Consequently, these equations were eliminated from the problem by leaving the final Euler parameters unspecified. Of the two remaining kinematic equations, one was also eliminated because of symmetry. The one kinematic equation retained and the appropriately

specified joint motion were sufficient to achieve the final spin-stabilized state. The results of the optimal open loop control investigation, however, pointed out that virtually nothing was lost from these simplifications since the orientation of the spin axis of the retriever spacecraft was very nearly constant during capture. Control requirements seem quite reasonable for maneuver times of five minutes and with control constraints more typical of an actual system. Finally, the constraint loads on the joint seem to impose no prohibitive structural requirements or control requirements to effect the prescribed joint motion.

A second approach to the nonlinear control problem was to develop a feedback control law by using Liapunov stability theory. The Liapunov indirect method showed how linear feedback could produce an asymptotic approach to the spin-stabilized equilibrium from within some local region of the equilibrium. Difficulty in determining the size of that region led to a nonlinear feedback control law derived from Liapunov's direct method and LaSalle's theorem. The nonlinear control law, when applied to the dynamic equations, transformed the original nonlinear system to a linear system, which was analyzed numerically to determine control and constraint load profiles. The analysis was keyed to achieving desired

system response with little attention to limiting controls and constraint loads. Consequently, when a very close approach to spin-stabilized equilibrium was required in a maneuver time of five minutes, peak controls and constraint loads were significantly greater than those for optimal open loop control. However, even here peak magnitudes were not large. Furthermore, these peaks might be reduced significantly by a more systematic approach to parameter selection in the control law and the system describing the joint motion.

The final approach considered for solving the capture problem used optimal open loop control first. Then residual errors were eliminated by nonlinear feedback control. Here again, specifying system performance led to significant increases in peak controls and constraint loads at the initiation of feedback control. On the other hand, these peaks were at least 65% less than those obtained by using only feedback control for capture. A much further reduction was expected, but this again pointed out the need for further investigation into parameter selection for the feedback control law and the joint motion.

As with optimal open loop control, the feedback control approach did not control the complete absolute orientation of the two-body system. However, feedback

control was initiated with the retriever spacecraft in or near a state of pure spin about its symmetry axis. Then by design the controls either maintained pure spin or produced pure spin with little change in spin axis orientation. Consequently, the two control approaches are consistent, producing similar results.

To summarize, the work presented here is significant in several respects. First, the field of multi-body dynamics has been extended by the general equations of motion derived in Chapter 2. Second, optimal control theory has been applied to the problem of remote orbital capture through these equations to address control requirements more realistically than previous work. Third, a nonlinear feedback control approach to orbital capture has been demonstrated. Finally, structural requirements of the joint in the two-body system have been considered by solving for the constraint loads on the joint during capture.

5.5 Suggestions for Further Research

While this work has addressed a very special capture problem, a foundation has been laid to move forward to more general problems. The equations of motion can be extended to asymmetric target satellites and to retriever spacecraft with reaction wheel control systems. Rendezvous and docking strategies must be developed that consider more

general dynamic states of the target. Convenient rigid appendages may not be present on prospective targets, so deployment of grappling devices from the joint on the retriever spacecraft needs to be considered. These are only three of many possible extensions of the work presented here, but they point out significant areas that require investigation.

VITA

Joseph William Widhalm Jr. was born on October 8, 1944 in Temple, Texas. He earned a B.S. in Aeronautical and Astronautical Engineering at the University of Illinois at Urbana-Champaign in 1967 and an M.S. in Astronautical Engineering at the Air Force Institute of Technology, Wright-Patterson AFB, Ohio in 1974. He was commissioned as a second lieutenant in the U.S. Air Force in 1967 and graduated from Air Force pilot training in 1968. He served on operational flying assignments to the F-105 aircraft in Thailand and the F-111 aircraft in England. He also served as an instructor pilot in the T-38 aircraft. From 1975 until 1979 he was an orbital operations engineer at the Air Force Space and Missile Systems Organization, participating in the procurement, launch, and on-orbit test and operation of such satellites as NATO III, DSCS II, FLTSATCOM, and DSCS III. As a result of his research for the Ph.D. degree he co-authored two papers for the AIAA Journal of Guidance, Control, and Dynamics. At the Air Force Institute of Technology he received the Commandant's Award for Outstanding Thesis Research. His military decorations include the Distinguished Flying Cross, two Meritorious Service Medals, seven Air Medals, and two Air Force Commendation Medals.

LIST OF REFERENCES

1. Onega, G. T. and Clingman, J. H., "Free-Flying Teleoperator Requirements and Conceptual Design," Proceedings of the First National Conference on Remotely Manned Systems (edited by E. Heer), California Institute of Technology, 1973, pp. 19-32.
2. Smith, G. W. and DeRocher, W. L., "Orbital Servicing and Remotely Manned Systems," Mechanism and Machine Theory, Vol. 12, 1977, pp. 65-76.
3. Faile, G. C., Counter, D. N. and Bourgeois, E. J., "Dynamic Passivation of a Spinning and Tumbling Satellite Using Free-Flying Teleoperators," Proceedings of the First National Conference on Remotely Manned Systems (edited by E. Heer), California Institute of Technology, 1973, pp. 63-73.
4. Kaplan, M. H. and Nadkarni, A. A., "Control and Stability Problems of Remote Orbital Capture," Mechanism and Machine Theory, Vol. 12, 1977, pp. 57-64.
5. Conway, B. A., Tuligowski, J. E. and Webber, P. D., "Dynamics of Remote Orbital Capture," Proceedings AAS/AIAA Astrodynamics Specialist Conference, Lake Placid, NY, 1983.
6. Hooker, W. W. and Margulies, M., "The Dynamical Attitude Equations for an N-Body Satellite," J. of the Astronautical Sciences, Vol. 12, 1965, pp. 123-128.
7. Hooker, W. W., "A Set of Dynamical Attitude Equations for an Arbitrary N-Body Satellite Having r Rotational Degrees of Freedom," AIAA Journal, Vol. 8, No. 7, 1970, pp. 1205-1207.
8. Greenwood, D. T., Principles of Dynamics, Prentice-Hall, Inc., Englewood Cliffs, NJ, 1965, Chapter 8.
9. Conway, B. A. and Widhalm, J. W., "Equations of Attitude Motion for an N-Body Satellite with Moving Joints," AIAA J. of Guidance, Control, and Dynamics, to appear.

10. Conway, B. A. and Widhalm, J. W., "Optimal Continuous Control for Remote Orbital Capture," AIAA J. of Guidance, Control, and Dynamics, to appear.
11. Bryson, A. E., Jr. and Ho, Y., Applied Optimal Control, Ginn and Co., Waltham, MA, 1969, Chapters 2 and 3.
12. Pereyra, V., "PASVA3: An Adaptive Finite Difference FORTRAN Program for First Order Nonlinear Ordinary Boundary Problems," Lecture Notes in Computer Science, Vol. 76, Springer-Verlag, Berlin, 1978, pp. 67-88.
13. Junkins, J. L. and Turner, J. D., "Optimal Continuous Torque Attitude Maneuvers," AIAA J. of Guidance and Control, Vol. 3, No. 3, May-June 1980, pp. 210-217.
14. Vadali, S. R., Kraige, L. G. and Junkins, J. L., "New Results on the Optimal Spacecraft Attitude Maneuver Problem," AIAA J. of Guidance, Control, and Dynamics, Vol. 7, No. 3, May-June 1984, pp. 378-380.
15. Vidyasagar, M., Nonlinear Systems Analysis, Prentice-Hall, Inc., Englewood Cliffs, N.J., 1978, Chapter 5.
16. Meirovitch, L., Methods of Analytical Dynamics, McGraw-Hill, Inc., New York, N.Y., 1970, Chapter 6.

END

FILMED

5-85

DTIC